

Martine Evensen
Solveig So-Sun Garen
Elin Karlsen Paulsrud

Design and Build Up of a Tribometer to Work Under Corrosive and Fatigue Conditions for the Offshore Renewable Energy Sector

A Top Sliding Motion Approach

Bachelor's thesis in Mechanical Engineering
Supervisor: Nuria Espallargas
Co-supervisor: Hamid Khanmohammadi
May 2024



Norwegian University of
Science and Technology

Martine Evensen
Solveig So-Sun Garen
Elin Karlsen Paulsrud

Design and Build Up of a Tribometer to Work Under Corrosive and Fatigue Conditions for the Offshore Renewable Energy Sector

A Top Sliding Motion Approach

Bachelor's thesis in Mechanical Engineering
Supervisor: Nuria Espallargas
Co-supervisor: Hamid Khanmohammadi
May 2024

Norwegian University of Science and Technology
Faculty of Engineering
Department of Mechanical and Industrial Engineering



Norwegian University of
Science and Technology

REPORT BACHELOR THESIS

Title

Design and Build Up of a Tribometer to work Under Corrosive and Fatigue Conditions for the Offshore Renewable Energy Sector

Design og bygging av et tribometer som skal fungere under korrosive og utmattende forhold for offshore fornybar energisektor

Project number

MTP-K-2024-20

Author(s)

Evensen, Martine

Garen, Solveig So-Sun

Paulsrud, Elin Karlsen

Supervisor NTNU

Espallargas, Nuria

Khanmohammadi, Hamid (co-supervisor)

Report is OPEN/~~CLOSED~~

Date

21.05.2024

Short abstract (Both in Norwegian and English)

This project aims at designing and building up a tribometer capable of testing metallic samples under three conditions simultaneously. The conditions that are being tested for are friction, corrosion and bending fatigue.

I dette prosjektet skal det designes og bygges opp et tribometer som er i stand til å teste metalliske prøver under tre forhold samtidig. Forholdene som skal testes er friksjon, korrosjon og utmatting.

Stikkord:

Testrigg med flere parametere

Tribometer

Korrosjon

4-punkts statisk og syklisk bøyning

Utmatting

Tribologi

Keywords:

Multi-degrading test rig

Tribometer

Tribocorrosion

4-point static and cyclic bending

Fatigue

Tribology

Preface

This bachelor's thesis is written at the Department of Mechanical and Industrial Engineering at the Norwegian University of Science and Technology (NTNU) in Trondheim. The group consists of Martine Evensen, Solveig So-Sun Garen and Elin Karlsen Paulsrud. We are all studying mechanical engineering with a specialization in machine design.

For this Bachelor's thesis we designed and built a tribometer that will be used to test metal samples for three different conditions simultaneously and thus find the material that will be best suited for different purposes. This tribometer will be used in an international project to study the behavior of different metals that will be used in the offshore renewable energy sector.

We would like to raise a special thanks to our supervisors:

Nuria Espallargas

Hamid Khanmohammadi

We would also like to thank the Bachelor group that has worked along side us on this project. This group consists of Harald Aase, Ansgar Korsæth and Kjetil Sørensen

21. May, Trondheim

Abstract

A tribometer is an instrument that can test how different materials interact with each other, and it is used to study the friction and wear between surfaces. Knowledge about the behaviour of materials under different conditions is very useful as it can help engineers and project managers choose the right materials for their projects, and thus improve the quality of the products.

The main focus of this Bachelor's thesis has been the designing and building up of a tribometer that can test metallic samples exposed to friction, corrosion and bending fatigue simultaneously. The goal for the project has been to create a prototype of a tribometer that can later be used in the tribology laboratory at NTNU in Trondheim.

The tribometer designed in this project is a ball-on-plate tribometer with four-point bending and an electrochemical cell. It will perform tests on small metallic test samples, with a fatigue load applied from the underside and friction and corrosion tests performed on the top. There is also another Bachelor group that has been working in the same project, but with the load applied from the top of test sample and the friction and corrosion tests performed on the underside of the test sample. In collaboration with the other group and the supervisors a common size of the test samples was agreed upon for both groups' tribometer.

With the great guidance from the supervisors throughout this project, as well as the knowledge gained over the three years of studying mechanical engineering, the group was able to make great progress toward finalizing a design for the tribometer.

Through working on this project, the group has met many of the goals that were set prior to starting the project. The group has also gained experience that will be valuable in their future careers.

Sammendrag

Et tribometer er et instrument som kan teste hvordan ulike materialer interagerer med hverandre, og det brukes for å studere friksjon og slitasje mellom overflater. Kunnskap om materialers oppførsel under ulike forhold er veldig nyttig da det kan hjelpe ingeniører og prosjektledere med å velge de riktige materialene for sine prosjekter, og dermed forbedre kvaliteten på produktene.

Hovedfokuset for denne bacheloroppgaven har vært å utvikle et design for et tribometer som kan teste metalliske prøver som er utsatt for friksjon, korrosjon og utmatting samtidig. Målet for prosjektet har vært å lage en prototype av et tribometer som senere kan bli brukt i tribologilabben på NTNU i Trondheim.

Tribometeret som er designet i dette prosjektet er et ball-on-plate tribometer med four-point bending og en elektokjemisk celle. Det vil utføre tester på små metalliske prøver, med en utmattingslast påført fra undersiden og friksjons- og korrosjonstester utført på oversiden. Det er også en annen bachelorgruppe som har jobbet på det samme prosjektet, men med lasten påført fra oversiden og friksjons- og korrosjonstestene utført på undersiden av prøven. I samarbeid med den andre gruppen og veilederne ble det bestemt en felles størrelse på prøvene for begge gruppernes tribometer.

Med god veiledning fra veilederne gjennom dette prosjektet, i tillegg til den kunnskapen som gruppen har tilegnet seg over de tre årene på maskiningeniørstudiet, ble det gjort store fremskritt mot å ferdigstille et design for tribometeret.

Gjennom arbeidet med dette prosjektet, har gruppen oppnådd mange av de målene som ble satt før prosjektet ble startet. Gruppen har også tilegnet seg erfaringer som vil være verdifulle i fremtidige karrierer.

Contents

Preface	i
Abstract	ii
Notation	xii
Abbreviation	xiv
1 Introduction	1
1.1 Background	1
1.2 Project Description	1
1.3 Performance Goals	2
2 Theory	3
2.1 Tribology	3
2.1.1 Friction	3
2.1.2 Wear	4
2.2 Electrochemical Corrosion	5
2.3 Tribocorrosion	7
2.3.1 Effect of Corrosion on Wear	7
2.3.2 Effect of Wear on Corrosion	8
2.3.3 The Impact of Third Bodies	8
2.4 Four-Point Bending	9
2.4.1 Equations Surrounding Four-Point Bending	9
2.5 S-beam Load Cell	11
2.6 Motors	12
2.6.1 Brushless DC Motor	12
2.6.2 Stepper Motor	14
2.7 Captive Linear Actuator	15
2.8 Materials	15
2.8.1 Silicone Rubber	15
2.8.2 PEEK	15
2.8.3 PLA	15
2.8.4 Steel	16

2.9	Equations Needed for Calculating the Dimensions of the Dead Weight . . .	16
3	Digitalisation and Sustainability	17
3.1	Digitalisation	17
3.2	Sustainability	17
3.3	How can Tribometers Contribute to Digitalisation and Sustainability? . . .	18
4	Methodology	19
4.1	Design Thinking	19
5	Design and Build up	21
5.1	Inspiration	21
5.2	The Test Piece	22
5.2.1	Finding the Max Moment	23
5.2.2	Size of the Test Piece	25
5.2.3	Overview of Materials and Their Mechanical Properties	28
5.3	Optical board	30
5.4	Friction Mechanism	30
5.4.1	Friction Mechanism - First Design	31
5.4.2	Friction Mechanism - Second Design	33
5.4.3	Friction Mechanism - Third Design	34
5.4.4	The Motor for Friction Mechanism	36
5.4.5	Ball Holder - First Design	37
5.4.6	Ball Holder - Second design	39
5.4.7	Ball Holder Hat	41
5.4.8	Dead Weight	41
5.4.9	Test Piece Holder - First Design	44
5.4.10	Test Piece Holder - Second Design	46
5.4.11	Support for the Friction Mechanism - First Design	48
5.4.12	Support for the Friction Mechanism - Second Design	48
5.5	The Load Cell for the Friction Mechanism	52
5.5.1	Load Cell Mount	52
5.5.2	BLDC Motor Mount - First Design	54
5.5.3	BLDC Motor Mount - Second Design	55

5.6	Electrochemical Cell	56
5.6.1	Seal	56
5.6.2	Compartment for the Electrochemical Cell - First Design	59
5.6.3	Compartment for the Electrochemical Cell - Second design	60
5.6.4	Compartment for the Electrochemical Cell - Third design	61
5.6.5	Compartment for the Electrochemical Cell - Fourth design	65
5.7	Fatigue Load Application	66
5.7.1	Design Criteria	66
5.7.2	Fatigue Load Application - First Design	67
5.7.3	Fatigue Load Application - Second Design	69
5.7.4	Fatigue Load Application - Third Design	69
5.7.5	Fatigue Load Application - Fourth Design	71
5.7.6	Motor for the Fatigue Load Application	74
6	Final Design	76
6.1	Entire Friction Mechanism	77
6.1.1	Friction Mechanism - Materials	78
6.1.2	Further Improvements of the Friction Mechanism	78
6.2	Fatigue Load Application	79
6.2.1	Fatigue Load Application - Materials	79
6.2.2	Further Improvements of the Fatigue Load Application	79
6.3	Electrochemical Cell	80
6.3.1	Electrochemical Cell - Material	80
6.3.2	Further Improvements of the Electrochemical Cell	80
6.4	Materials	81
6.5	How to Assemble the Tribometer	81
6.6	Performing the Tribotest	82
7	Limitations	84
8	Conclusions	86
	Appendices	91
	A Calculations	91

B Machine drawings

95

List of figures

2.1.1	Ball-on-plate	3
2.1.2	Adhesive wear	4
2.1.3	Abrasive wear	5
2.2.1	Corrosion of iron	6
2.2.2	Three electrode setup	7
2.4.1	Four-point bending	9
2.4.2	Parameters of the test piece	10
2.5.1	Simplified Diagram of a S-beam Load Cell	11
2.6.1	Simplified Diagram of an Outer Rotor BLDC Motor	13
2.6.2	Coil Polarity	13
2.6.3	Rotation of the BLDC Motors Rotor	13
2.6.4	Simple Drawings of the Main Parts of a Hybrid Motor	14
5.1.1	Tribometer in the tribology lab	21
5.2.1	Free Body Diagram (FBD)	22
5.2.2	Sections of the test piece	23
5.2.3	Cut in section 1 of the test piece	23
5.2.4	Cut in section 2 of the test piece	24
5.2.5	Cut in section 3 of the test piece	24
5.2.6	Shear force diagram	25
5.2.7	Moment diagram	25
5.2.8	Sizes of the test piece	27
5.2.9	Finale sizes of the test piece	28
5.3.1	Optical Board	30
5.4.1	First Design of the Friction Mechanism	32
5.4.2	First Design of Friction Mechanism	32
5.4.3	Second Mockup of Friction Mechanism	33
5.4.4	Second design of Friction Mechanism	33
5.4.5	Third Design of Friction Mechanism	34
5.4.6	Third Design of Friction Mechanism	35
5.4.7	Assembled Motor and Components	36
5.4.8	Dimensions of the BLDC motor	37

LIST OF FIGURES

5.4.9	Ball Holder - First Design	38
5.4.10	Ball Holder - First Design - Separated Parts of the Ball Holder	39
5.4.11	Second design of ball holder with a length of 118.50 mm.	40
5.4.12	Ball Holder - Second Design - Separated Parts of the Ball Holder	40
5.4.13	Ball Holder Hat	41
5.4.14	Two Dimensions of 20 N dead weight	43
5.4.15	Two Dimensions of 50 N dead weight	44
5.4.16	Test Piece Holder - First Design	45
5.4.17	Parts of the First Design of Test Piece Holder	46
5.4.18	Test piece holder - Second Design	47
5.4.19	Adjustment of Second Design of Test piece holder	47
5.4.20	Support for the Friction Mechanism - First Design	48
5.4.21	Support for Friction Mechanism - Second Design	49
5.4.22	Support on the Right Side of Friction Mechanism	50
5.4.23	Parts of the Support on the Right Side of the Friction Mechanism	50
5.4.24	Support on the Left Side of the Friction Mechanism	51
5.4.25	Parts of the Support on the Left Side of the Friction Mechanism	51
5.5.1	Machine Drawing of RES2 S-Beam Jr. Load Cell	52
5.5.2	Different Angles of the Load Cell Mount	53
5.5.3	Bolt Connecting the Load Cell to the Test Piece Holder	54
5.5.4	BLDC Motor Mount - First Design	54
5.5.5	BLDC Motor Mount Parts - First Design	54
5.5.6	BLDC Motor Mount - Second Design	55
5.5.7	Motor Mount - Second Design	55
5.6.1	Silicone moulding kit	57
5.6.2	First design for electrochemical cell	59
5.6.3	Second design for electrochemical cell	60
5.6.4	Third design for the compartment containing the electrochemical cell	62
5.6.5	Seal in third design	63
5.6.6	Fourth design for compartment with the electrochemical cell	65
5.6.7	Seal in fourth design	66
5.7.1	Sketch of the Load Application Mechanism	67
5.7.2	Sketch for the load application mechanism	68

LIST OF FIGURES

5.7.3	Load application - First design	68
5.7.4	Load applicator - Second design	69
5.7.5	Support applicator - Third design	70
5.7.6	Load Applicator Mechanism - Applicators	70
5.7.7	Fatigue Load Application - Fourth Design	71
5.7.8	Support Applicator - Fourth Design	72
5.7.9	Support Applicator Parts - Fourth Design	72
5.7.10	Load Applicator - Fourth Design	73
5.7.11	Load Applicator parts - Fourth Design	74
5.7.12	Captive Linear Actuator - Technical Drawing	75
5.7.13	Captive Linear Actuator - Stroke Specification	75
6.0.1	Final design of the multi-degradation tribometer.	76
6.1.1	The final design of the friction mechanism.	77
6.2.1	Final design of the load application mechanism.	79
6.3.1	Electrochemical Cell	80

List of tables

3.2.1 Objectives to improve eco-efficiency 18

5.2.1 Materials and their mechanical properties 29

5.6.1 The casting process of the silicone seal. 58

Notation

Symbol	Meaning
μ	Coefficient of friction
F_f	Friction force
F_n	Normal load from ball
b	Width
h	Height / thickness
L	Length between the two support beams
a	Length between the support beam and the load applicator
F	Applied force
M(x)	Moment at distance x
M_{max}	Max moment
I_z	Moment of inertia around the z axis
σ_y	Yield strength
σ_{max}	Maximum stress
δ	Deflection
E_b	Modulus of elasticity in bending, tension
V	Shear force
Σ	Sum
F_y	Force along the y axis
w	Width for the inside of the compartment containing the electrochemical cell
l	Length for the inside of the compartment containing the electrochemical cell
d_{10}	The diameter of the 10mm ball holder
l_{wt}	The length of the wear track
$A_{exposed}$	Area of the test piece that is exposed to the electrolyte
$V_{electrolyte}$	Volume of electrolyte
H	Height from the top of the test piece to the top of the compartment for the electrochemical cell's walls.
V_{side}	Volume of electrolyte that is below the top surface of the test piece

NOTATION

Symbol	Meaning
A_{cell}	Horizontal area of the inside of the compartment for the electro-chemical cell
m	Mass
a	Acceleration
Ag	Silver
AgCl	Silver chloride
$V_{deadweight}$	Volume of the dead weight
V_{hole}	Volume of the cylindrical shaped hole in the dead weight
r	Radius

Abbreviation

Abbreviation	Meaning
AI	Artificial Intelligence
BLDC	Brushless Direct Current
CE	Counter Electrode
FBD	Free body diagram
IoT	Internet of Things
NTNU	Norwegian University of Science and Technology
PEEK	Polyetheretherketone
PLA	Polylactic Acid
RE	Reference Electrode
SDGs	Sustainable Development Goals
SS316L	Stainless steel 316L
SDSS UNS S32750	Super Duplex Stainless Steel UNS S32750
Inconel	A family of nickel-chromium-based superalloys
Ti6Al4V	Titanium alloy with 6 % Aluminum and 4 % Vanadium
UN	United Nations
UNDP	United Nations Development Programme
WE	Working Electrode

1 Introduction

1.1 Background

Tribocorrosion is degradation caused by the simultaneous action of corrosion and wear in a metallic material. Tribocorrosion and multi-degradation reduce the lifetime of components. This has a major impact on both the economy and the environment as equipment failure due to wear and corrosion stands for more than 1% of the losses to the gross national product of countries. In the offshore and marine industry, many machine components are subjected to both wear and corrosion simultaneously. Especially in a country like Norway, where the offshore industry is huge, thorough exploration of tribocorrosion is imperative (SINTEF, 2013).

Tribocorrosion studies show that when wear and corrosion appears simultaneously the loss of materials happens at a much higher rate than it would have, had they happened separately (C. B. von der Ohe and R. Johansen and N. Espallargas, 2011). Additionally there is not done a lot of research in the synergy effect of wear, corrosion and bending.

1.2 Project Description

This project aims at designing and building up a tribometer that can test metallic samples exposed to friction, corrosion and bending fatigue simultaneously. The first version of this type of tribometer was built in 2009 (C. B. von der Ohe and R. Johansen and N. Espallargas, 2011). However, that tribometer is of a larger scale than the tribometer that will be designed in this project.

The tribometer of this project will be a bench prototype of a ball-on-plate tribometer. A ball-on-plate tribometer is a tribometer where the test piece is a flat plate or a flat beam, and the friction is applied to the test piece with the help of a ball. In this tribometer the applied friction will be on top of the test piece and the fatigue load will be applied from the bottom of the test piece. To test the material for corrosion, the wear track is going to be submerged in salt water.

The materials that will be tested with the help of this tribometer is primarily SS316L, SDSS UNS S32750, mild steel, bearing steel, Inconel 625 and Ti6Al4. In this Bachelor's project there will only be made a prototype of the tribometer. This prototype will primarily be 3D-printed with PLA. If possible it is also preferred if the tribometer can perform the four-point bending test in both directions.

1.3 Performance Goals

Before this project started, the group decided on some goals that they would like to achieve while working on the Bachelor's thesis.

First of all, the group wanted to improve their ability to work effectively in groups and collaborate on solving the problems that may occur. By collaborating with each other, the supervisors and alongside the other group on challenges that may occur, the group hopes to develop stronger team-working skills.

Secondly, the group hopes to improve their ability in writing academic text by going through the research process and documenting the work that is done, while following the standards given for academic reports.

The group also hopes to be able to use the knowledge obtained through all the different courses that they have taken during their bachelors degree to develop an innovative solution for the Bachelor's thesis.

Lastly the group hopes this report will be helpful in future work within the tribology and tribocorrosion field.

2 Theory

2.1 Tribology

Tribology is the study of different surfaces interacting against each other. This includes the study of both friction and wear. There are hundreds of different apparatus used in tribo-testing, but this paper will focus on a ball-on-plate method (illustrated in Figure 2.1.1). A ball-on-plate tribometer works by having a ball, with a given normal load, sliding in reciprocating motions on a rigid metal test piece (the plate) (Morshed et al., 2021, p. 27 - 29). The ball is moving at a constant speed in an alternating linear movement. The speed that the ball is moving in is likely substantially higher than the speed that a metal component would experience friction, but this is done to be able to simulate the life cycle of the metal component in a significantly reduced time span.

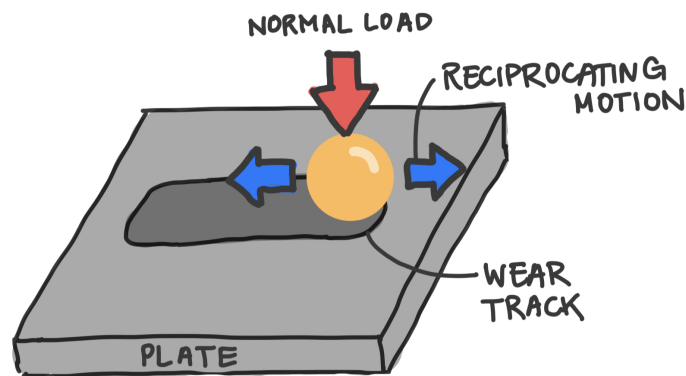


Figure 2.1.1: This illustration of the ball-on-plate method is inspired by (Morshed et al., 2021, p. 28).

2.1.1 Friction

When two solid surfaces are in contact with each other and an external tangential force is applied, the force that appears to resist the relative motion between the two surfaces is what is called friction (Igual et al., 2020). While discussing friction, the concepts of friction force (F_f) and friction coefficient (μ) come up. The friction coefficient is a measurement that describes the strength of friction between two surfaces. The friction force is the force that occurs when two surfaces are interacting against each other. The

friction coefficient is given by the formula:

$$\mu = \frac{F_f}{F_n} \quad (2.1.1)$$

This formula is based on Amonton's first law of friction. This law states that the friction force is directly proportional to the applied normal load, F_n (Lehigh University, n.d.).

As mentioned earlier, the normal load from the ball is given. The friction force can then be measured with the help of a force transducer. From this it is possible to calculate the coefficient of friction using Equation 2.1.1 (Lehigh University, n.d.). The friction will vary depending on the size of the normal load given from the ball (Igual et al., 2020).

2.1.2 Wear

When two surfaces interact with each other, especially when they are sliding against each other, some of the material can detach from the surface. The loss of material is what is called wear. Adhesive wear and abrasive wear are the most common types of wear (Society of Tribologist and Lubrication Engineers, n.d.).

Adhesive wear happens when these two surfaces slide against each other and material from one of the surfaces will stay adhered to the other, meaning that one of the surfaces loses material while the other gains material. Adhesive wear is illustrated in Figure (2.1.2) (Society of Tribologist and Lubrication Engineers, n.d.).

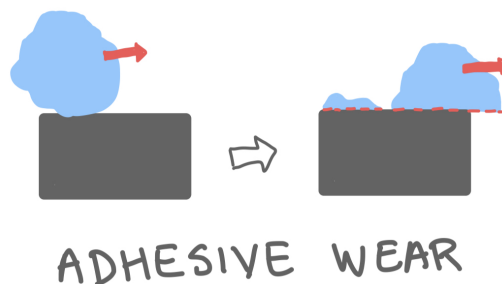


Figure 2.1.2: This illustration of adhesive wear is inspired by (Society of Tribologist and Lubrication Engineers, n.d.).

Abrasive wear happens when the two surfaces that are interacting with each other don't have the same level of hardness. This causes the harder material to remove some of the material from the surface of the softer material. Abrasive wear is illustrated in Figure (2.1.3)(Society of Tribologist and Lubrication Engineers, n.d.).

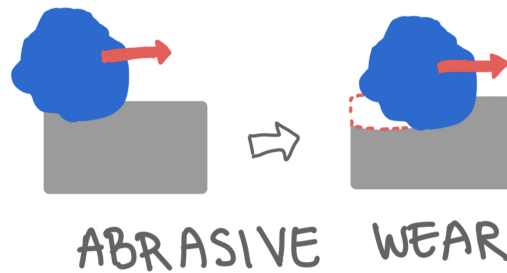


Figure 2.1.3: This illustration of adhesive wear is inspired by (Society of Tribologist and Lubrication Engineers, n.d.).

2.2 Electrochemical Corrosion

Corrosion is defined as the deterioration of materials caused by reactions with their environments (Stansbury and Buchanan, 2000, p. 1). For metallic materials in aqueous solutions, corrosion refers to the electrochemical reactions in which atoms, in the form of dissolved ions, are transferred from the metal into the solution. These reactions, in which the metal atoms lose electrons, are known as oxidation or anodic reactions. To sustain the corrosion reaction, the electrons that are left in the metal after the oxidation reactions need to be taken up by other dissolved substances in the solution. Reactions that include the consumption of electrons are known as reduction or cathodic reactions. In aqueous solutions the reduction of hydrogen ions and/or dissolved oxygen molecules are the most common cathodic reactions, and these reactions occur on the surface of the corroding metal (Igal et al., 2020, p. 8). The corrosion process of iron is illustrated in Figure 2.2.1.

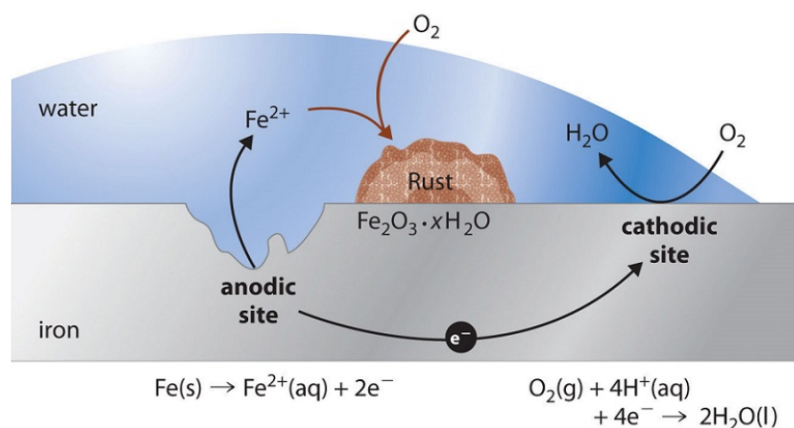


Figure 2.2.1: Corrosion process of iron. The metal ions at the anodic site dissolve and the electrons migrate to the cathodic site, where they are taken up by a depolarizer (Lower, n.d.).

When a critical concentration of metal ions in the solution is reached, solid corrosion products, such as hydroxides, oxides or sulfides, may form. In cases where these solid products does not adhere to the metal surface, the continual removal of metal ions from the solution, as well as the compensating transfer of ions from the metal to the solution, causes the corrosion-rate to be high. In other cases, the solid products adhere to the metal surface and form passive films (passivation) that slow down the diffusion of metal ions into the solution, and thus reducing the corrosion rate (Stansbury and Buchanan, 2000, p. 18-19).

Corrosion processes can be studied using several different electrochemical techniques, which involves applying and measuring currents and electrode potential (ETH Corrosion, 2021). A three-electrode setup, which includes a working electrode (WE), a reference electrode (RE) and a counter electrode (CE), is utilized for most electrochemical tests. The corroding material of interest is the WE. The RE provides a stable electrode potential, which works as a reference point for other potential measurements. A silver-silver chloride (Ag/AgCl) electrode is one of the most commonly used REs. The CE induces the corrosion reactions by providing a current to the WE. Platinum or gold, in the form of a mesh or a wire, are among the most commonly used CEs (Kutz, 2012, p. 51-52).

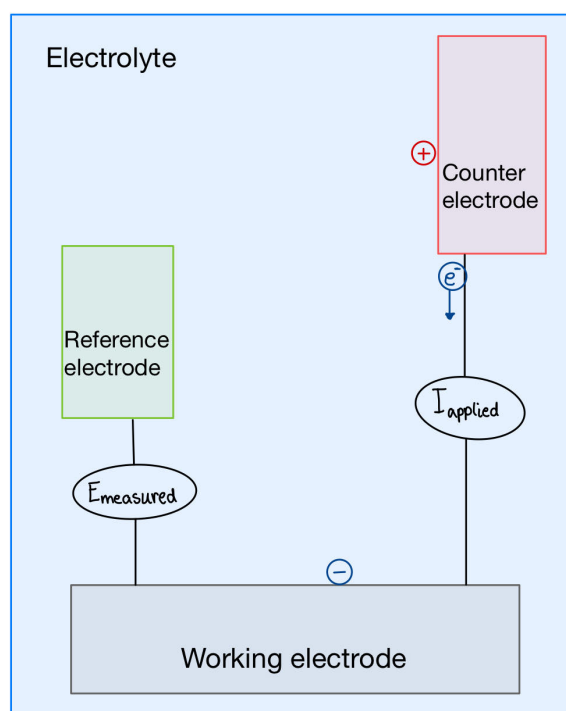


Figure 2.2.2: In a three electrode setup, the counter electrode can be seen as a source of electrons for the reactions that are happening on the working electrode (ETH Corrosion, 2021).

2.3 Tribocorrosion

Tribocorrosion is the degradation caused by the combination of wear and corrosion. Wear comes from the mechanical contact where two surfaces are sliding against each other and corrosion comes from the deterioration of materials caused by their reaction with their environments. The results of the combination of these two can differ compared to if they happened separately.

There are different types of interaction between wear and corrosion:

2.3.1 Effect of Corrosion on Wear

If one or more of the metal components are subject to localized corrosion or selective dissolution, it can lead to mechanical weakening of the material. One example of how corrosion can affect wear is selective corrosion of grain boundaries in the materials, which can contribute to wear as the cohesion of the grains at the surfaces are weakened. Another example is the formation of pits, that are caused by chloride attacks in seawater, and can

behave as initiation sites for cracks, and thus affect the fatigue wear of the material. The oxide films in passive metals are also thought to have a big impact on the metals' surface mechanical response (Igal et al., 2020, p. 36-37).

2.3.2 Effect of Wear on Corrosion

Passive metals tend to corrode faster when wear occurs simultaneously. The abrasive wear removes the passive film that coats the metal (depassivation) and the regrowth of this passive layer (repassivation) takes time. Under the depassivation, when parts of the passive layer that coats the metal is either gone or damaged, corrosion will happen at a much faster rate than normally (Igal et al., 2020, p. 37).

Active materials has a minimal change in corrosion rate while being simultaneously subjected to wear, compared to the passive materials (Igal et al., 2020, p. 37).

2.3.3 The Impact of Third Bodies

When wear occurs, part of the material detaches from the surfaces due to adhesion, abrasion or depassivation and this causes a change in the contact conditions. There is a sliding contact between the test piece (the first body) and the friction ball (the second body), but when the metal particles detaches from the surface of the test piece, they will act as a third body in the sliding contact. This is due to the third bodies (the detached metal particles) being trapped between the other two bodies (Igal et al., 2020, p. 38).

These third body particles might get dissolved in the electrolyte. The metal particles might then get oxidized and become metal ions or metal oxides. The third body particles might also have already oxidized by the time it detaches from the test piece. The metal ions or the metal oxides is then dissolved in the electrolyte (Igal et al., 2020, p. 38).

The metal particles can also adhere back to the first or the second body by smearing, creating a transfer film. Smearing causes the surface of the body that the metal particles adhered to, to become rougher, thus causing increased friction and wear (Igal et al., 2020, p. 38).

2.4 Four-Point Bending

Four-point bending is a flexural strength test. Flexural strength is a materials ability to resist bending deflection when it is exposed to applied loads. When the test piece is exposed to applied loads it will bend. Across the depth of the test piece there are different amounts of stress. The stress is at its maximum compressive value on the concave surface of the test piece, and the stress is at its maximum tensile value on the convex surface. This is illustrated in Figure 2.4.1. Normally materials fail because of tensile stress before they fail because of compressive stress (University of Pennsylvania, n.d.).

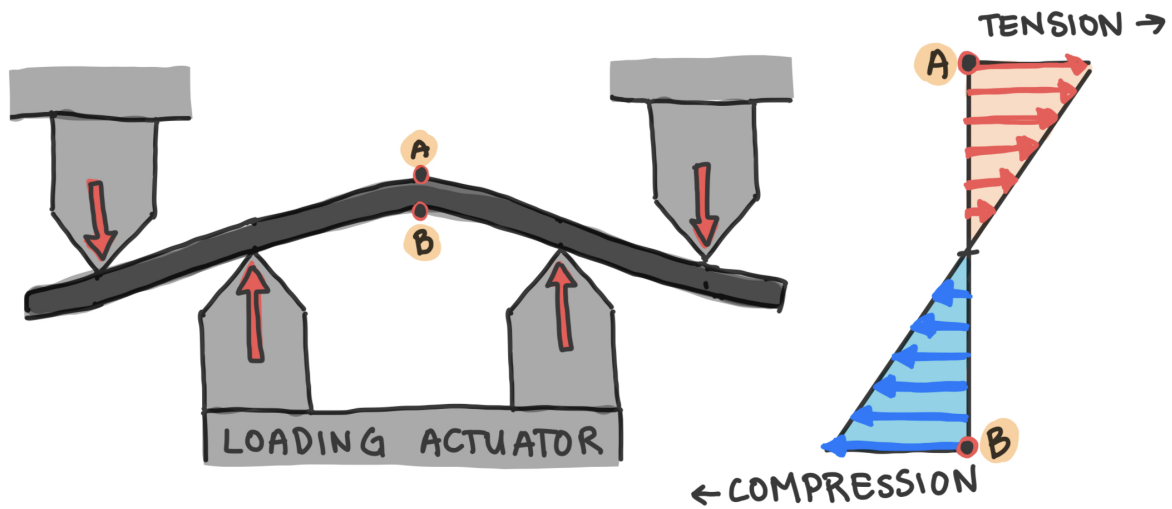


Figure 2.4.1: Four-point bending illustration, with a stress diagram where A shows the highest compressive stress and B shows the highest tensile stress. This illustration is inspired by (University of Pennsylvania, n.d.).

2.4.1 Equations Surrounding Four-Point Bending

Newton's first law of motion states that "An object at rest remains at rest, and an object in motion remains in motion at constant speed and in a straight line unless acted on by an unbalanced force." (NASA, n.d.) Meaning that if the object is at rest there is either no forces working on the object or the sum of the forces that are working on the object is equal to zero. In a four-point bending test the test piece is at rest meaning that the sum of the forces working on the test piece are equal to zero.

$$\Sigma F_y = 0 \quad (2.4.1)$$

Since the forces that are working on the test piece is balanced the test piece is in static equilibrium (Tennessee Tech University, n.d.).

In the following equations, some of the parameters are illustrated in Figure (2.4.2), where L is the length between the two support beams, a is the length between the support beam and the load applicator, h is the thickness of the test piece and b is the width of the test piece.

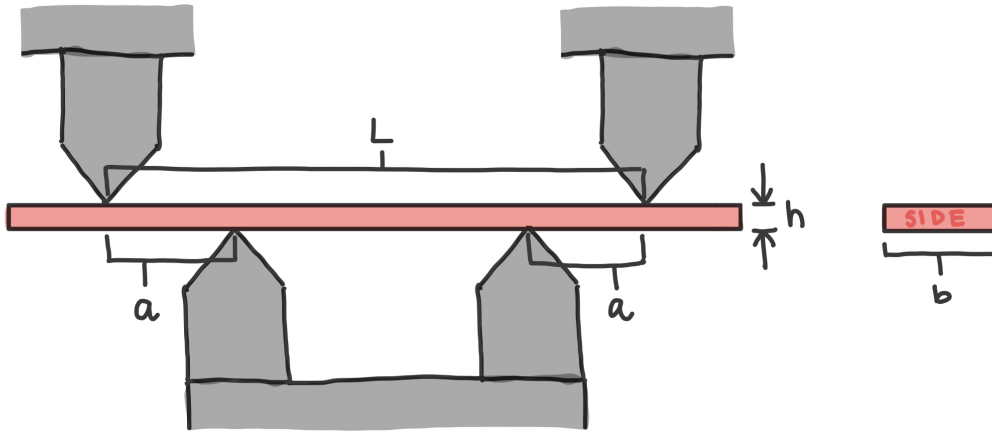


Figure 2.4.2: Illustration showing paramet L , a , b and h on the test piece.

When given the maximum stress of the test piece, the size of the fatigue load can be calculated. The formula for bending stress is: $\sigma = \frac{M \times y}{I}$, where M is the moment, y is the distance to the neutral axis and I is the moment of inertia (Boston University, n.d.). If the formula is given considering the maximum stress and it ends up being:

$$\sigma_{max} = \frac{M_{max} \times \frac{h}{2}}{I_z} \quad (2.4.2)$$

Where M_{max} is the maximum moment of the test piece and the distance to the neutral axis is given by $\frac{h}{2}$. The reason for this is because, as mentioned earlier, the highest level of stress on the test piece is at the top and bottom surface of the test piece. The neutral axis of the test piece is the x -axis that cuts through the middle of the beam, so the perpendicular distance between the surface of the test piece to the neutral axis is half of the height of the test piece. I_z is the moment of inertia around the z -axis.

$$I_z = \frac{b \times h^3}{12} \quad (2.4.3)$$

This formula is found in (Johannessen, 2018, p. 63).

To find the deflection of the test piece in a four-point bending test the given formula, found in (ASTM International, 2013, p. 6), can be used:

$$\delta = \frac{F \times a \times (3 \times L^2 - 4 \times a^2)}{4 \times b \times h^3 \times E_b} \quad (2.4.4)$$

2.5 S-beam Load Cell

Load cells are force transducers that convert mechanical force into a readable output signal, most commonly electrical, pneumatic or hydraulic pressure (Zemic Europe, 2024). There are many types of load cells, where each is designed to measure different sizes and types of forces. The S-beam load cell is optimal for measuring tension and compression loads (Flintec, 2024).

The S-beam load cell gets its name due to their "s" shape (Figure 2.5.1). The central beam holds the strain gauge, and the arms with the mounting holes curving outwards. When the load cell experiences a compressive or tensile force it will deform slightly, and the strain gauges bonded to the beam will follow, thus altering the shape of the strain gauges and its electrical conductivity and resistance (RS, 2023). The force is measured by sending a voltage or current through the sensor. The output signal is proportional to the applied load (Flintec, 2024).

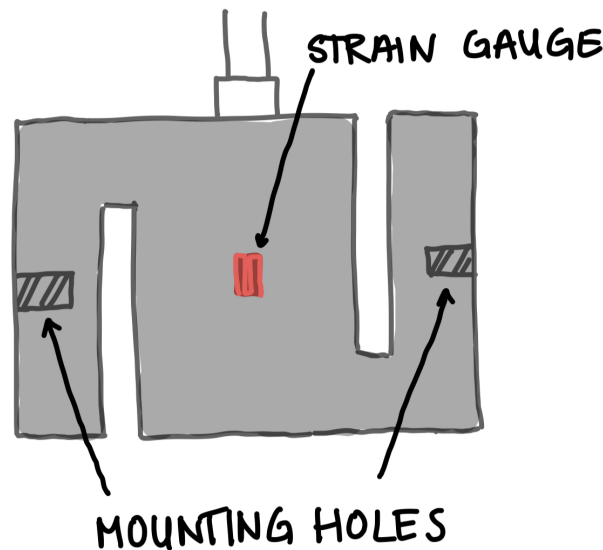


Figure 2.5.1: Simplified diagram of an s-beam load cell.

2.6 Motors

2.6.1 Brushless DC Motor

A BLDC motor, short for brushless direct current motor, is an electrical component that converts electrical energy into a mechanical force. Inside the motor are two main parts, the rotor and stator (Figure 2.6.1). In essence, the rotors, made of permanent magnets, rotates when the stators coils are energized. There are two configurations, the outer and inner rotor. The outer rotor will be used to explain the workings of the BLDC motor. When a current is sent through the coils of the stator it will create a magnetic field, turning them into an electromagnet (Lesics, 2014). The polarity of the coil is determined by the direction of the current (Figure 2.6.2). A stator coil is energized so that the polarity of the coil attracts the permanent magnet on the rotor. Simultaneously, the stator coil behind the rotor's magnet is energized so the polarity is identical to the permanent magnet to aid the rotation (Figure 2.6.3). This increases the motor's torque and power output.

The coils have to be energized at the precise moment to contain a smooth rotation and effectively use energy. In a brushed DC motor the commutation, which is a process of changing the electrical currents direction, is controlled mechanically by the brushes and the commutator. A BLDC motor uses electronic commutation. Sensors inside the motor, typically Hall effect sensors, detect the positioning of the rotor and send a signal to the connected motor controller. With the help of transistor switches the motor controller can timely energize the correct coils (Zhoa and Yu, 2011).

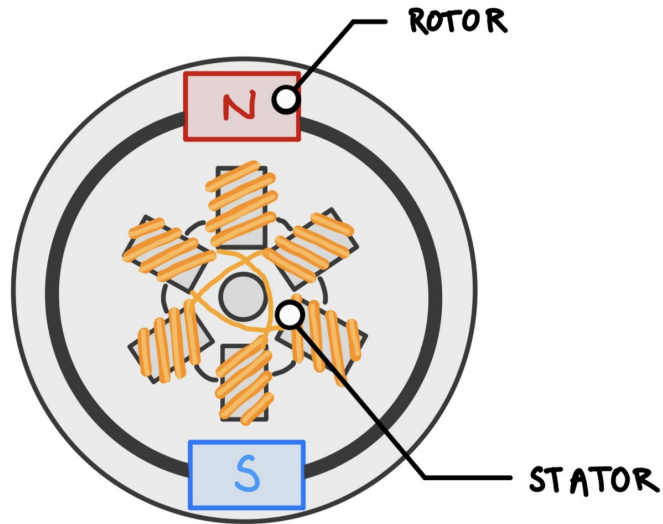


Figure 2.6.1: Simplified diagram of an outer rotor BLDC motor.

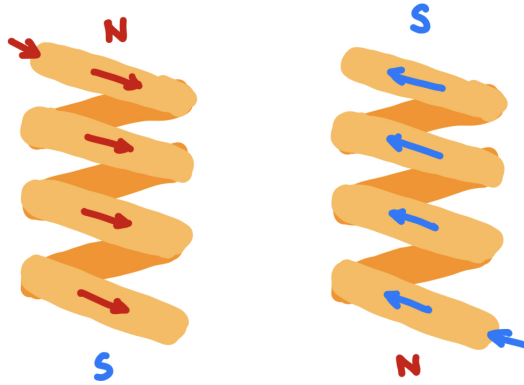


Figure 2.6.2: Polarity of a coil determined by current direction.

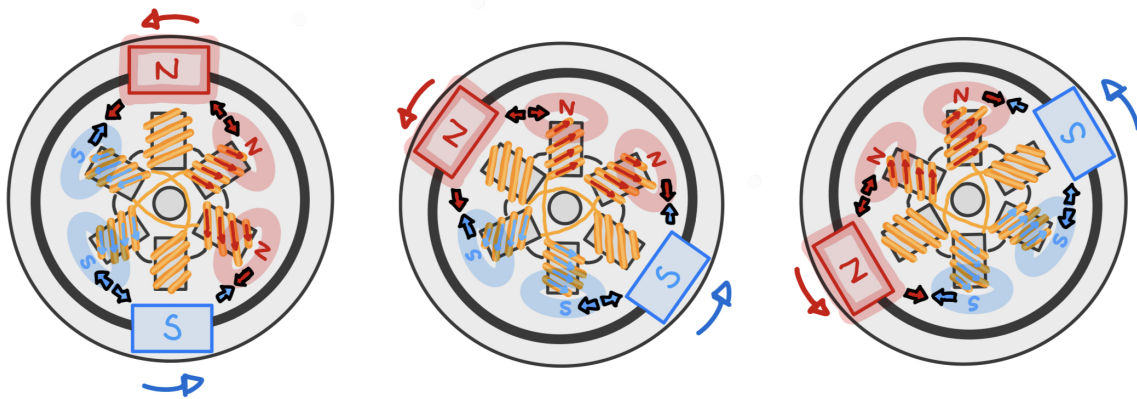
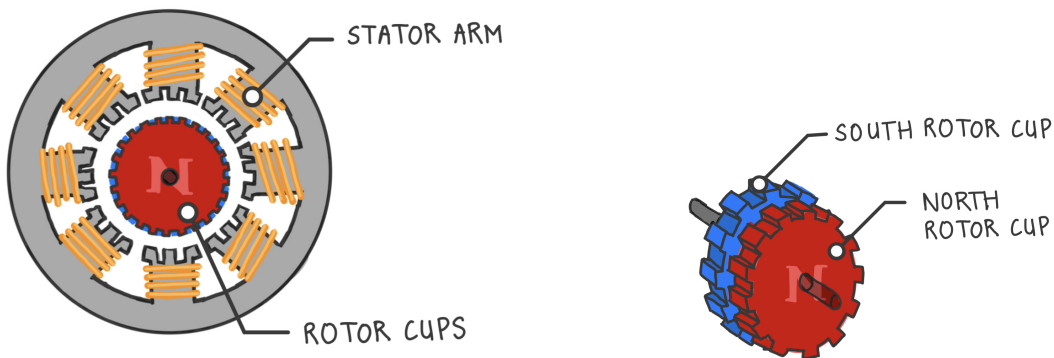


Figure 2.6.3: Rotation of the BLDC motors rotor by the electromagnetized stator coils.

The brushes and commutator in a regular DC motor wear over time due to friction, and demands regular replacements. Sparking and heat is also a concern with brushed DC motors. Removing the brushes avoids these issues, while also reducing noise and increasing the motors longevity (RS, 2023).

2.6.2 Stepper Motor

Similarly to a BLDC motor, the stepper motor is brushless and utilizes electromagnetism to rotate. However, unlike a DC motor that can only rotate continuously, the stepper motor is characterized by its ability to take short angled rotations, also called "steps". The most commonly used is the hybrid stepper motor, which uses both permanent magnets and variable reluctance. The rotor of a hybrid stepper motor is made of two permanent magnet cups, that typically have 50 teeth each (Figure 2.6.4b). Hybrid stepper motors have stationary stators with multiple pares of electromagnetic coils (Figure 2.6.4a). Each stator arm also have teeth that in total exceed the number of teeth of the rotor cups. The amount of teeth determine the smallest angle that the stepper motor can turn. The difference in teeth increases the amount of steps, smoothens torque ripple and reduces step loss (Faulhaber, n.d.).



(a) Simple diagram of a hybrid stepper motor (b) Hybrid stepper motors rotor cups

Figure 2.6.4: Simple drawings of the main parts of a hybrid stepper motor.

A stepper motor does not need a feedback sensor or encoder to monitor the positioning of the rotor. It is connected to a motor driver that contains the switches placed in H-bridges. The switches are electronic and precisely turned off and on through code on a controller (The Engineering Mindset, 2021).

2.7 Captive Linear Actuator

A captive linear actuator converts rotational motion into linear motion. Its main components consist of a threaded rod which is turned by a spline connected to the motor. Additionally, the actuator is integrated with an anti-rotation mechanism that prevents the actuator rod from rotating, making it captive. This makes the movement purely translational (Solutions, 2019).

2.8 Materials

2.8.1 Silicone Rubber

Silicone rubber is a material that offers many advantages and can be used for a lot of different applications. One very important advantage is that silicone rubber is very flexible. It has high elasticity, which allows the material to keep its shape and functionality even when exposed to repeated stress like compression, stretching and bending. The flexibility also allows for moulding of complex shapes. Other advantages of silicone rubber is the good electrical insulation properties and the ability to resist the effects of moisture. All of these properties makes silicone rubber an excellent material for several applications, including seals (SRM Industries, 2023).

2.8.2 PEEK

Polyetheretherketone (PEEK) is a polymer that is often used in engineering. The material has a very good strength-to-wear ratio, and it is resistant to wear, abrasion and fatigue (IMETRA, n.d.). PEEK can withstand high temperatures without losing its high strength, and it also has corrosion resistance, which means it can resist corrosive effects of surrounding media (WAYKEN Rapid Manufacturing, 2022).

2.8.3 PLA

Polylactic Acid (PLA) is one of the most common plastics used in desktop 3D-printing. The material is made from resources that are natural and renewable, making it one of the more sustainable and eco-friendly filament options for 3D-printers. PLA is a semi-crystalline polymer and the melting point is between 170-180°C. Even though PLA has disadvantages like being fragile and sensitive to high temperatures and sunlight, the accessibility and ease of use makes it a great material for prototyping (Carlota, 2023).

2.8.4 Steel

Steel, an iron alloy, is the most used material globally. It is used in a variety of constructions and appliances. It is used to make cars, buildings, construction equipment, surgical scalpels, washing machines, et cetera (Worldsteel Organisation, 2024). Pure iron is ductile, therefore carbon, and in other instances nickel or manganese, is added in small amounts to harden and strengthen the material. The carbon content in steel ranges up to two percent. An iron alloy with a higher carbon content is considered cast iron. Steel has exceptional mechanical properties, low cost of forming and processing, and there is an abundance of its raw material (Wente et al., 2023).

In the last decades the steel industry has made an effort to reduce their environmental impact. Newer lightweight steels save energy and resources. On top of that, steels magnetic property makes easy recovery of scrap and can be recycled infinitely without any reduction of the materials quality (Worldsteel Organisation, 2024). Stainless steel 316L

(SS316L) is a favoured material for constructing various offshore and marine applications. SS316L offers high corrosion resistance and good weldability (Ajay et al., 2019, p. 658). The density of SS316L is 8000 kg/m^3 (Yakout et al., 2019, p. 403).

2.9 Equations Needed for Calculating the Dimensions of the Dead Weight

From Newton's Second Law of Motion "The acceleration of an object depends on the mass of the object and the amount of force applied." (NASA, n.d.) The following formula, taken from (Johannessen, 2018, p. 23), is given to show this:

$$F = m \times a \tag{2.9.1}$$

To calculate the volume of a cylinder, the following formula, taken from (Johannessen, 2018, p. 19) can be used:

$$V = \pi \times r^2 \times h \tag{2.9.2}$$

3 Digitalisation and Sustainability

3.1 Digitalisation

Digitalisation involves using technology to improve, simplify and renew the way things are done. Automation and robotisation, as well as artificial intelligence (AI) are some of the digital solutions that have transformed society. Another example is Internet of Things (IoT), which makes it possible to connect physical and digital systems. This is done with sensors that are placed in the physical system and sends data to the digital system (SINTEF, n.d.).

3.2 Sustainability

Sustainability means utilizing the world's resources in a way that meets the needs of today's generation, without compromising future generations ability to meet their needs (United Nations, n.d.-b). The United Nations (UN) has a list of 17 Sustainable Development Goals (SDGs) proposed to improve health and education and reduce inequality, while also trying to prevent further climate change and preserve the world's resources (United Nations, n.d.-a). According to the United Nations Development Programme (UNDP) the number of people using electricity increased from 78 to 90 percent between 2000 and 2018, and the number will continue to increase as the world's population grows. To minimize further climate change caused by fossil fuels as the demand for energy increases, one of the goal targets of SDG 7 is to substantially increase the share of energy coming from renewable sources (United Nations Development Programme, n.d.).

In chapter 17.2 of the book *Sustainable Engineering: Principles and Practice* , the author writes about eco-efficiency which is about "creating more value with less impact" (Bakshi, 2019). Eco-efficiency covers a lot of the requirements for sustainability, including the environmental aspect and the life cycle impact. There are three main objectives businesses should follow in order to improve their eco-efficiency. These three objectives are listed in table 3.2.1.

Table 3.2.1: Objectives to improve eco-efficiency (Bakshi, 2019).

Objective	Description
Reduce the use of resources	The goal is to reduce the amount of resources, e.g. materials and energy, that is being used. This can be done by improving the recyclability of the materials and by closing the material loops.
Reduce the impact on the environment	The goal is to reduce the amount of pollutants that are emitted, and to reduce the pollutants impact.
Increase the value of the product or service	The goal is to improve the functionality and flexibility of the product, and with that provide more benefits to costumers.

3.3 How can Tribometers Contribute to Digitalisation and Sustainability?

With the use of tribometers, the behaviour of materials can be studied under different conditions, and the use of sensors is helpful to gather data during the tests. The knowledge gained from the research can be very useful and it can help engineers chose the best suited materials for their projects. This means that the products can operate longer before needing to be repaired or replaced, which will reduce the consumption of materials.

The tribometer in this project is designed to work under corrosive, wear/friction and fatigue conditions. These are conditions that the offshore renewable energy sector has to take into consideration when designing their products. A tribometer that can perform tests with these conditions will therefore be beneficial in the further development within the offshore renewable energy sector. By developing this energy sector, the availability of renewable energy increases, something that could potentially mean that the need for non-renewable energy decreases. This will help reach SDG 7.

4 Methodology

Product development comprises all the stages that are involved in a products journey from concept or idea to market release. There are several different methodologies and processes that can be used in product development, but the most common stages in the process includes identifying a problem or a need, creating a concept, validating the concept and making a prototype, and testing and making changes (ProductPlan, n.d.). Some of the methodologies that are often used for product development are the engineering design process, the agile methodology and the design thinking process.

4.1 Design Thinking

For working on this project the group decided to follow the design thinking process. This process is non-linear and iterative, which means that even though it consists of different stages, more than one stage may be conducted at the same time (Dam, 2024).

The first stage of the design thinking process is to research the users needs. This involves empathizing with the intended user and gathering information about what they want and need from the product(Dam, 2024). Through the project description and the information provided by the supervisors, the group was able to develop a good understanding of what their needs and wishes for the tribometer were.

The second stage is the definition stage, where the problem needs to be defined based on the information that was gathered in the first stage (Dam, 2024). By going through and organizing the information that was given, the group was able to define the specific problem that needed to be solved with this project.

In the next stage of the design thinking process, the goal is to come up with ideas and solutions to the defined problem. This can be done through techniques like brainstorming, brainwriting and Worst Possible Idea (Dam, 2024). For this project, the group chose to use brainstorming. Everyone shared their different ideas, and at the end of the brainstorming session they were all discussed and the best ideas were chosen to move forward with.

Under the process of brainstorming and sketching ideas, the group found great help in course material from previous subjects like MAST2008 *Produksjonsteknikk(Manufacturing Technology)* and MAST2001 *Maskindeler 1(Maskin Elements 1)*. Knowledge about threads, screws, bearings, coupling, machining, manufacturing and technical drawings helped with conceptualizing the designs.

Stage four involves developing the ideas further, creating prototypes and finding the best possible solution for the problems (Dam, 2024). The design ideas from the brainstorming session were developed into a prototype of the tribometer, and a 3D model was made using Fusion 360. The design was then presented to the supervisors and feedback was given. Based on this feedback, changes were made in order to improve the design.

The fifth stage is to test and try out the solutions and prototypes. Even though this is the final stage in the five-stage model, the results from the testing often lead to going back to a previous stage. This is what makes the design thinking process iterative. By moving back and forth between the steps, the solution can be developed even further and a final product can become even better (Dam, 2024). One of the biggest challenges with this project was finding a way to make sure the electrochemical cell was sealed. The seal was tested and redesigned multiple times in order to try to make the best possible solution.

5 Design and Build up

5.1 Inspiration

The tribometer designed in this project was inspired by the tribometers already in use in the tribology laboratory at NTNU for some of its parts. One of these tribometers uses a similar design for the friction mechanism, as shown in Figure 5.1.1. The design for the ball holder and the dead weight is also highly inspired by another tribometer that was made by a previous Bachelor group.



Figure 5.1.1: The tribometer that inspired the friction mechanism.

5.2 The Test Piece

Early on it was decided to go with four-point bending over three-point bending to apply the fatigue on the test piece. The reason for this was that with four-point bending the deflection of the test piece is more evenly spread out between the two points of applied load, while in a three-point bending test the deflection is very high in the middle as this is the only point of applied load. This means that in a four-point bending test the middle of the test piece is flatter than in a three-point bending test. The reason this is important is because it will be easier to perform the friction test and design the compartment containing the electrochemical cell on a flatter test piece.

To figure out the optimal size of the test piece, all the forces that were going to work on the test piece had to be taken into consideration. When doing this the normal load given from the friction ball is not taken into consideration. This is done after discussions with the supervisor of this project where it was decided that since the normal load given from the friction ball will vary considerably from test to test, it was not seen as appropriate to take it into consideration when designing the size of the test piece. The highest normal load for the tribotest that will be used on this tribometer is 50N.



Figure 5.2.1: Free body diagram that shows the forces working on the test piece, with the exception of the force from the normal load given from the friction ball.

In the free body diagram, Figure 5.2.1, it is shown that the applied force is $F/2$. The reason for this is that the load applicator is designed with two points connected to the same arm and the same motor. Since F is the force given from the motor to the arm, the force splits between the two points. The support beams will also have a force that is working on the test piece with the same magnitude as the applied force is working on the test piece. This is because the test piece is in static equilibrium as explained in Equation 2.4.1, $\sum F_y = 0$.

5.2.1 Finding the Max Moment

To find the max moment the sections between the loads are analysed.

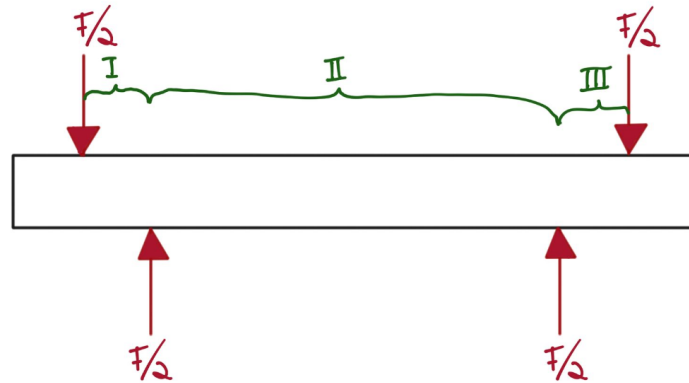


Figure 5.2.2: Illustration that shows the three sections of the test piece that gets analysed.

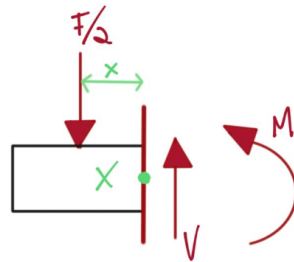


Figure 5.2.3: Cut in section 1.

The moment and the shear force is added to make sure that the section of the test piece stays in static equilibrium. The direction that the moment and the shear force is drawn in are here defined as the positive direction. From section 1:

$$\Sigma F_y = 0 \rightarrow -\frac{F}{2} + V = 0$$

$$V(x) = \frac{F}{2}$$

$$\Sigma M_{cut} = 0 \rightarrow \frac{F}{2} \times x + M = 0$$

$$M(x) = -\frac{F}{2} \times x$$

This means that in the first section of the test piece there is a constant shear force equal to $\frac{F}{2}$. There is also a moment in this section. Right were the force from the support beam works on the test piece the moment is 0 and where the test piece is cut the moment is equal to $-\frac{F}{2} \times x$. The change in moment through the section decreases linearly.

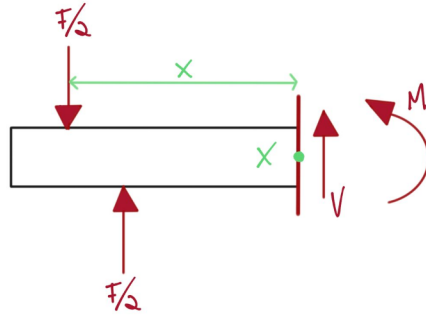


Figure 5.2.4: Cut in section 2.

From section 2:

$$\Sigma F_y = 0 \rightarrow -\frac{F}{2} + \frac{F}{2} + V = 0$$

$$V(x) = 0$$

$$\Sigma M_{cut} = 0 \rightarrow \frac{F}{2} \times x - \frac{F}{2} \times (x - a) + M = 0$$

$$M(x) = -\frac{F}{2} \times a$$

This means that in the second section of the test piece there is no shear force, but there is a moment. The moment is the same throughout section 2 and it is equal to $-\frac{F}{2} \times a$.

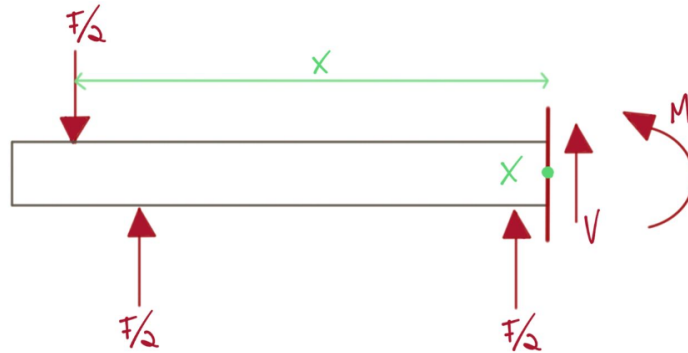


Figure 5.2.5: Cut in section 3.

From section 3:

$$\Sigma F_y = 0 \rightarrow -\frac{F}{2} + \frac{F}{2} + \frac{F}{2} + V = 0$$

$$V(x) = -\frac{F}{2}$$

$$\Sigma M_{cut} = 0 \rightarrow \frac{F}{2} \times x - \frac{F}{2} \times (x - a) - \frac{F}{2} \times (x - a - (L - 2a)) + M = 0$$

$$M(x) = -\frac{F}{2} \times x + \frac{F}{2} \times L$$

This means that in the third section of the test piece, there is a constant shear force equal to $-\frac{F}{2}$. There is also a moment in this section. Right were the force from the support beam that is the closest to the cut works on the test piece the moment is equal to $-\frac{F}{2} \times a$ and where the test piece is cut the moment is equal to $-\frac{F}{2} \times x + \frac{F}{2} \times L$. The change in moment through the section increases linearly.

The shear force diagram and the moment diagram can then be drawn:

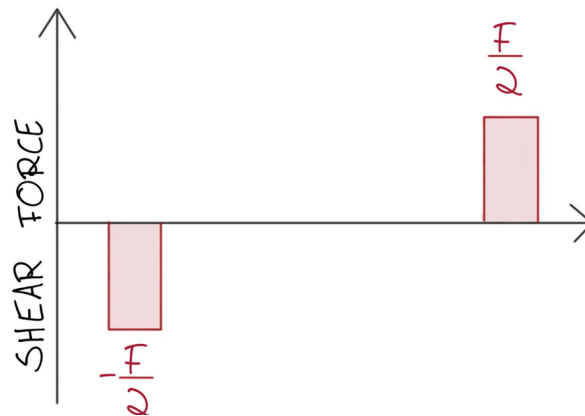


Figure 5.2.6: Shear force diagram.

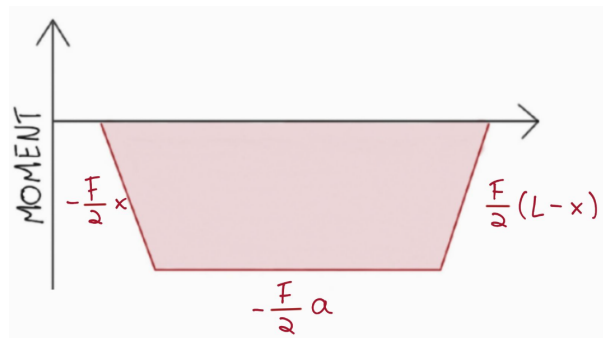


Figure 5.2.7: Moment diagram.

5.2.2 Size of the Test Piece

Originally, it was decided to take inspiration from the ASTM E855-08 Standard Test Methods for Bend Testing of Metallic Flat Materials for Spring Applications Involving Static Loading. (ASTM International, 2013) This standard states, among other things, that the length of a equals a sixth of the length of L. With this in mind, the length of the test piece was set to 81 mm, and therefore a was set to 13.5 mm. In this design b was set to 15 mm and h was 2.5 mm.

Originally, the project was only focused around SS316L. For these measurements, the force came out to 574 N and the deflection was 0.812 mm. These calculations were performed with a yield strength of 310 MPa. This is a different yield strength that what is given in Table 5.2.1 for the same material. This is because SS316L has a yield strength that ranges in value between 170 MPa to 310 MPa.

The reason for using the highest value of yield strength for the material was that the group knew that there was a possibility of the tribometer performing tests on different materials and not just SS316L. By calculating around the highest value of yield strength for the material, the tribometer would be able to perform tests on a bigger selection of materials than if it was designed around a lower yield strength.

After redesigning the load application and how the tribometer would be able to perform the fatigue in both directions, the length between the support beam and the applied fatigue load became adjustable (see Subsubsection 5.7.4).

After discussions with the supervisors it was decided that the size of the test piece should be the same for the two groups working on this project. The reasoning for this was that the laboratory will only need to order one size that would work on both tribometers. The following are the sizes that were agreed upon:

Total length of the test piece = 100 mm

$L = 90$ mm

$a = 30$ mm

$h = 2.5$ mm

$b = 15$ mm

These parameters are also illustrated in Figure (5.2.8):

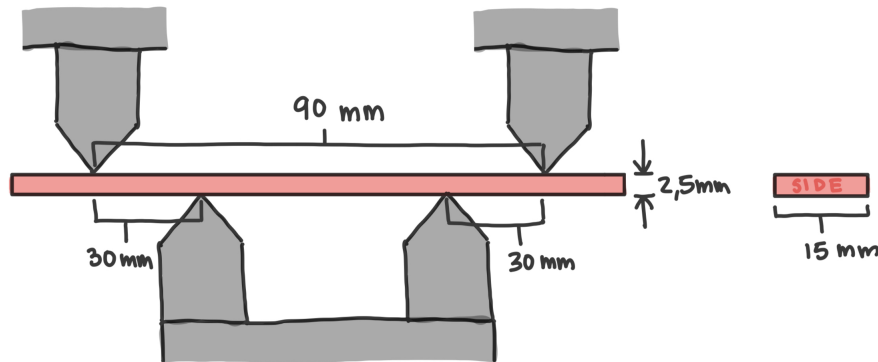


Figure 5.2.8: Illustration showing the agreed upon sizes of the test piece.

Because of the compartment for the electrochemical cell being 38 mm (See Subsubsection 5.6.5), as well as needing a bit of clearance between the compartment and the fatigue load applicators/support beams, it was not possible to get an a of 30 mm. It was then decided that the two tribometers would have different a values as the sizes that was deemed most important to have the same were the width, the height and the length so that the test pieces could be ordered in the same size.

Because the test piece holder is going 10mm into the test piece (see Subsubsection 5.4.9), and the need for clearance between the test piece holder and the fatigue load applicator/the support beams, the total length of the test piece had to be 30 mm longer than the length of L . This means that the test piece had to be 15 mm longer than L on each side. The test piece holder takes up 10 mm, the clearance between the test piece holder and the fatigue load applicator/the support beams takes up 2.5 mm, and the distance created by the load applicator and the support beams being rounded off is another 2.5 mm (See Subsubsection 5.7.4).

The final sizes of the test piece was then decided as:

Total length of the test piece = 120 mm

$L = 90$ mm

$a = 20$ mm

$h = 2.5$ mm

$b = 15$ mm

This is also illustrated in Figure (5.2.9):

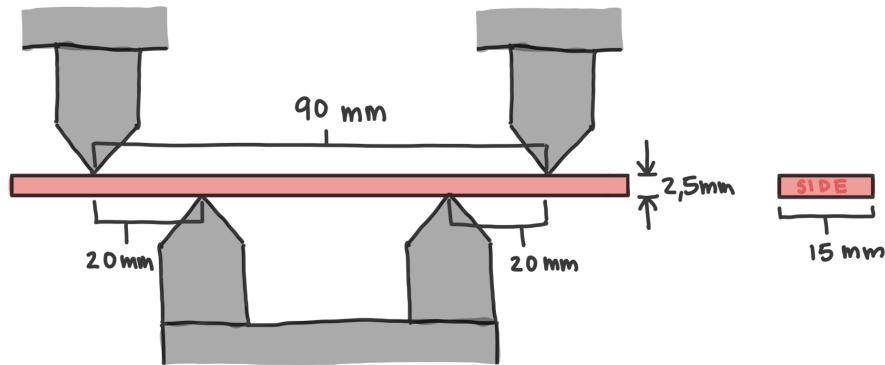


Figure 5.2.9: Illustration showing the finale sizes of the test piece.

5.2.3 Overview of Materials and Their Mechanical Properties

After the size of the test piece is determined, the force needed to reach the maximum stress can be calculated. Part of the project description for this tribometer was that the maximum stress that the material would have, had to be 90 % of the yield strength of said material.

As mentioned earlier the materials that this tribometer would mainly be testing were already given. In table 5.2.1 the different materials, their yield strength, max stress, the applied force needed to reach the max stress, the modulus of elasticity of the different materials and the max deflection that will occur in the center of the test piece with the given force, is shown. The values for yield strength and the modulus of elasticity was something that was given from the supervisors. The calculations for sigma max, the applied force and the maximum deflection can be found in Appendix A.

Table 5.2.1: Overview of materials and their mechanical properties including max stress, applied force and deflection.

Material	Yield strength (MPa)	Sigma max ($\frac{N}{mm^2}$)	F(N)	E($\frac{N}{mm^2}$)	Max deflection (mm)
SS316L	170	153	230.0625	193 000	0.5772621762
SDSS UNS S32750	550	495	773.4375	210 000	1.783571429
Mild steel	350	315	492.1875	210 000	1.135
Bearing steel	520	468	731.25	210 000	1.686285714
Inconel 625	580	522	815.625	208 000	1.898942308
Ti6Al4	880	792	1237.5	113 800	5.266080844

From this table one can see that the force needed to get to the max stress for Ti6Al4, is higher than the force that the motor can give (Subsubsection 5.7.6). In addition to this the deflection of the Ti6Al4 test piece is extremely high and it would come with extreme difficulties to design a compartment for the electrochemical cell that could handle this deflection without leaking. After discussions with the supervisor, it was therefore decided that this tribometer would not perform tests on Ti6Al4.

5.3 Optical board

The multi-degradation tribometer will be secured to an optical board (Figure 5.3.1). An optical board is a heavy platform with threaded mounting holes that the components will be stabilized and supported on. The holes are threaded to fit M6 screws and spaced out on a 25×25 mm grid.

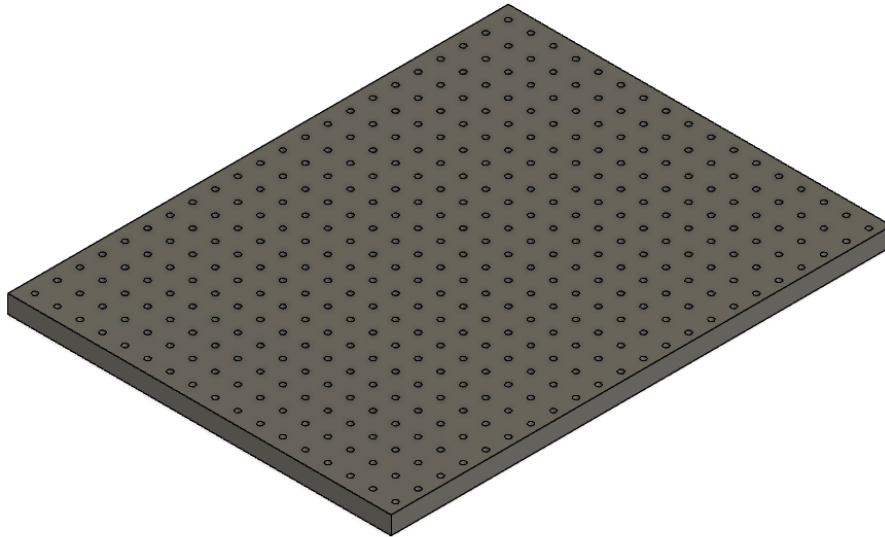


Figure 5.3.1: Optical board.

5.4 Friction Mechanism

The friction mechanism was heavily inspired by the tribometer that is located in the tribology laboratory at NTNU. The advantages of replicating the design was knowing beforehand that the mechanism will work and that the users of the tribometer will be familiar with its functionality.

Preceding the designing and modelling, there were criteria that the friction mechanism had to meet. It was known that two different sized alumina balls were to be used, and the design had to be suitable for a ball with a diameter of 6 mm and 10 mm. Later in the project a ball with a diameter of 4.76 mm was also added. Additionally, it was decided that the friction mechanism would oscillate so that the wear track from the alumina ball has a 10 mm in length.

5.4.1 Friction Mechanism - First Design

The first design (Figure 5.4.1) was an approximate, scaled down replica of the tribometer in the lab. At this stage, the project was missing a lot of parameters and designs of other tribometer parts, so many of the dimensions did not have reasoning. The initial design prioritized the wear track length and the possibility to use different ball sizes.

The tribometer in the lab utilizes a screw to apply the normal load, however in this tribometer a dead weight will be used instead. When the test piece deflects in reaction to the applied fatigue load, the mechanism with the screw will not be able to apply a constant normal load on the test piece. The screw mechanism that was fixed in horizontal direction would not be able to follow the deflection of the test piece. The dead weight, which is free in vertical direction, will be able to follow the deflection without change in the normal load.

The main body of the friction mechanism (Figure 5.4.2a) had a hole meant for a ball holder with a 10 mm alumina ball. This is where the ball holder will stand under the tribotest. If the user wishes to test with a 6 or 4.67 mm ball a cork (Figure 5.4.2b) can be placed into the main body. The main body is mounted onto two rods at four points by attachments (Figure 5.4.2c).

To achieve a wear track length of 10 mm, the motor attachment (Figure 5.4.2e) had a pin distanced 5 mm from its center. When the motor attachment moved half a rotation, the main body, connected with an arm (Figure 5.4.2d), slid 10 mm.

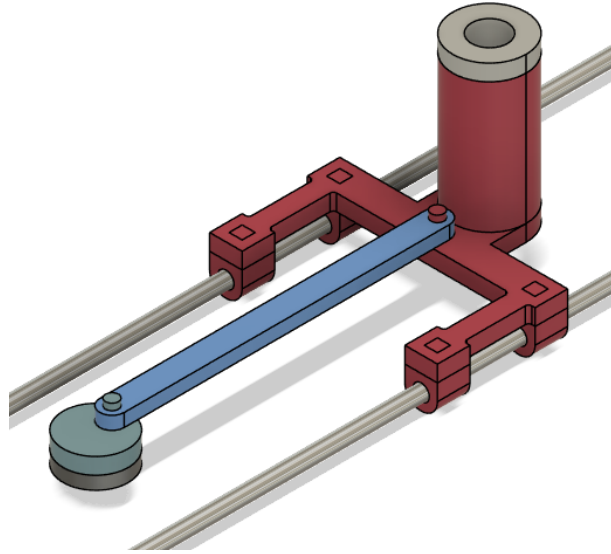
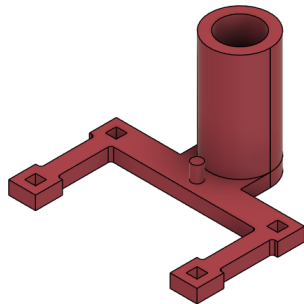
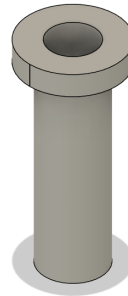


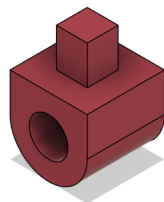
Figure 5.4.1: The first design of the friction mechanism.



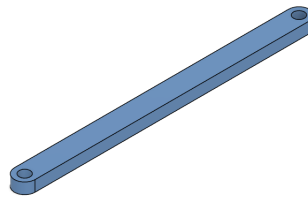
(a) First design of the main body



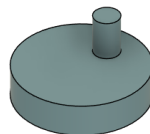
(b) First design of the cork



(c) First design of the rod attachments



(d) First design of the arm



(e) First design of the motor attachment

Figure 5.4.2: First design of friction mechanism.

5.4.2 Friction Mechanism - Second Design

There were made minimal changes to the friction mechanism in the second design (Figure 5.4.3). The hole for the ball holder was moved to the center to distribute the weight more evenly through the main body (Figure 5.4.4a). In addition, the rod attachments (Figure 5.4.4b) and the main body were modified with holes to secure the parts together by using bolts.

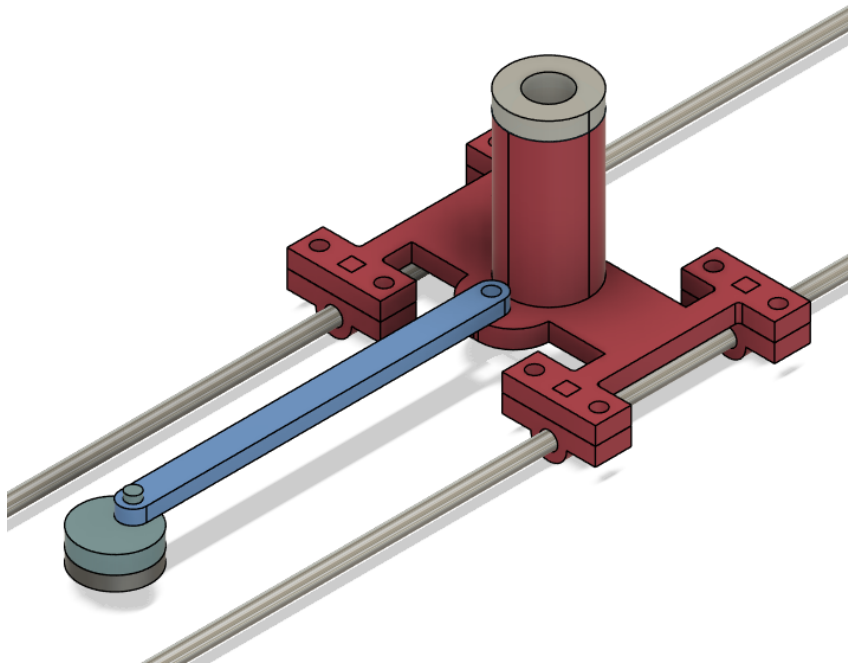


Figure 5.4.3: The second mockup of the friction mechanism.



(a) Second design of the main body

(b) Second design of the rod attachments

Figure 5.4.4: Second design of friction mechanism.

5.4.3 Friction Mechanism - Third Design

The third and final design (Figure 5.4.5) was changed and dimensioned to fit with the other parts of the tribometer. The height of the main body (Figure 5.4.6a) and cork (Figure 5.4.6b) was lowered to reduce the height of the tribometer, as there were concerns that it would become topheavy. The rod attachments (Figure 5.4.6c) were redesigned to accommodate for a thicker rod and were flattened on the top to simplify manufacturing. To have a more robust connection between the BLDC motor and the main body, the arm (Figure 5.4.6d) is widened and made thicker.

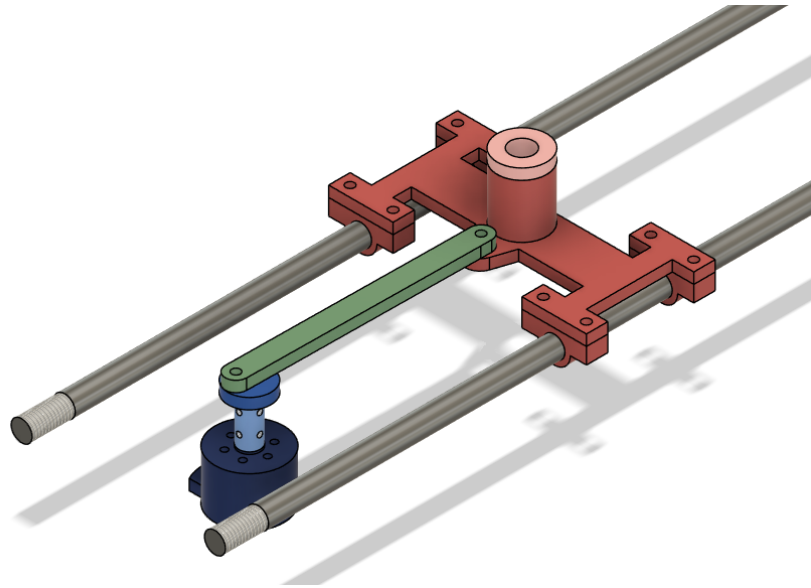
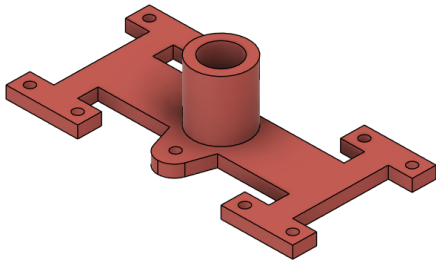
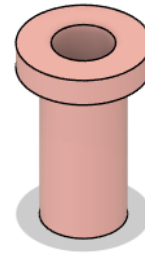


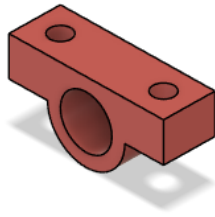
Figure 5.4.5: The third design of the friction mechanism.



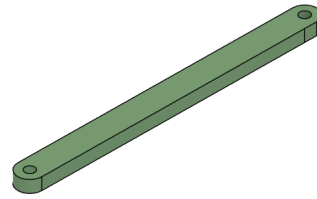
(a) Third design of the main body.



(b) Third design of the cork.



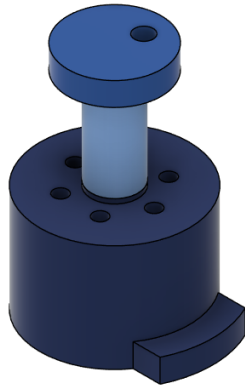
(c) Third design of the rod attachment.



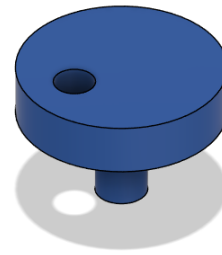
(d) Third design of the arm.

Figure 5.4.6: Third design of friction mechanism.

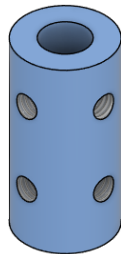
A small BLDC motor, was found to complete the design for the friction mechanism. Using the drawings from the datasheet (Figure 5.4.8), a 3D model could be made (Figure 5.4.7d). The motor attachment (Figure 5.4.7b) was connected to the motor shaft by a coupling (Figure 5.4.7c) with four threaded holes to secure it in place. Assembled, the BLDC motor and the attachments will look like (Figure 5.4.7). The motor attachment has a hole instead of a pin. The motor attachment, arm, and main body will be connected by pins.



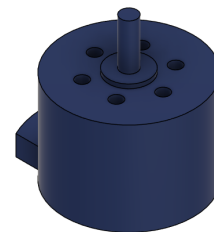
(a) Motor with assembled attachments



(b) BLDC motor attachment.



(c) BLDC motor coupling.



(d) BLDC motor for the friction mechanism.

Figure 5.4.7: Assembled motor and components.

5.4.4 The Motor for Friction Mechanism

The motor that drives the friction mechanism had to be able to withstand the frictional force. Through calculations of estimated sized for the frictional force the minimum torque that the motor has to run could be found. With these numbers, A sales representative from FAulhaber recommended The series 4221G024BXTH SC BLDC motor (Figure 5.4.8). The BLDC motor is small and has a rated torque up to 92 mN/m (Faulhaber, 2021), that was said to be suitable for this application.

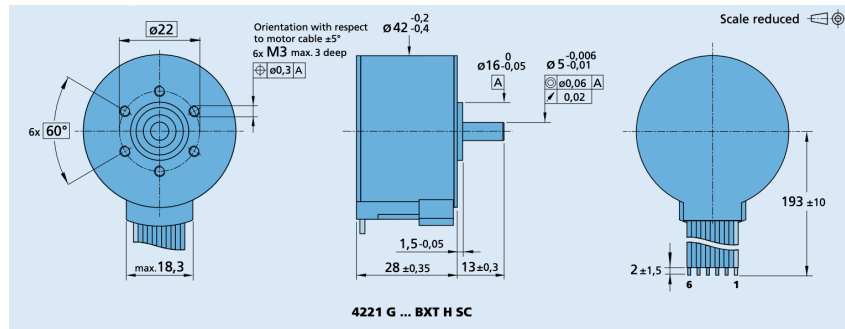
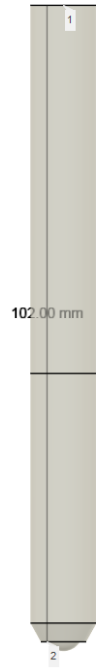


Figure 5.4.8: Dimensions of the BLDC motor for the friction mechanism from the datasheet (Faulhaber, 2021).

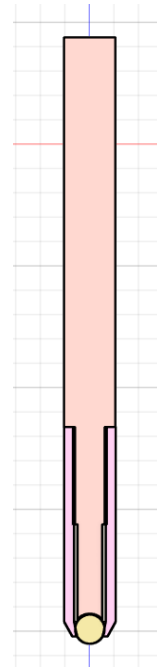
5.4.5 Ball Holder - First Design

The first ball holder design (Figure 5.4.9a) was inspired by an existing one in the tribology laboratory at NTNU. The ball holder resembled a ballpoint pen. There were three parts to the ball holder, the holder top (Figure 5.4.10a), the cap (Figure 5.4.10b) and the alumina ball. After the ball was dropped into the cap, the holder was screwed in, pushing the ball further into the tip thus securing it. During the tribotest, the ball must not roll inside of the holder. Figure 5.4.9b) show a cross section of the assembled ball holder. The cap was dimensioned so the ball protrudes 1.5 mm out of the cap tip (Figure 5.4.9c) without slipping out. The walls of the ball holder cap were set at 2 mm. To save space inside compartment for the electrochemical cell, the ball holder had to be as small as possible. If the walls were to be thinner it would make the ball holder cap fragiler.

There will be made separate ball holders to fit each alumina ball size. The design is the same but the diameter of the ball holder is adjusted to suit the 4.76 mm, 6 mm and 10 mm ball.



(a) First design of ball holder with length of 102 mm.

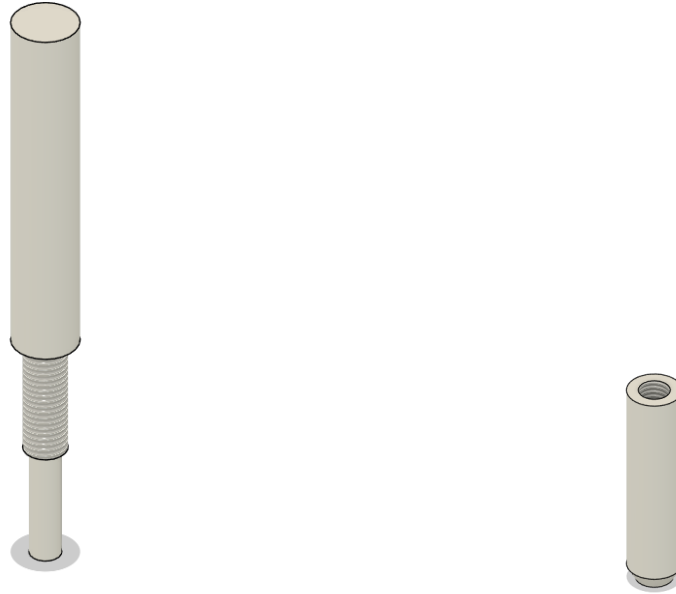


(b) Cross section of first ball holder design.



(c) Length of the alumina ball protrusion at 1.50 mm.

Figure 5.4.9: First design of the ball holder.



(a) First design of the ball holder top.

(b) First design of the ball holder cap.

Figure 5.4.10: Separated parts of the first design of the ball holder.

5.4.6 Ball Holder - Second design

The length of the second ball holder (Figure 5.4.11) was increased to 118.50 mm from 102 mm in the previous design. The ball holder was not tall enough to hold the ball holder hat. Due to the increased height of the ball holder, the pushing part of the ball holder top (Figure 5.4.12a) same with the ball holder cap (Figure 5.4.12b). This change was made to lessen the chance of breakage or buckling of the pushing part of the ball holder top.

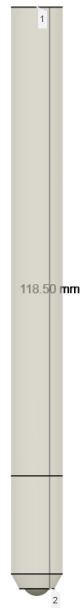


Figure 5.4.11: Second design of ball holder with a length of 118.50 mm.



(a) Second design of ball holder top.

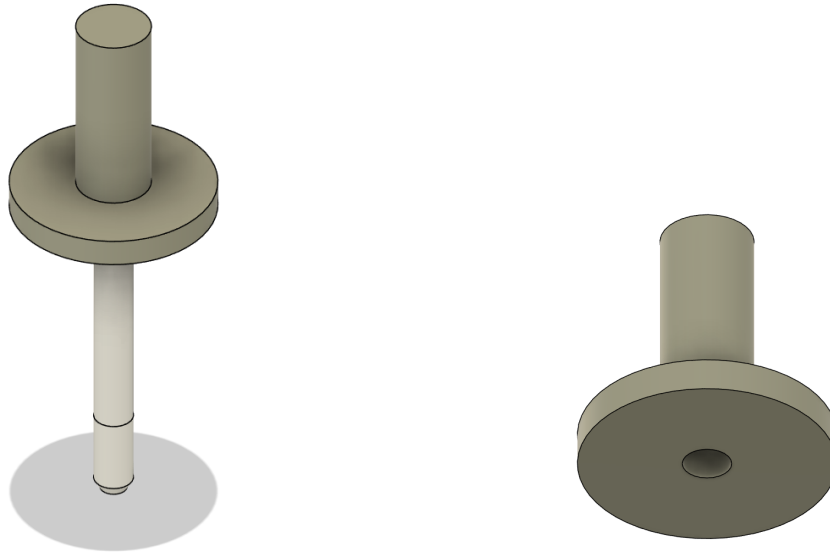


(b) Second design of ball holder cap.

Figure 5.4.12: Separated parts of the second design of the ball holder.

5.4.7 Ball Holder Hat

The ball holder hat (Figure 5.4.13a) was placed on top of the ball holder, and was made to hold the doughnut-shaped dead weight. There will be three different hats to fit each ball holder size.



(a) Ball holder with hat

(b) Ball holder hat

Figure 5.4.13: Ball holder hat on and off ball holder.

5.4.8 Dead Weight

The ball holder will apply a normal load of either 20 N or 50 N during testing. The dead weight will be made out of steel, and the shape will be cylindrical with a hole to fit the ball holder hat. This density is used to calculate the dimensions of the weight.

To find the dimensions of the dead weight the volume of the weight has to be determined. To find the volume the mass is needed. The mass is calculated by flipping formula 2.9.1, making the mass, m , the subject of the equation:

$$m = \frac{F}{a}$$

Where F is the Normal load from the dead weight, a is the gravitational acceleration and m is the mass of the dead weight.

First, the mass needed to apply the 20 N load is calculated:

$$\frac{20 \text{ N}}{9.81 \text{ m/s}^2} = 2.039 \text{ kg}$$

The volume can be found by dividing the weight in kilograms with the materials density:

$$V_{20Ndeadweight} = \frac{2.039 \text{ kg}}{8000 \text{ kg/m}^3} = 2.549 \times 10^{-4} \text{ m}^3 = 2.549 \times 10^5 \text{ mm}^3$$

The volume of the 20 N steel dead weight is $2.549 \times 10^5 \text{ mm}^3$.

For the 50 N dead weight, the mass is:

$$\frac{50 \text{ N}}{9.81 \text{ m/s}^2} = 5.097 \text{ kg}$$

The volume is then calculated:

$$V_{50Ndeadweight} = \frac{5.097 \text{ kg}}{8000 \text{ kg/m}^3} = 6.371 \times 10^{-4} \text{ m}^3 = 6.371 \times 10^5 \text{ mm}^3$$

The volume of the 50 N steel dead weight is $6.371 \times 10^5 \text{ mm}^3$.

The proportions of the dead weight do not have a standard, and were therefore decided by the group. To determine the final dimensions of the dead weight the supervisor wished to see two different sizes, a short and tall weight. The heights of the weights are set to 30 mm and 60 mm for the 20 N dead weight, and 30 mm and 80 mm for the 50 N dead weight. A size for the height was set instead of the radius to make manufacturing of the weight easier, if it was to be made with a CNC cutter. To find the diameter, the formula for the volume of a cylinder (Equation 2.9.2) was flipped so that the radius, r , becomes the subject of the equation (Equation 5.4.1):

$$r = \sqrt{\frac{V_{total}}{\pi \times h}} \quad (5.4.1)$$

The calculation of the dead weight dimensions have to account for the hole through the center. The hole in the center has a diameter of 20 mm. To calculate the correct dimensions of the dead weight the volume of the hole is added in the equation (Equation 5.4.2).

$$V_{total} = V_{deadweight} + V_{hole} \quad (5.4.2)$$

The radius and diameter can then be calculated:

$$r_{20N,short} = \sqrt{\frac{2.549 \times 10^5 \text{ mm} + (\pi \times (20 \text{ mm})^2 \times 30 \text{ mm})}{\pi \times 30 \text{ mm}}} = 55.719 \text{ mm}$$

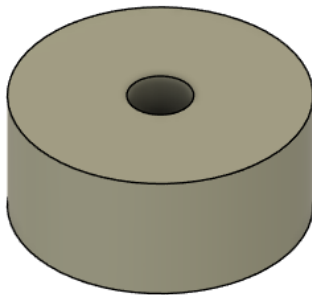
$$d_{20N,short} = 55.719 \text{ mm} \times 2 = 111.44 \text{ mm}$$

The short 20 N dead weight (Figure 5.4.14a) has a height of 30 mm and a diameter of 111.44 mm.

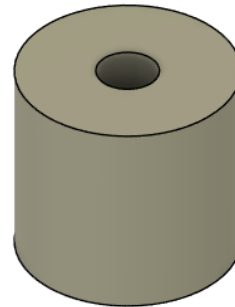
$$r_{20N,tall} = \sqrt{\frac{2.549 \times 10^5 \text{ mm} + (\pi \times (20 \text{ mm})^2 \times 60 \text{ mm})}{\pi \times 60 \text{ mm}}} = 41.860 \text{ mm}$$

$$d_{20N,tall} = 41.860 \text{ mm} \times 2 = 83.72 \text{ mm}$$

The tall 20 N dead weight (Figure 5.4.14b) has a height of 60 mm and a diameter of 83.72 mm.



(a) Short 20 N deadweight



(b) Tall 20 N deadweight

Figure 5.4.14: Two options for the 20 N dead weight.

The same calculations were then done for the 50N dead weight:

$$r_{50N,short} = \sqrt{\frac{6.371 \times 10^5 \text{ mm} + (\pi \times (20 \text{ mm})^2 \times 30 \text{ mm})}{\pi \times 30 \text{ mm}}} = 84.616 \text{ mm}$$

$$d_{50N,tall} = 84.616 \text{ mm} \times 2 = 169.23 \text{ mm}$$

The short 50 N dead weight (Figure 5.4.15a) has a height of 30 mm and a diameter of 169.23 mm.

$$r_{50N,tall} = \sqrt{\frac{6.371 \times 10^5 \text{ mm} + (\pi \times (20 \text{ mm})^2 \times 80 \text{ mm})}{\pi \times 80 \text{ mm}}} = 54.175 \text{ mm}$$

$$d_{20N,tall} = 54.62 \text{ mm} \times 2 = 108.35 \text{ mm}$$

The tall 50 N dead weight (Figure 5.4.15b) has a height of 80 mm and a diameter of 108.35 mm.

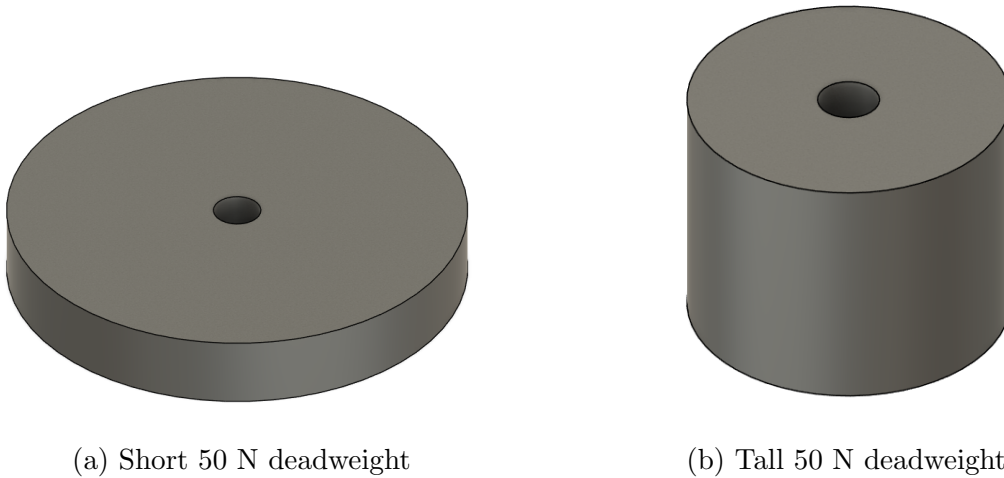


Figure 5.4.15: Two options for the 50 N dead weight.

After consulting with the supervisors it was agreed that the short 20 N and the tall 50 N dead weight were the better alternatives.

5.4.9 Test Piece Holder - First Design

The design for the tribometer did not have a test piece holder initially, as the idea was to rest the test piece on the load applicators similar to a classic fatigue bending test. To measure the frictional force with a load cell, the test piece has to be able to move horizontally. A holder mounted on spring plates would allow for movement and return the test piece to its starting point. The first design (Figure 5.4.16) was drafted with inspiration from one of the tribometers in the tribology laboratory at NTNU and suggestions from the projects supervisor.

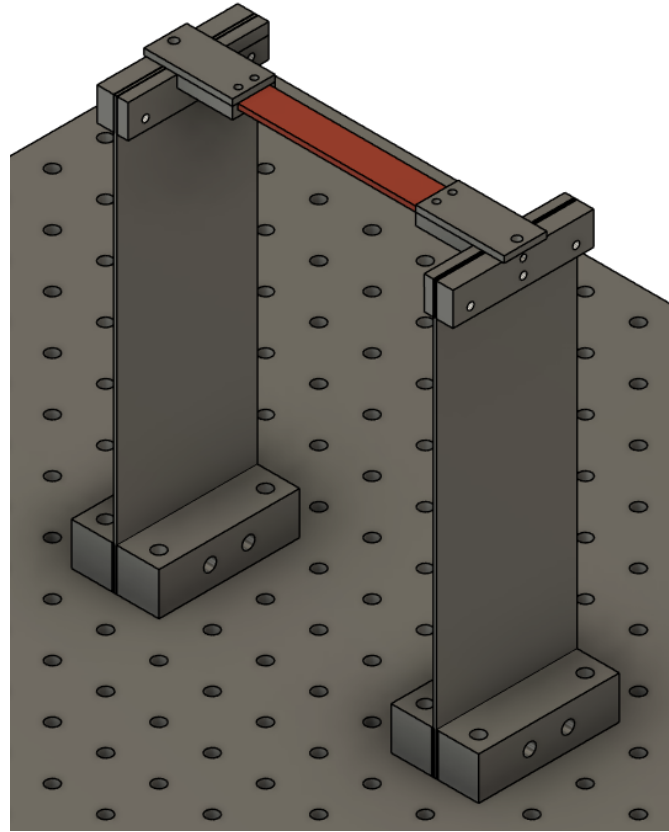


Figure 5.4.16: First design of test piece holder.

With this design the test piece will have two holes on each end. The test piece was installed by placing it into the fitted slot on the upper attachment (Figure 5.4.17c), closing the lid that was connected by a pivot hinge (Figure 5.4.17c & 5.4.17d), and fastening with screws and nuts. The end of the test piece will sit perfectly 10 mm into the slot. The upper attachment consisted of two components enclosing a spring plate (Figure 5.4.17b), connected by screws. The spring plate was pinched and secured to the optical board by two attachments (Figure 5.4.17a). At the top of the spring plates were holes where the test piece holder upper attachments were screwed in. The test piece holders on both sides of the test piece were almost identical.

The issue with this design lies in the way the test piece is fastened to the test piece holder. There is a concern that under fatigue bending the test piece will also bend at the point where it was screwed. This will turn the four-point bending test into a six-point bending test. It was not applicable to rely on the spring plate to counteract this bending, so the issue was solved in the second design of the test piece holder.

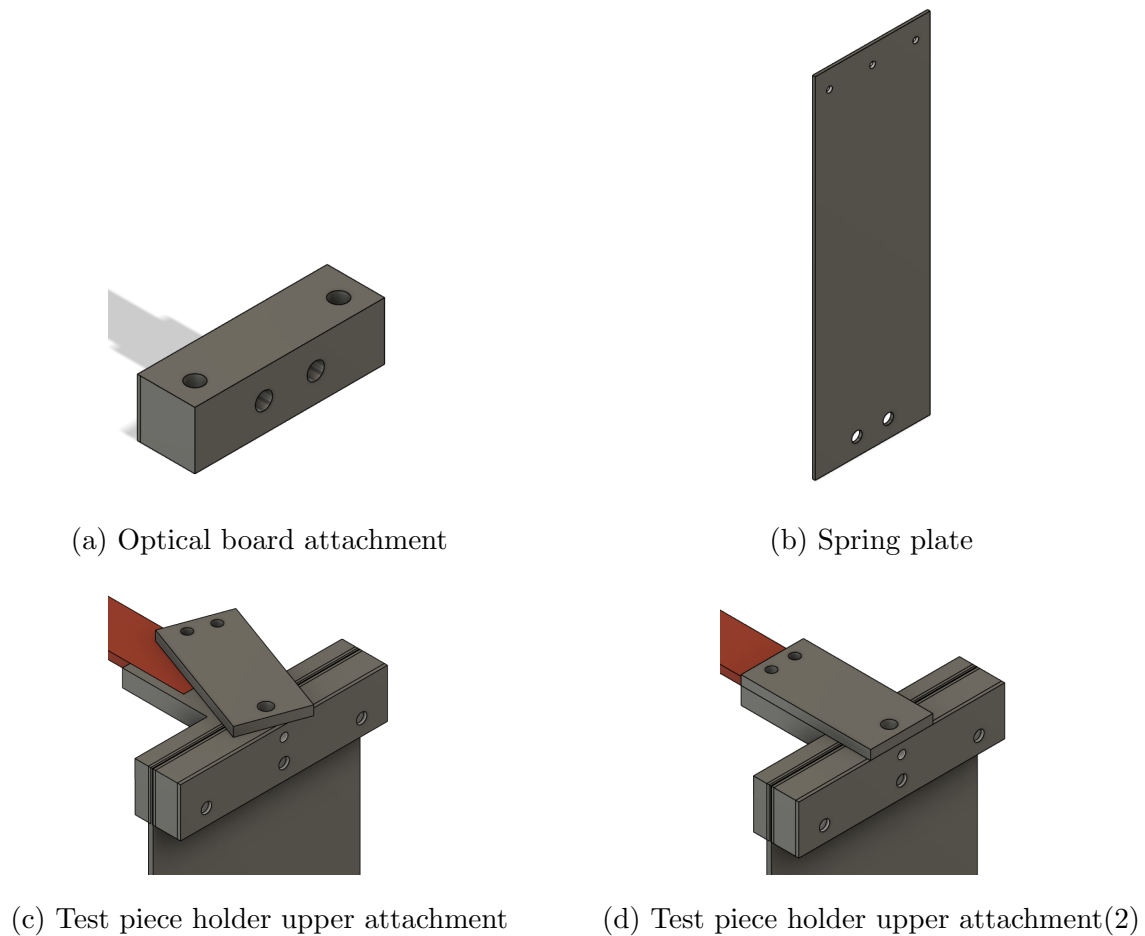


Figure 5.4.17: First design of test piece holder.

5.4.10 Test Piece Holder - Second Design

The second design (Figure 5.4.18) was altered to avoid bending at the point where the test piece was fastened. The cover of the upper attachment is removed and the screws are replaced with a pin (Figure 5.4.19a). The pin will allow the test piece to curve while still being fixed to the holder.

The support applicators (Figure 5.7.8) are fixed at a height that exactly touches the top of the test piece. Since there is virtually no room between these two parts, sliding the test piece into the slot of the test piece holder in the Figure 5.4.19a would be difficult. The wall facing the front is opened (Figure 5.4.19b), making installation easier.

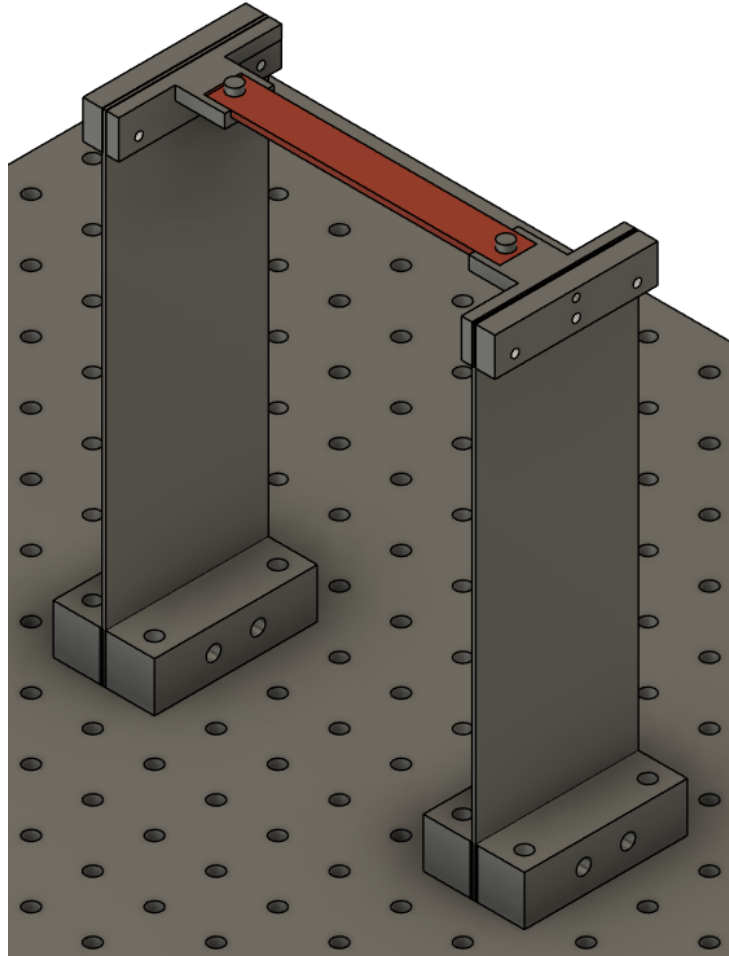
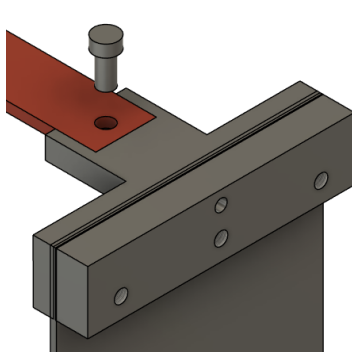
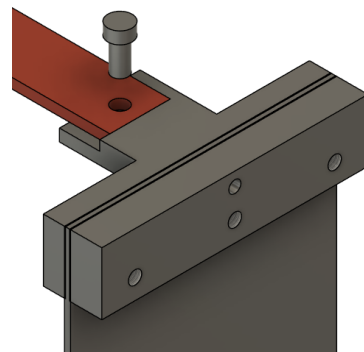


Figure 5.4.18: Second design of test piece holder.



(a) Second design of holder



(b) Adjustment to second design

Figure 5.4.19: Adjustment of second design of friction mechanism.

5.4.11 Support for the Friction Mechanism - First Design

The purpose of the first design (5.4.20) was to roughly estimate the size of the tribometer, and give an idea of the support beam dimensions. The draft was helpful when deciding the dimensions of the rest of the tribometer parts.

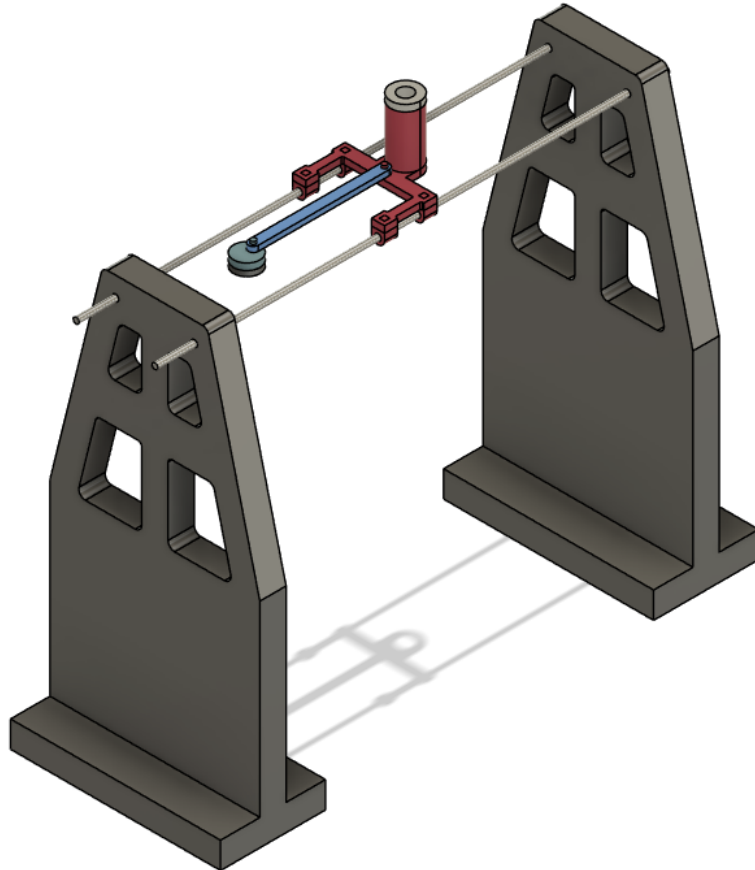


Figure 5.4.20: First design of the support for the friction mechanism.

5.4.12 Support for the Friction Mechanism - Second Design

The supports for the friction mechanism (Figure 5.4.21) were placed on the optical board where they are not in the way but close enough to the other tribometer parts to minimize space. The support on the right side of the friction mechanism (Figure 5.4.22) has a larger opening than the left to make room for the load cell mount (See Subsubsection 5.5.1). In the situation where maintenance or replacement of the load cell is necessary, there should be easy access to the screws that secures the load cell mount together. That is the reason why the left support for the friction mechanism (Figure 5.5.1) for the was asymmetrical to the right.

The geometry of the first design makes it difficult to manufacture. A solution is to divide the support into multiple simple parts. The supports from the second design include two triangular beams (Figure 5.4.23a or 5.4.25a), a support beam or wall (Figure 5.4.23b or 5.4.25b) and a horizontal beam that hold the friction mechanism rods (Figure 5.4.23c or 5.4.25c). The support beams are attached together by M6 screws.

One could argue that there is no need for a support wall or beam. However, because of the height of the tribometer, measured to be roughly 300mm tall, the supports are added to strengthen the construction.

The diameter of the rod was set to 10mm and is threaded at each end. The rod slides into the holes of the horizontal top beam (Figure 5.4.23c), and is secured by nuts. As maintenance or repair of the holder might be necessary, the rods are designed to be easily installed and removed.

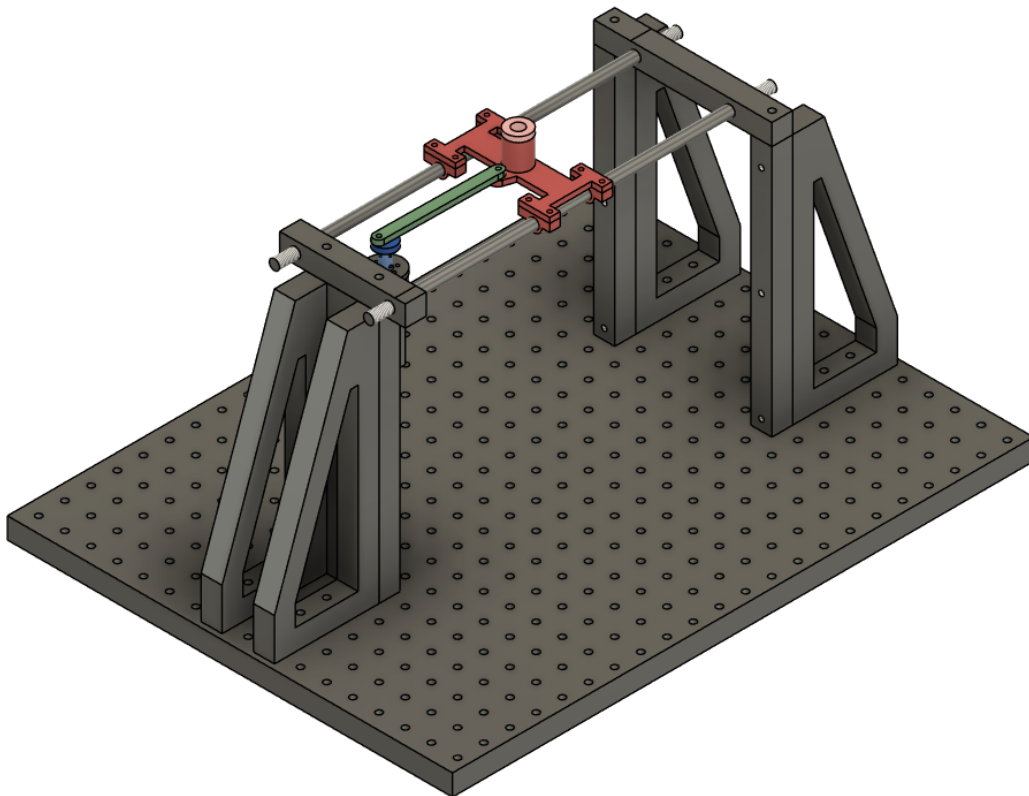


Figure 5.4.21: Second design of the support for the friction mechanism.

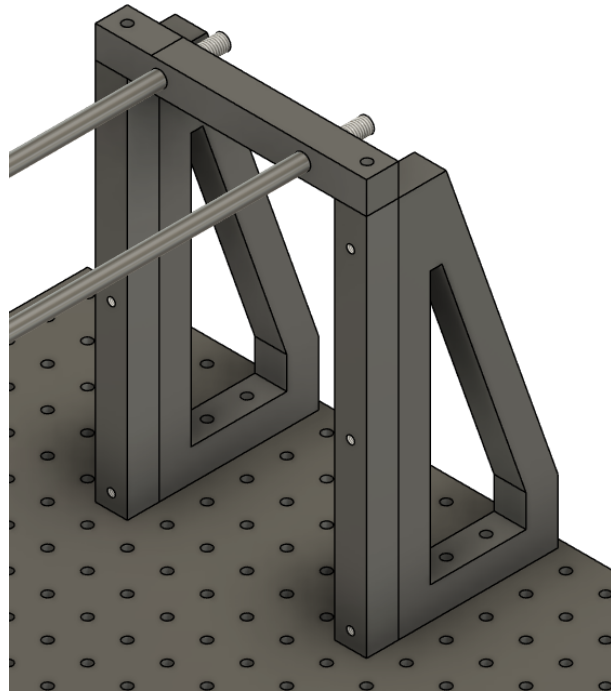
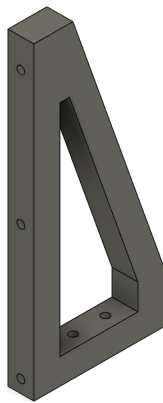


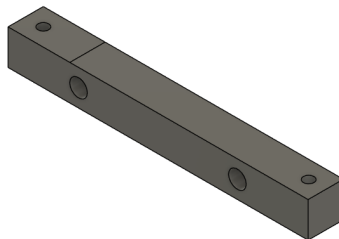
Figure 5.4.22: Support on the right side of the friction mechanism.



(a) Triangular Beam



(b) Support beam - right



(c) Support for rods - right

Figure 5.4.23: Parts of the support on the right side of the friction mechanism.

The support wall (Figure 5.4.25b) on the left will hold the motor. Extra M6 holes are threaded to fit the motors bracket (Figure 5.5.7).

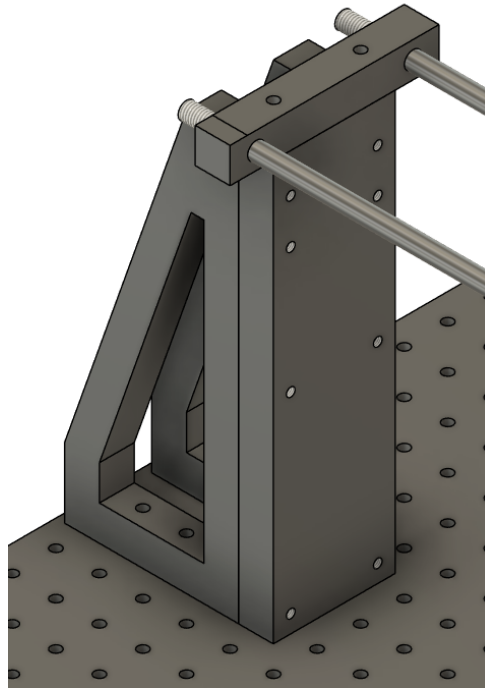
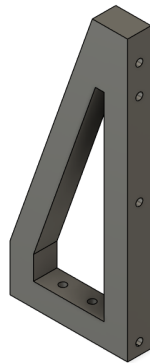


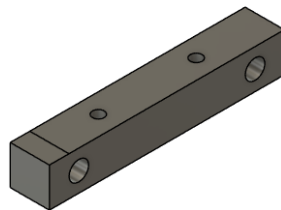
Figure 5.4.24: Support on the left side of the friction mechanism.



(a) Triangular beam



(b) Supportwall - left



(c) Support for Rod - left

Figure 5.4.25: Parts of the support on the left side of the friction mechanism.

5.5 The Load Cell for the Friction Mechanism

Through contact from a sales representative from Loadstar sensors the RES2 S-Beam Jr. load cell with overload protection (Loadstar Sensors, n.d.) was picked for the friction mechanism. The sensor was small in size and are available in capacities from 5 kg up to 50 kg. The load cell will be not be measuring a load higher that 50 N, assuming a friction coefficient of 1. A selling point for this load cell was that an interface and software is available together, making the setup of the tribometer an easier task.

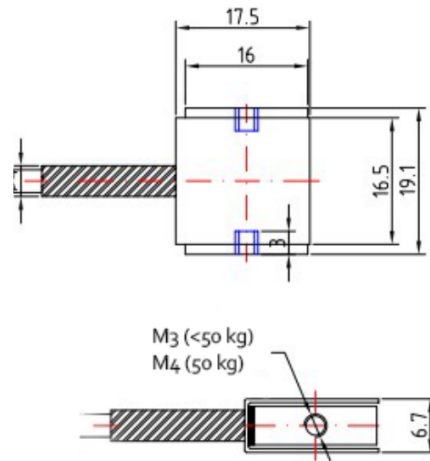


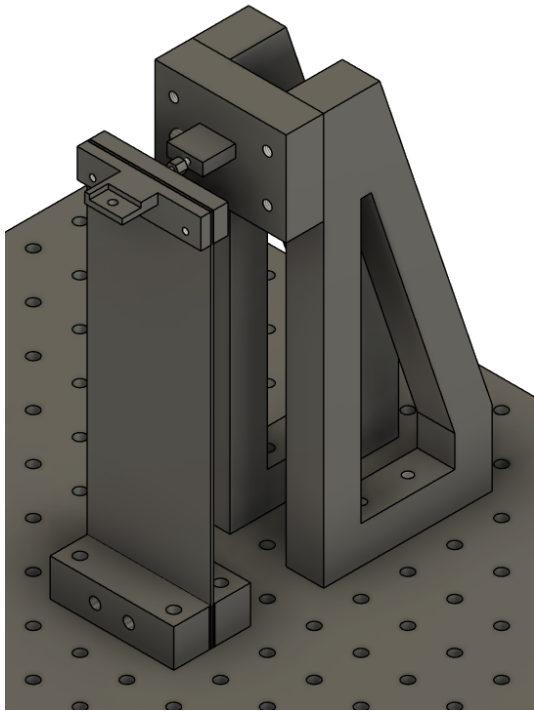
Figure 5.5.1: Machine drawing of RES2 S-beam Jr. load cell.

5.5.1 Load Cell Mount

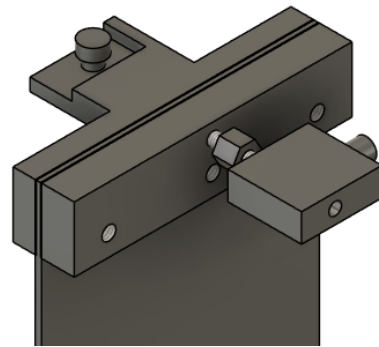
The load cell mount was anchored in between the triangular support beams of the right friction mechanism (Figure 5.4.22). Oscillation of the friction mechanism could interfere with the results of the load cell if it was to be mounted to the same support beams as the friction mechanism. As the friction mechanism moves, it could cause movement or vibrations in the supports that the load cell would pick up. The load cell was only meant to measure the frictional force between the alumina ball and the test piece. For that reason the load cell was mounted on a separate support.

The load cell was oriented with its arms facing the test piece holder and the support wall (Figure 5.5.2a). On each side of the load cell are threaded holes for mounting. The load cell sits directly against the support wall (Figure 5.5.2c) and was secured in place by a screw from the backside (Figure 5.5.2d). The load cell and the test piece holder was connected by a double ended hexagonal bolt (Figure 5.5.2b). The bolt (Figure 5.5.3) has

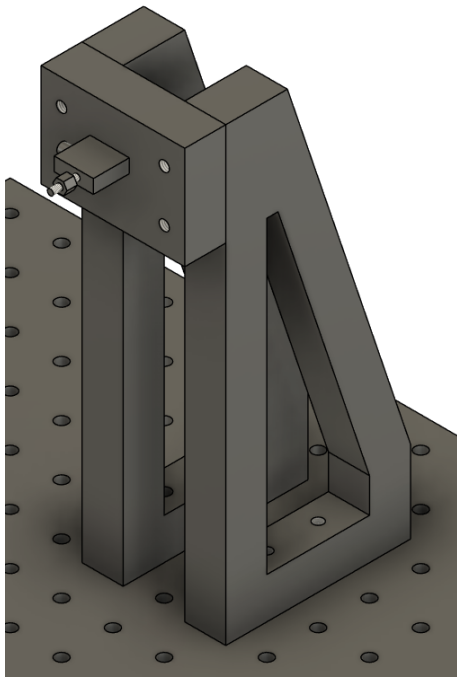
a hexagonal head to be easily adjusted.



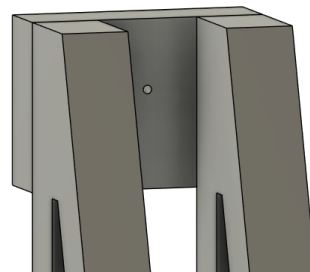
(a) Load cell mount with test piece holder



(b) Load cell screwed into test piece holder



(c) Load cell mounted to support wall



(d) Support wall from backside

Figure 5.5.2: Different angles of the load cell mount.

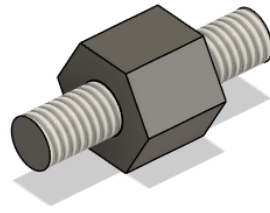


Figure 5.5.3: Bolt connecting the load cell to the test piece holder.

5.5.2 BLDC Motor Mount - First Design

The BLDC motor was mounted on the left support wall. The first design for the motor mount (Figure 5.5.4) consisted of a shelf (Figure 5.5.5b) and a simple L-shaped bracket (Figure 5.5.5a) with holes designed after the mounting threads on the motor. The shelf was meant as an extra precaution to stabilize the motor when running. Both motor mount parts had holes that aligned with threaded holes on the support wall, and was fixed with M6 screws.

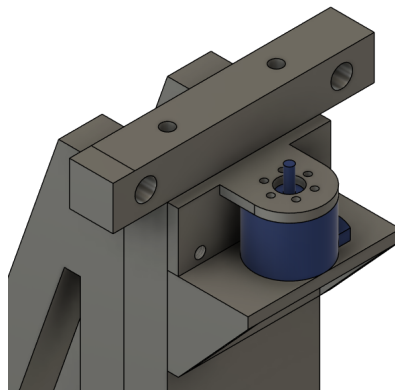
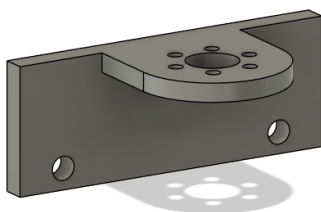
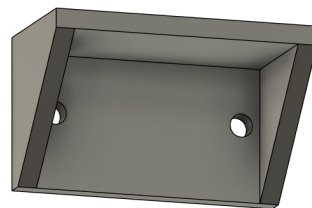


Figure 5.5.4: First design of BLDC motor mount.



(a) BLDC Motor Bracket



(b) Shelf for BLDC motor

Figure 5.5.5: BLDC Motor mount parts.

5.5.3 BLDC Motor Mount - Second Design

In the second design for the motor mount (Figure 5.5.6) the shelf was removed and the length of the L-bracket was extended. The hole that attached the L-bracket to the support wall from the first design would not stabilize the motor well, and could not be moved upwards due to the screws that connected the rod support beam (Figure 5.4.25c) to the support wall. The length of the new bracket (Figure 5.5.7) was adjusted and had additional mounting holes. As the bracket would be made of sturdy metal the L-bracket would sufficiently stabilize the motor, thus the shelf was removed.

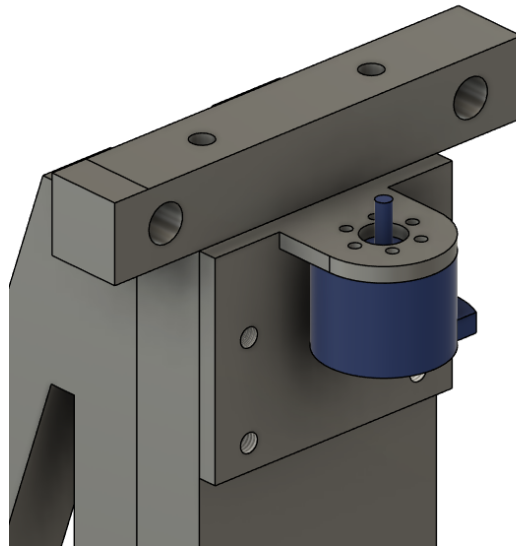


Figure 5.5.6: Second design for BLDC motor mount.

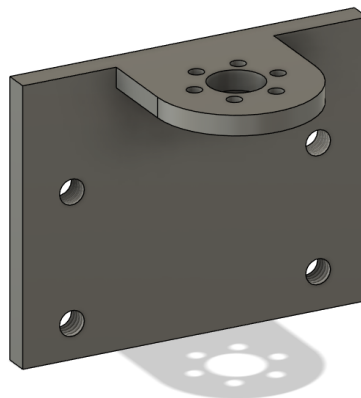


Figure 5.5.7: Second Design of motor mount.

5.6 Electrochemical Cell

Early on in the design phase of this project it was decided that the electrolyte should only be on a portion of the test piece, instead of the whole tribometer being submerged. This meant that the compartment containing the electrochemical cell had to be designed with the size of the ball holder in mind, since the ball holder needs to go into this compartment in order for the tribometer to do tests with both friction and corrosion simultaneously. The biggest concern with this setup was if the electrolyte would leak out when the fatigue load was applied to the test piece.

The tribometer will use the counter and reference electrodes that are already in use in the tribology lab: a platinum wire counter electrode and a Ag/AgCl reference electrode.

5.6.1 Seal

After brainstorming ideas of how to make sure the electrolyte would not leak out of the compartment containing the electrochemical cell, it was concluded that a seal made out of silicone rubber would be a good solution. This was because of the material's flexibility and ability to withstand compression. It was also decided that in order to get the seal to have the desired shape, as well as being able to test multiple different shapes if needed, the best solution would be for the group to cast the silicone. The group decided to cast the silicone themselves because this would allow for a more efficient prototyping and testing process. An efficient prototyping and testing process was deemed important as it was expected that the seal would need redesigning quite a few times to make it work as intended. A silicone moulding kit, shown in Figure 5.6.1, was used for casting the seal.



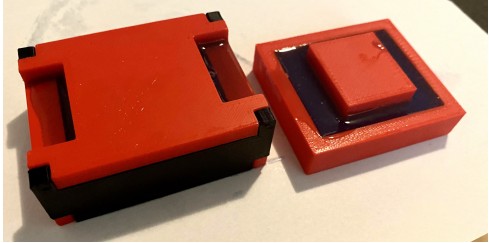
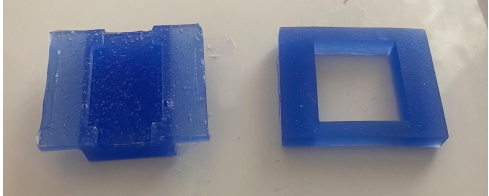


Figure 5.6.1: The silicone moulding kit that was used for making the silicone seal (Panduro, n.d.).

In order to cast the silicone, a mould was needed. To get the desired shape, the group opted for 3D-printed moulds. 3D-models of these were made in Fusion 360 and printed in PLA at Ubåten, a part of the Rapid prototyping laboratory at NTNU Gløshaugen.

Table 5.6.1 describes the process of casting the silicone seal. The pictures are from the casting of the seal in the final design of the compartment containing the electrochemical cell (subsubsection 5.6.5), which consists of a top and a bottom seal. A similar process can be used for any of the designs.

Table 5.6.1: The casting process of the silicone seal.

	Description	Picture
1	As specified in the instructions that came with the silicone moulding kit, component A was first added to a cup. An equal amount of component B was then added to the same cup, and the two components were stirred well for approximately 30 seconds.	
2	The mixture was then poured into the 3D-printed moulds. The amount of air bubbles in the silicone was reduced by tapping the bottom of the silicone filled moulds on a hard surface.	
3	In order to get the silicone to the desired shape for the bottom seal a lid was added, shown to the left in the picture. Since the top seal, shown to the right in the picture, is flat, that mould did not need a lid.	
4	After about 1 hour the silicone had cured and the seals were taken out of the moulds.	

5.6.2 Compartment for the Electrochemical Cell - First Design

In the first suggestion for the design, the compartment for the electrochemical cell is placed around the test piece as illustrated in Figure 5.6.2, with hinges on the back and a clasp on the front to hold the two parts of the compartment together. The compartment should never directly touch the test piece. The reason for this is that the test piece has to be able to deflect when the fatigue load is applied. Therefore, there is a seal formed as a rectangle where the walls of the compartment meet the top of the test piece. On the bottom, there is a solid rectangular layer of silicone between the test piece and the compartment. The electrolyte will only be on the top of the test piece. The reason for the compartment going around the whole test piece is to make the seal between the top of the test piece and the compartment compressed, so the electrolyte does not leak out.

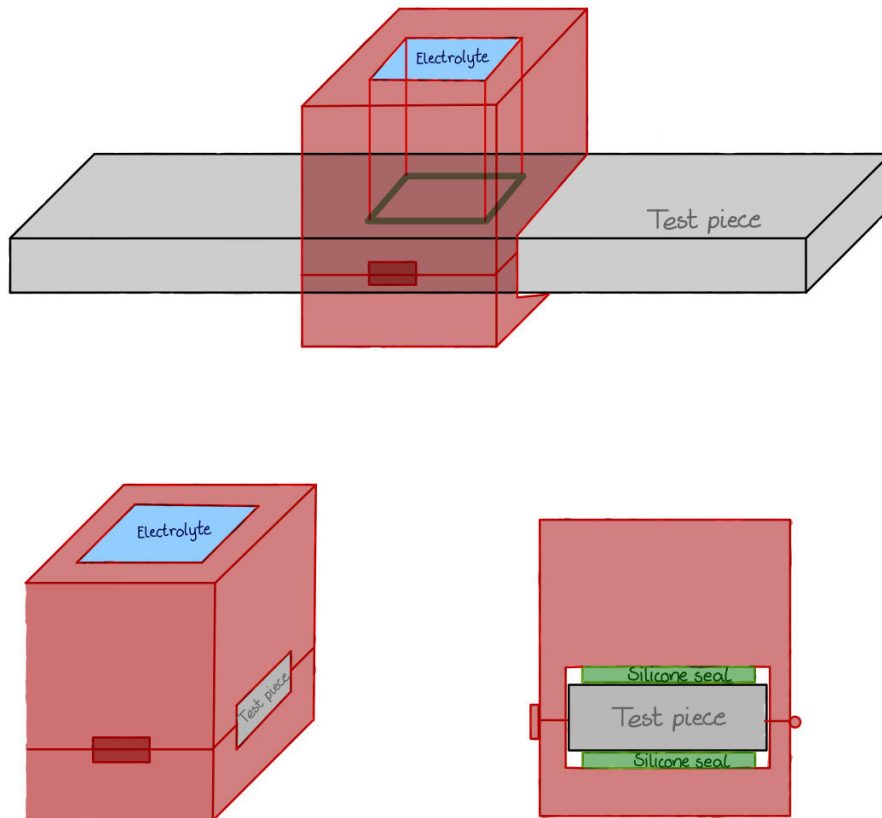


Figure 5.6.2: Sketch of the first design suggestion for the compartment containing the electrochemical cell.

5.6.3 Compartment for the Electrochemical Cell - Second design

In order to reduce the amount of materials needed, a new design was suggested. In this design the whole compartment for the electrochemical cell is placed on top of the test piece, with a beam on each side to secure it to the ground of the tribometer. Similar to the previous design, there is a silicone seal between the test piece and the walls of the compartment (illustrated in Figure 5.6.3), and the beams are there in order to compress the seal and preventing the electrolyte from leaking out.

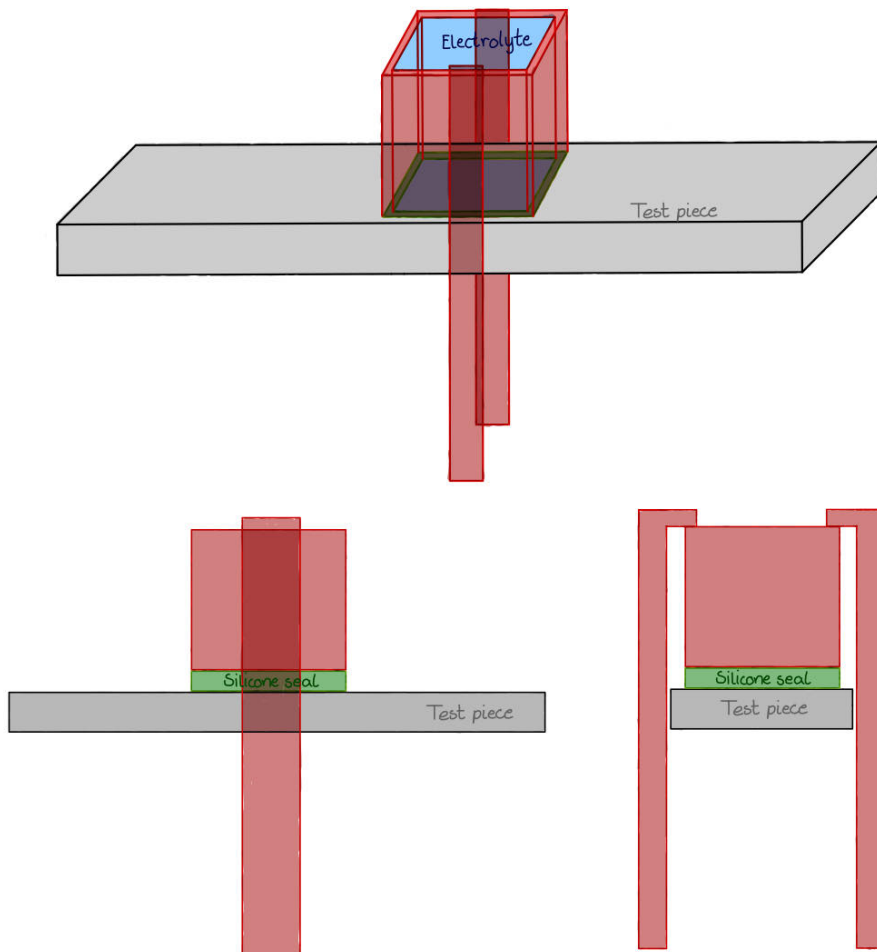


Figure 5.6.3: Sketch of the second design suggestion for the compartment containing the electrochemical cell.

One of the problems with this compartment was that it would be very challenging to secure the side beams in such a way that the silicone seal would be compressed enough and prevent leakage.

5.6.4 Compartment for the Electrochemical Cell - Third design

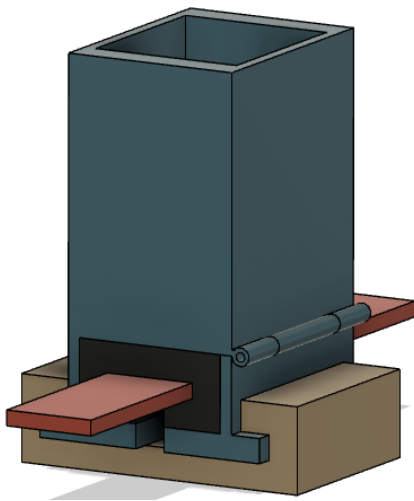
The two first designs were designed with a 6 mm friction ball in mind. After discussions with the supervisors it was decided that it would be preferable to be able to do tests with a 10 mm ball as well. Since the ball holder for the 10 mm friction ball has a diameter of 14 mm, and the width of the test piece is 15 mm, the use of the 10 mm friction ball would require the compartment for the electrochemical cell to be wider than the test piece. Therefore, having the whole compartment on top of the test piece would not be possible, and a new design had to be developed.

The minimum required size for the inner walls of the compartment for the electrochemical cell was calculated:

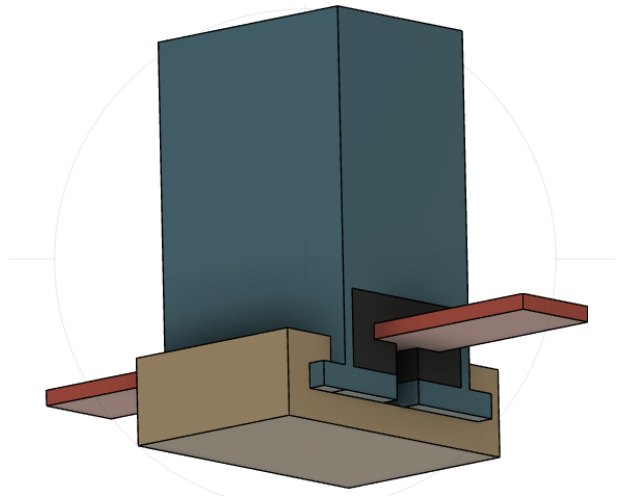
$$w_{min} = d_{10} + clearance = 14 \text{ mm} + 2 \times 2 \text{ mm} = 18 \text{ mm}$$

$$l_{min} = l_{wt} + d_{10} + clearance = 10 \text{ mm} + 14 \text{ mm} + 2 \times 2 \text{ mm} = 28 \text{ mm}$$

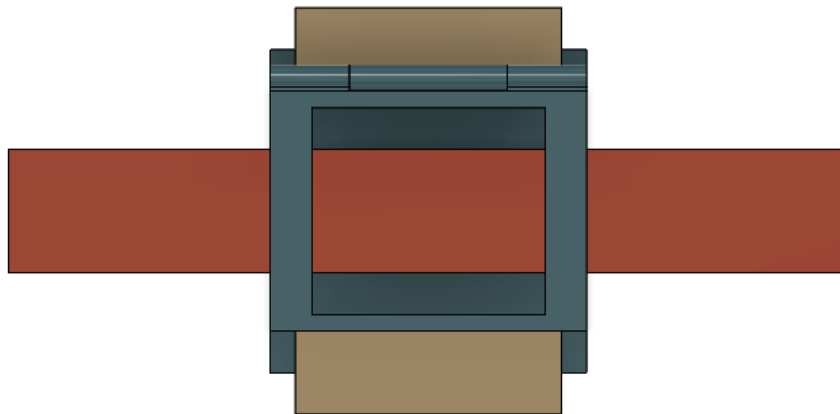
Here w_{min} is the minimum width for the inside of the compartment, l_{min} is the minimum length for the inside of compartment, d_{10} is the diameter of the ball holder for the 10 mm ball, and l_{wt} is the length of the wear track. The minimum clearance between the friction ball and the walls of the compartment was set to 2 mm. Since the width of the test piece is 15 mm and the minimum width of the compartment needed for the 10 mm friction ball is 18 mm the compartment needs to be extended past the width of the test piece. Therefore a new design was created. Figure 5.6.4 shows screenshots taken from Fusion 360 of this design's 3D model, and Figure 5.6.5 shows how the silicone seal is placed around the test piece.



(a) Hinges on one side



(b) Clasp, illustrated in brown, holding the compartment in place



(c) From the top showing the inside of the compartment

Figure 5.6.4: 3D model of the third design for the compartment containing the electrochemical cell.

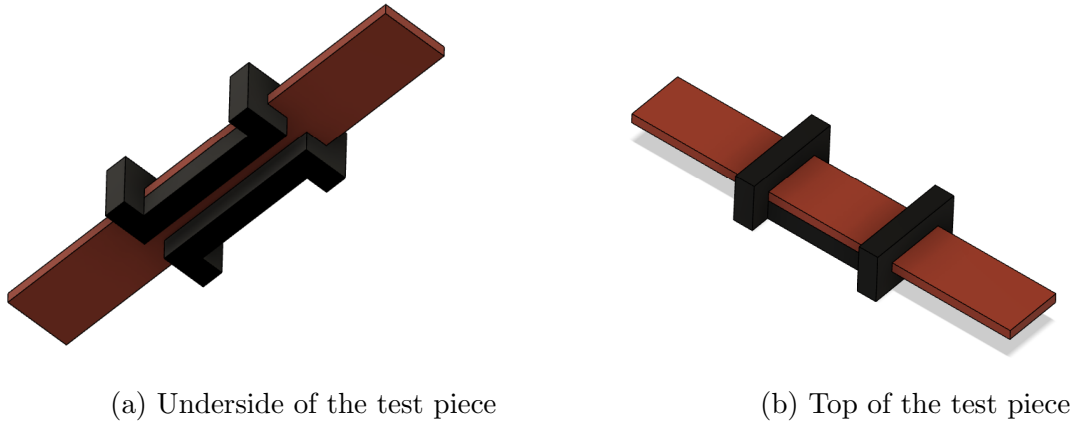


Figure 5.6.5: 3D model showing the seal around the test piece.

There are hinges on one side of the compartment, shown in Figure 5.6.4a, which makes it possible to open it and place it around the test piece. A clasp, shown in Figure 5.6.4b, slides onto the bottom of the compartment and holds it in place.

The seal, shown in Figure 5.6.5, was set to have a height of 6 mm and a width of 5 mm. The reason for this was because the group cast the seal themselves, and a thinner seal would be more likely to be unsuccessful. In addition to this, the seal needed a certain thickness to be able to compress enough and prevent leakage. The distance from the test piece to the compartment containing the electrochemical cell was set to 5 mm. By having the distance smaller than the height of the seal, the seal was compressed even when there was no fatigue load applied to the test piece.

With this design for the seal, the minimum length for the inside of the compartment did not change. However, the minimum width did:

$$w_{min} = b + 2 \times \text{compressed thickness of seal} = 15 \text{ mm} + 2 \times 5 \text{ mm} = 25 \text{ mm}$$

This means that the minimum width when just considering the size of the ball holder and the clearance needed between the ball holder and the wall is smaller than the minimum width when considering the width of the test piece and the thickness of the seal. Therefore, the latter width is the one that is used in the final design.

Through conversation with one of the supervisors, it was recommended that the ratio between the area of the test piece that is exposed to the electrolyte and the volume of the electrolyte should be at least 1:30. Based on this, the volume of the electrolyte was calculated:

$$A_{exposed} = b \times l_{min} + 2 \times h \times l_{min} = 15 \text{ mm} \times 28 \text{ mm} + 2 \times 2.5 \text{ mm} \times 28 \text{ mm} = 560 \text{ mm}^2$$

$$V_{electrolyte} = 30 \times A_{exposed} = 30 \times 560 \text{ mm}^2 = 16800 \text{ mm}^3$$

Here $A_{exposed}$ is the area of the test piece that is exposed to the electrolyte, and $V_{electrolyte}$ is the volume of electrolyte. Since the width of the compartment is now larger than the width of the test piece, as shown in Figure 5.6.4c, the sides of the test piece are also exposed to the electrolyte. However, $A_{exposed}$ can be adjusted by coating part of the test piece.

Then the minimum required height of the cell was calculated:

$$H_{min} = \frac{V_{electrolyte} - 2 \times V_{side}}{A_{cell}} = \frac{16800 \text{ mm}^3 - 2 \times 25 \text{ mm} \times 5 \text{ mm} \times 7.5 \text{ mm}}{28 \text{ mm} \times 25 \text{ mm}} = 21.32 \text{ mm}$$

Here V_{side} is the volume of the electrolyte that is below the top surface of the test piece. This will be equal to the difference in width between the test piece and the wall of the compartment times the combined height of the seal and the test piece. A_{cell} is the horizontal area of the inside of the compartment for the electrochemical cell. H_{min} is the minimum height from the top of the test piece to the top of the compartment's walls. To account for the displacement of the liquid because of the ball and the ball holder, as well as possible splashing caused by the back and forth motion of the ball holder, the height of the walls were set to $H = 50 \text{ mm}$.

This version of the cell was 3D-printed, and the seal was cast in a 3D-printed mould. For a more detailed description of the casting process see subsection 5.6.1. Using a 3D-printed test piece, the cell was tested for leaks by pouring water into it and bending the test piece to simulate the fatigue load being applied. The test showed that there was minimal leakage from the silicone seal. However, the hinges caused the water to leak out.

5.6.5 Compartment for the Electrochemical Cell - Fourth design

The hinges in the previous design caused the compartment with the electrochemical cell to not be sealed properly, so a new design was developed. This design used the same idea with the clasp to hold the compartment in place, but instead of hinges on one side, the cell consists of a top part and a bottom part held together by a clasp on each side. The width and length of the cell in this design are the same as in the previous design with $w = 25 \text{ mm}$ and $l = 28 \text{ mm}$. See subsection 5.6.4 for the calculations of these dimensions. After discussions with the supervisors, the height of the compartment was reduced from $H = 50 \text{ mm}$ to $H = 40 \text{ mm}$. The height was reduced in order to make the ball holder shorter, and thus reduce the risk of buckling. The wall thickness is set to 5mm, making the outer width 25 mm and the outer length 38 mm. The reason for the wall thickness is that the width of the seal is 5 mm and the wall should cover the whole width. As can be seen in Figure 5.6.6a, there were also added two loops to the top of the cell. These are there to hold the counter electrode and the reference electrode in place during the tests.

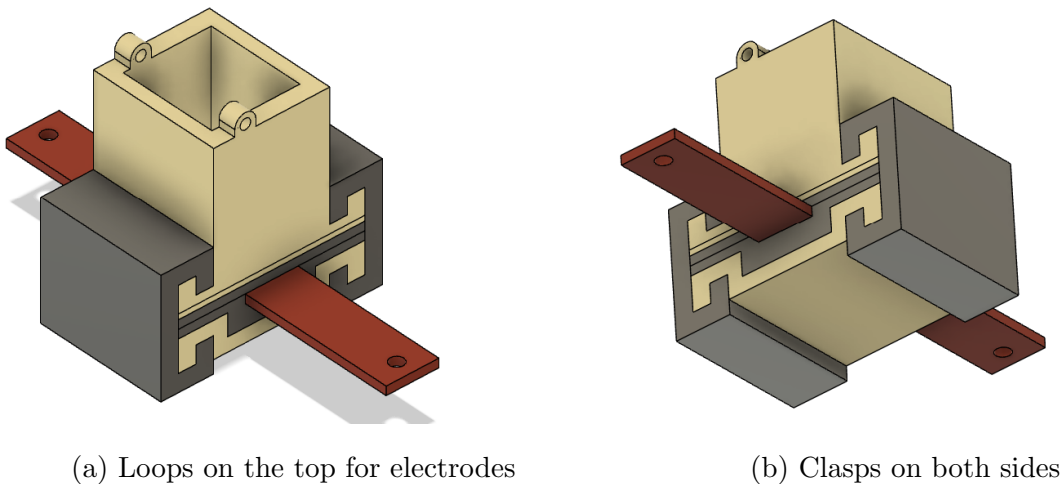


Figure 5.6.6: 3D model of fourth design for the compartment with the electrochemical cell.

The seal in this design consists of two parts: a top and a bottom, which sits around the test piece as shown in Figure 5.6.7. The two parts of the seal would preferably be glued or fixed onto their respective part of the compartment. This is to reduce the amount of steps needed in order to start the tribotest and make it more user friendly. The clasps will then be slid on and the sides of the seal will be compressed so no electrolyte leaks out.

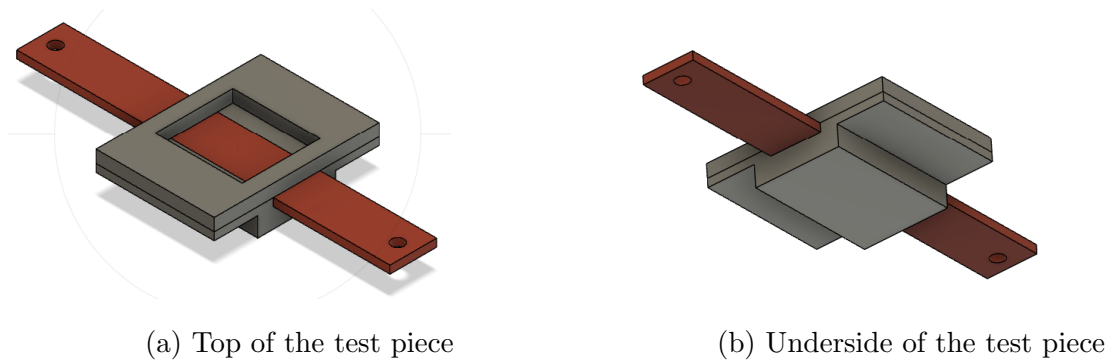


Figure 5.6.7: 3D model showing the seal around the test piece.

A 3D-printed test piece and a 3D-printed compartment for the electrochemical cell was used for the testing of the seals. The group found that the side of the test piece that was facing up while printing was rougher, and most of the leakage happened on this side. To try and eliminate errors caused by it, the sides of the test piece were polished. After this, there was no more leakage.

The height and the width of the seal, as well as the distance between the test piece and the wall of the compartment, is the same in this design as in the previous one (subsubsection 5.6.4). A few other heights for the top seal, 4mm and 8mm, were also tested, but it was found that the 6mm seal worked the best. A problem that was encountered with the 6mm seal was that the clasps were very difficult to slide on, especially without help from a second person. A clamp tool can be a possible solution to make this process easier.

5.7 Fatigue Load Application

5.7.1 Design Criteria

The load fatigue test was decided from early in the project to be four point bending. There was also a wish for load application to be able to bend the test piece back and forth, in positive and negative direction. To start with, the shape of the applicators was made following the ASTM international E885-08 standard for bend testing of metallic flat material. In this standard the applicators are pointed, but later are later rounded off by requested of the project supervisors. The components has to also be able to withstand the load that is applied by the fatigue test motor.

5.7.2 Fatigue Load Application - First Design

There are two main parts of the load application, the load and support applicators. A typical fatigue bending test is pneumatically or hydraulically driven and scaled much larger than the desired size for this project. An electrical motor would be suitable for this projects scale. At this stage, the type of motor was not decided. However, in which way the load applicator would apply the cyclic load on the test piece was explored.

Figure 5.7.1 was an early sketch where the project group attempted to figure out how to apply the load from both the bottom and top of the test piece. The idea in this sketch was that the load applicators clamp down on the test piece, locks in place and moves up and down.

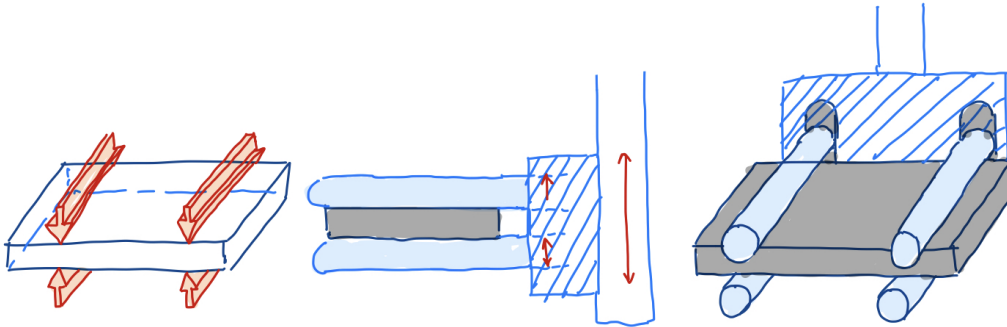


Figure 5.7.1: Sketches of the load application mechanism.

A first sketch and model of the load applicator mechanism (Figure 5.7.2 & 5.7.3) was drawn. There were load applicators on the top and bottom of the test piece and was secured by a component (Figure 5.7.2c) which the applicators slide into, then fastened into place. The tip of the applicator has an angle of 60 degrees. This follows the E885-08 standard by ASTM international. The supports applicator for the first design was drawn but did not get a 3d model. Most of the focus was on the load application mechanism in the start. The yoke mechanism was chosen at this stage to push the load applicator up and down, though there was scepticism around its functionality. Thinking of an idea for how the test piece was going to bend was difficult for the group at the start.

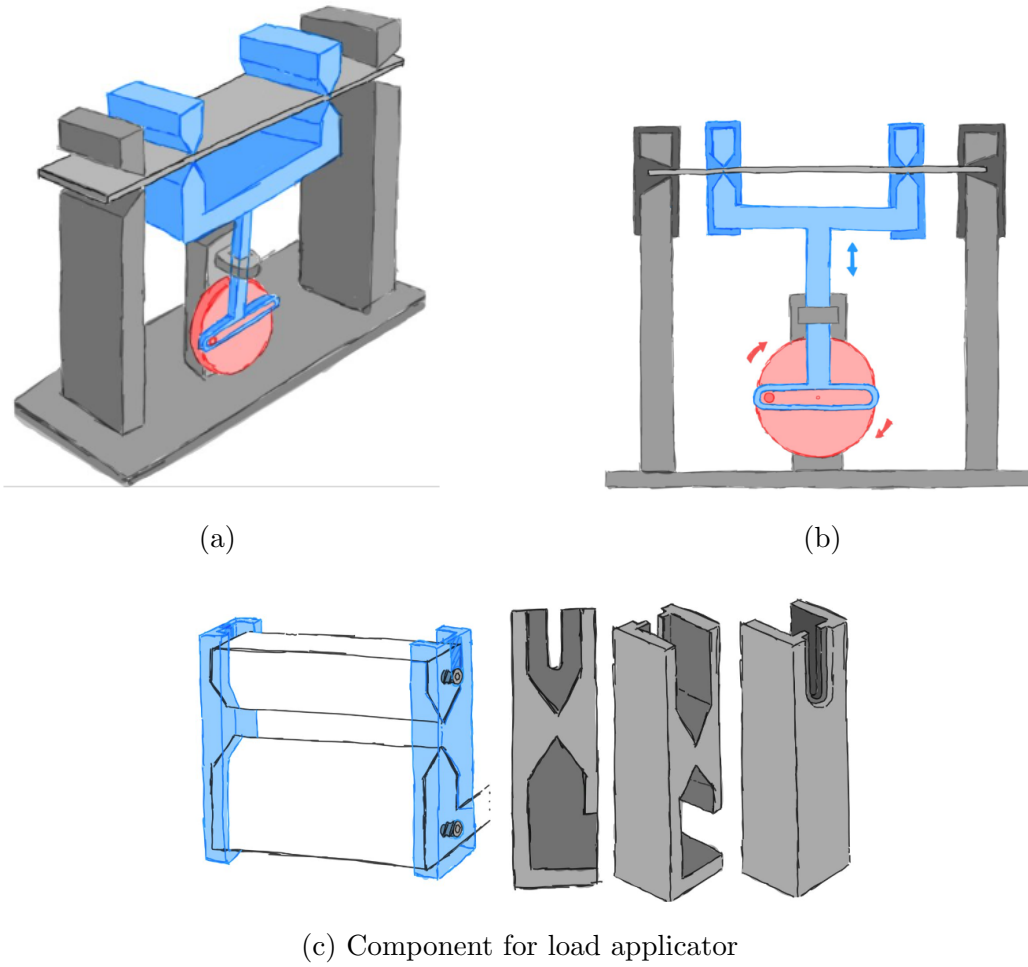


Figure 5.7.2: Sketches for the load application mechanism

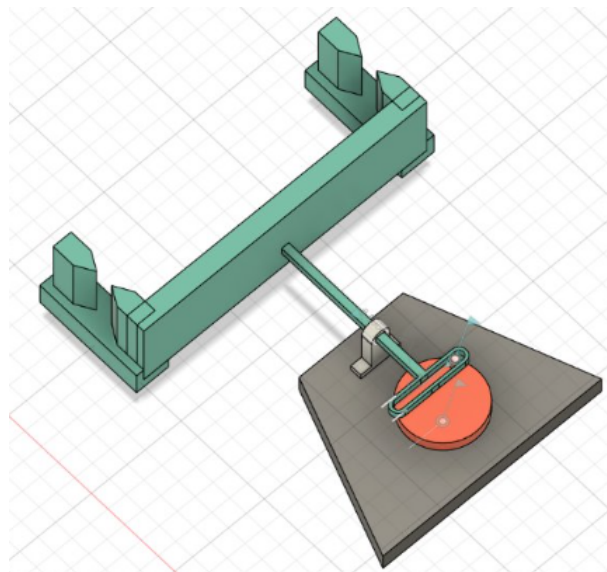


Figure 5.7.3: First design of load applicator

5.7.3 Fatigue Load Application - Second Design

After a discussion with the project supervisor, it was decided that this configuration would have either tensile or compressive bending, contrary to alternating. That was why in the second design (Figure 5.7.4) the load applicators on the top of the test piece are removed. A stand for the support applicators were also modelled.

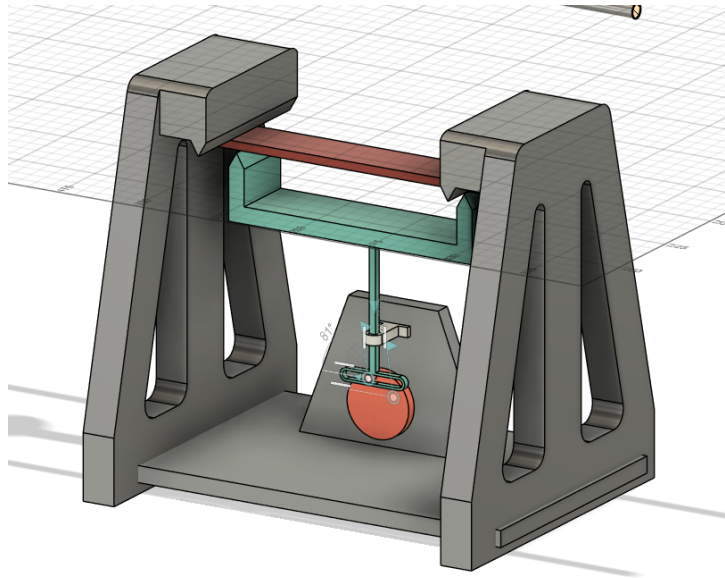


Figure 5.7.4: Second design of load applicator.

5.7.4 Fatigue Load Application - Third Design

The yoke mechanism is scrapped and exchanged for a captive linear stepper motor in the third design (Figure 5.7.5). When the third design was created the stepper motor was not finalized, that was why the load applicators are missing from this version. A large force would be applied to the support applicator by the motor, so the stand had to be shaped in a way that could sustain the load. The stand had a triangular shape with a wide base to counter this. The support applicators were also changed from rigid to adjustable. There were three parts to the support applicator, the stand, applicator and t-bolt (Figure 5.7.6). A t-rail stucked outwards at the top of the stand. The t-bolt, with a threaded hole, slid into the rail and was movable along the rails length. At the appropriate position the applicator was placed and screwed in and tightened with the T-bolt. The applicator was rounded off from a point to a 5 mm diameter half-circle.

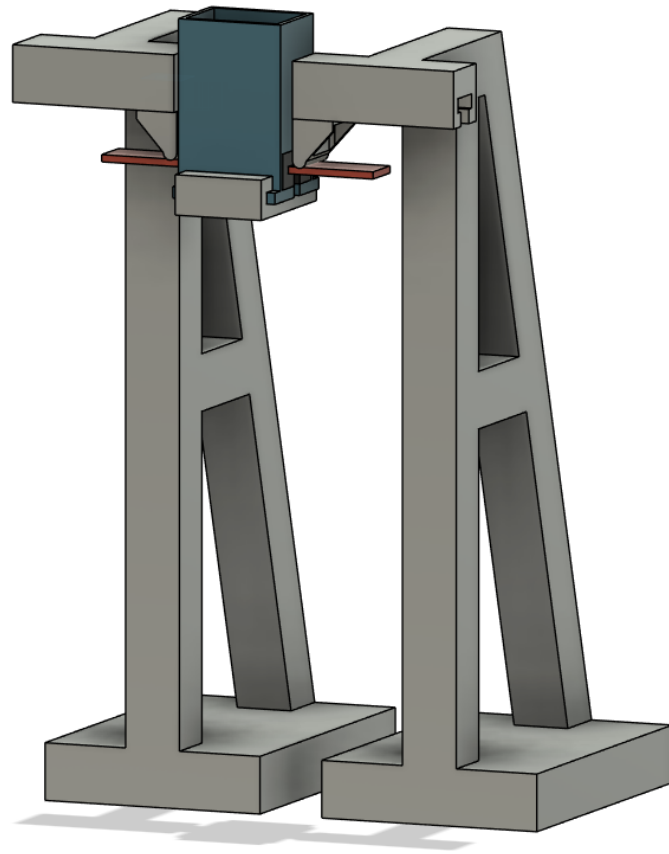
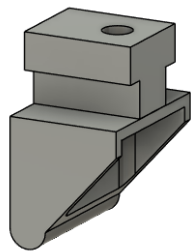
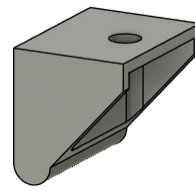


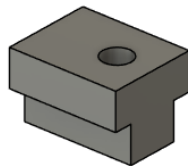
Figure 5.7.5: Third design of support applicators.



(a) Applicator with T-bolt



(b) Applicator



(c) T-bolt

Figure 5.7.6: Applicator with T-bolt for the third design.

5.7.5 Fatigue Load Application - Fourth Design

The fourth design (Figure 5.7.7) could be completed due to the interacting components reaching their final designs as well. The undetermined height of the motor was what stopped the progression of many load application parts. After the captive linear stepper motor (Figure 5.7.11a), from Dings' Intelligent Control Technology Co. Ltd was finalized, most of the components could reach their finished designs.

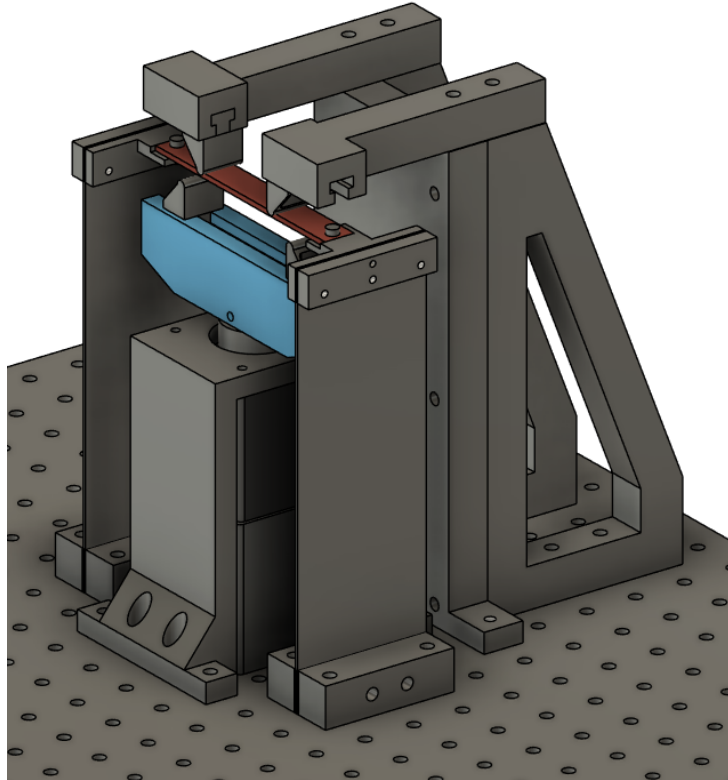


Figure 5.7.7: Fourth design of fatigue load application including the test piece holder.

The previous (third) design had a complicated geometry that would make it hard to manufacture. To solve this the support applicators in the fourth design (Figure 5.7.8) were separated into multiple simpler parts. Additionally, a support wall (Figure 5.7.9a) was added to the triangular support beams (Figure 5.7.9b), to create a sturdier structure that could withstand the loads from the stepper motor. The support applicator arms (Figure 5.7.9c and 5.7.9d) were mounted on top of the support wall and triangular beam. They have t-rails at the end for the applicators and t-bolts. All of these parts were screwed together and to the optical board with M6 screws.

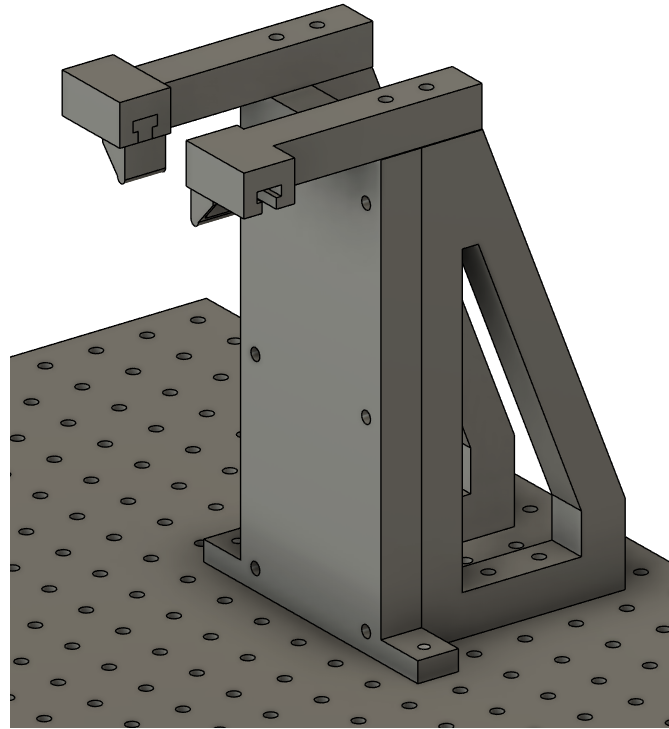
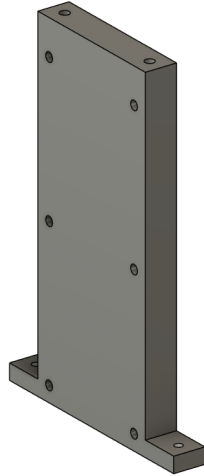
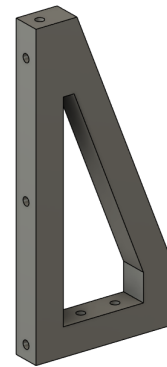


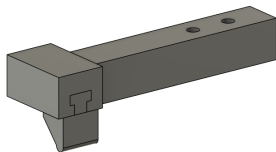
Figure 5.7.8: Fourth design of support applicators.



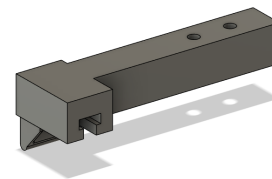
(a) Support applicator wall



(b) Triangular support beam



(c) Left support applicator arm



(d) Right support applicator arm

Figure 5.7.9: Support applicator parts.

At this stage the motor for the fatigue application load was finalized. Drawings and dimensions (See Subsubsection 5.7.6) were made available, so the design (Figure 5.7.10) and parts for the fatigue load motor could be created. The stepper motor (Figure 5.7.11a) was fastened to the optical board by a u-shaped bracket(Figure 5.7.11b). The top of the bracket had holes that aligned with the threaded mounting holes of the motor. The stepper motor attachment(Figure 5.7.11c) had a threaded hole on the underside to match the threaded axle on the motor. The motor attachment makes mounting the T-rail load applicator attachment(Figure 5.7.11d) easier. The load applicator attachment had a socket for a top of the motor attachment. A pin or screw was used to connect these parts. Two applicators (Figure 5.7.6b) slid into the load applicator attachment rails and were fixed at the desired position by tightening the screw in the t-bolt. To precisely adjust the applicators to the right position, a ruler would be attached to the front of the rail.

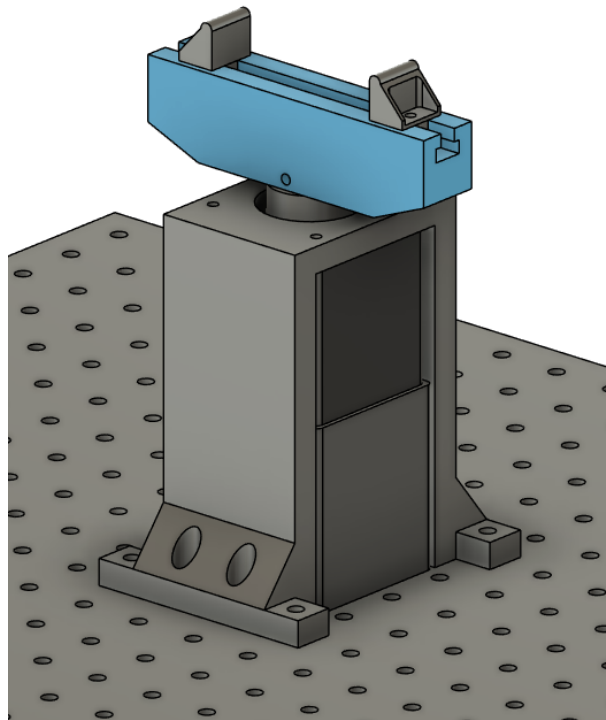


Figure 5.7.10: Fourth design of fatigue load applicator with motor.

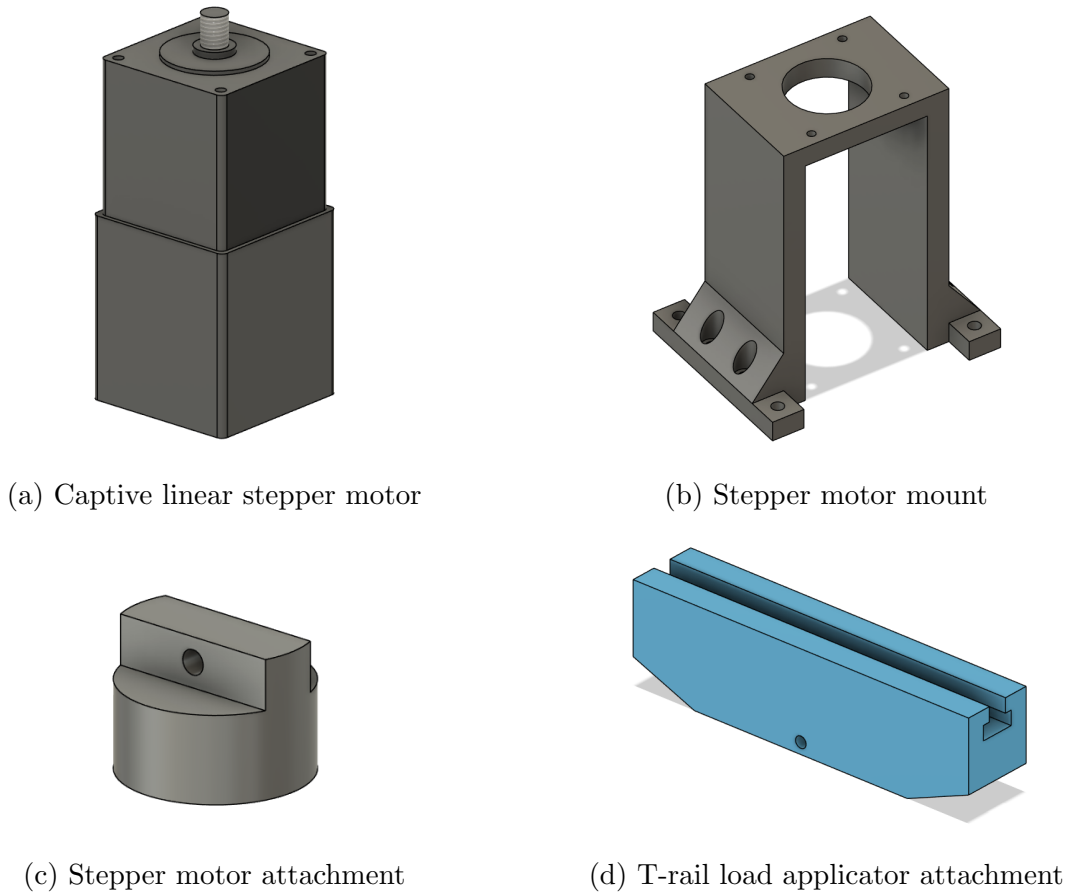


Figure 5.7.11: Load applicator parts for fourth design.

5.7.6 Motor for the Fatigue Load Application

The size 24 stepper lead screw linear actuator by Dings' Intelligent Control Technology Co. Ltd was chosen for the fatigue load application, with the help of the parallel group, the supervisor and the sales representative from Dings'. The fatigue load applicator has to apply a load of 815.625 N (See table 5.2.1) to the test piece in multiple cycles. This motor is capable of applied 1050 N with high performance under long working cycles (Dings' Intelligent Control Technology Co. Ltd, 2024).

The motors configuration had a multitude of options, but the following parameters were picked. As the deflection of the test piece will not exceed the minimum stroke length of the motor, Size A and Stroke B was decided to be 45.70 mm and 12.70 mm (Figure 5.7.13). By suggestion of the sales representative the motor would be double stacked, making the size of L 68.3 mm.

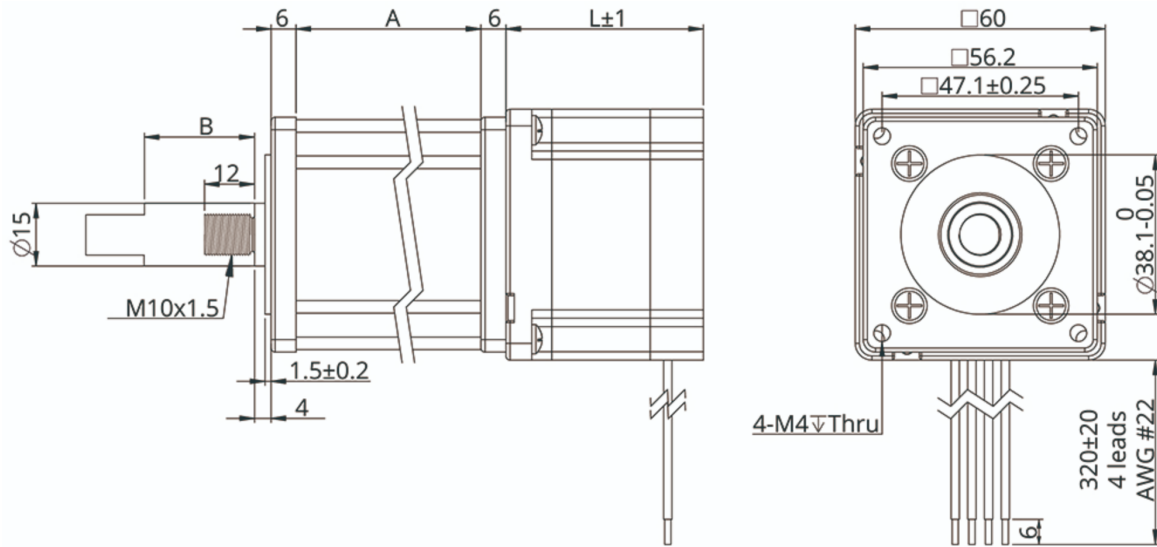


Figure 5.7.12: Technical drawing of the captive linear actuator (Dings’ Intelligent Control Technology Co. Ltd, 2024).

Stroke Specification

Size A (mm)	Stroke B (mm)	Size L (mm)	
45.70	12.70		
52.05	19.05		
58.40	25.40		
64.80	31.80	Single Stack Motor 47	Double Stack Motor 68.3
71.10	38.10		
83.80	50.80		
96.50	63.50		

Figure 5.7.13: Stroke specification table with marked size (Dings’ Intelligent Control Technology Co. Ltd, 2024).

6 Final Design

Figure 6.0.1 shows the completed 3D model of the tribometer. The prototype will be installed in the tribology laboratory at NTNU shortly after the submission of this Bachelor's thesis. The machine drawings of each part of the final design can be found in Appendix B.

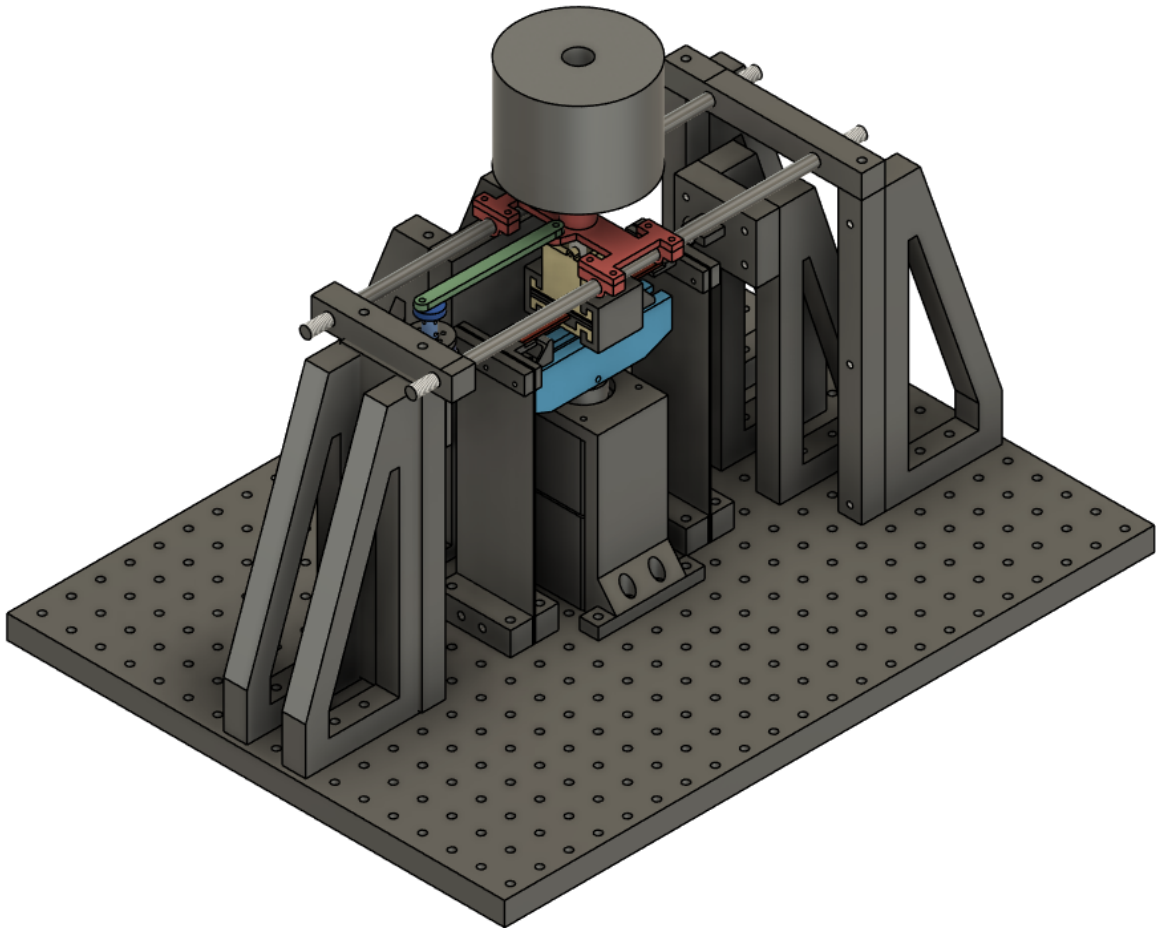


Figure 6.0.1: Final design of the multi-degradation tribometer.

6.1 Entire Friction Mechanism

The final configuration of the friction mechanism (Figure 6.1.1) consists of:

- The third design of the friction mechanism (Subsubsection 5.4.3)
- The second design of the friction mechanism supports (Subsubsection 5.4.12)
- The second design of the test piece holder (Subsubsection 5.4.10)
- The second design of the ball holder (Subsubsection 5.4.6)
- The ball holder hat (Subsubsection 5.4.7)
- The load cell mount (Subsubsection 5.5.1)
- The second design of the motor mount (Subsubsection 5.5.3)

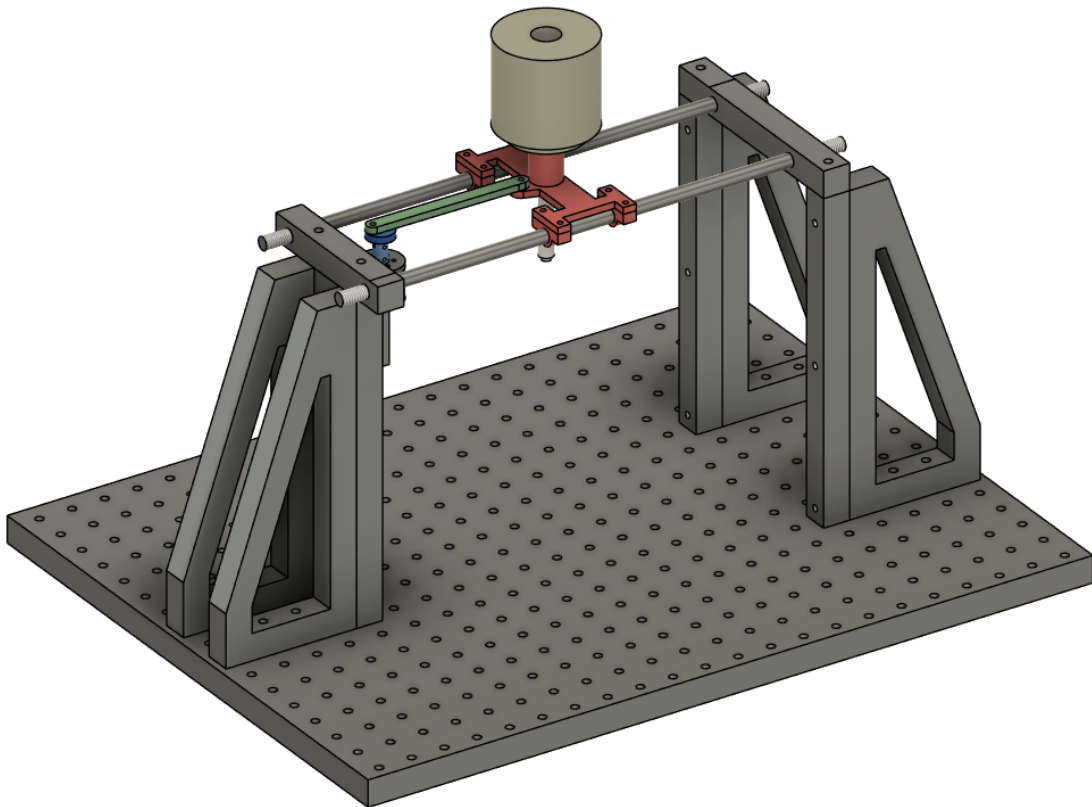


Figure 6.1.1: The final design of the friction mechanism.

6.1.1 Friction Mechanism - Materials

It is foreseen that most, if not all, of the parts of the friction mechanism will be made of stainless steel, with the exception of the ball holder and alumina ball that has to be made out of a non - corrosive material, like PEEK. The spring plates on the test piece holder will be made out of an elastic yet firm metal. The spring plates should allow movement in horizontal axis.

6.1.2 Further Improvements of the Friction Mechanism

Currently, the rod attachments are in direct contact with the rod. The friction between these parts can interfere with the results of the tribotest. To prevent as much friction as possible linear bearings should be implemented in the design.

The placement of the threaded hole where the load cell is connected to the test piece holder is acceptable but inconvenient. A lot of maneuvering is needed to connect the two parts with the screws. A suggestion for future development is to increase the height of the right part of the test piece holder so that it resembles a wall. The wall will have a hole that a screw can go through, and fasten to the load cell.

6.2 Fatigue Load Application

The final design for fatigue load application (Figure 6.2.1) consists of the fourth design of the load application (Subsubsection 5.7.5) and second design of the test piece holder (Subsubsection 5.4.10).

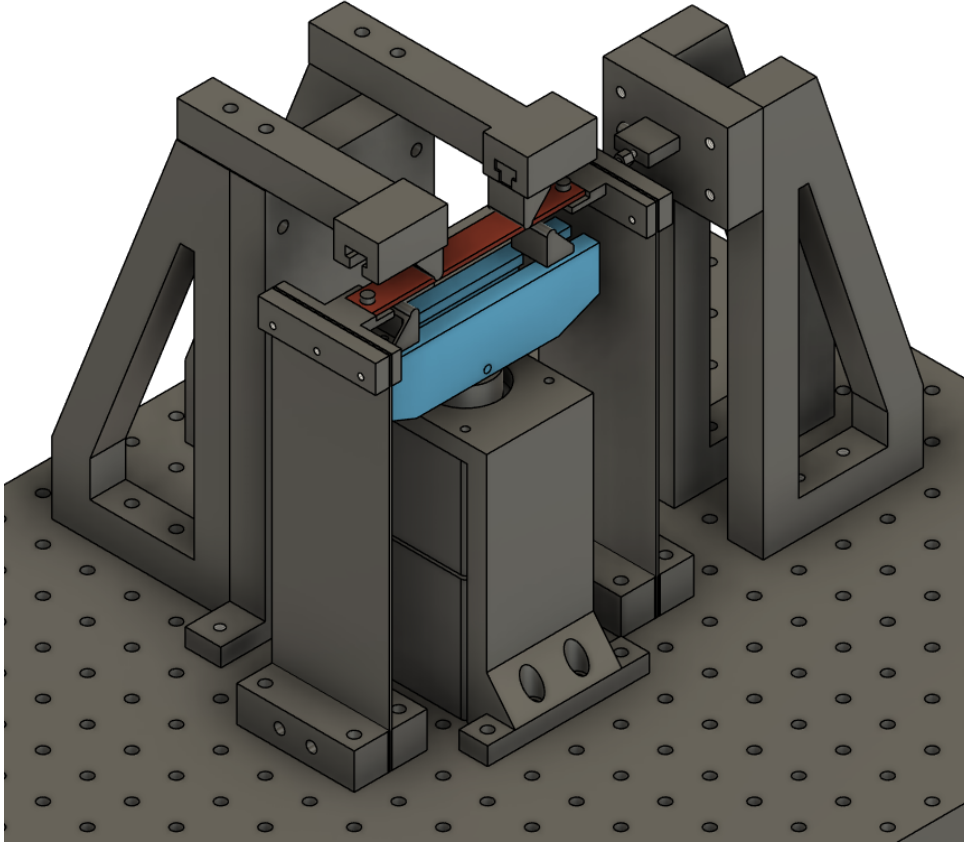


Figure 6.2.1: Final design of the load application mechanism.

6.2.1 Fatigue Load Application - Materials

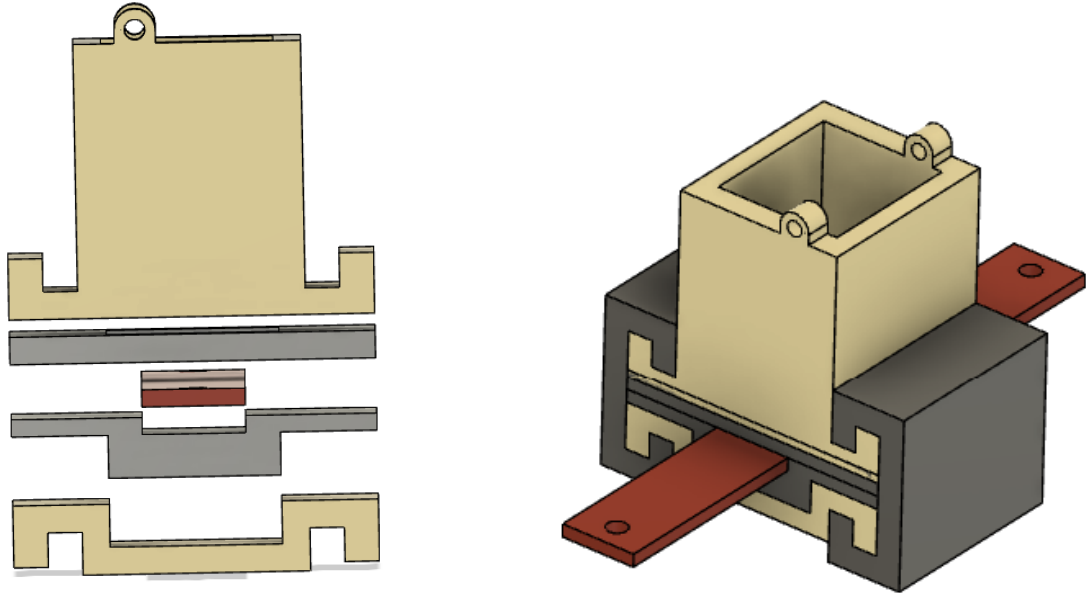
The fatigue load application parts will endure the heaviest loads of the whole tribometer. It is consequential that these parts are made out of strong and durable material like stainless steel.

6.2.2 Further Improvements of the Fatigue Load Application

A concern with the fatigue load application parts is that it has not been tested in practice. Whether or not the support applicator can withstand the force given from the load applicator is unknown. There is a possibility that the supports will bend due to the load applicator.

6.3 Electrochemical Cell

After multiple prototypes of the compartment for the electrochemical cell and seal, the configuration is concluded with the fourth design (Figure 6.3.1).



(a) Assembling order of the electrochemical cell. (b) The electrochemical cell with test piece.

Figure 6.3.1: The final design of the electrochemical cell.

6.3.1 Electrochemical Cell - Material

The compartment for the electrochemical cell must be made out of a non-conductive material, so stainless steel is not an option. PEEK is a good alternative as it is corrosion resistant and durable. The seal has to be made out of an elastic material for the compartment to be able to retain the electrolyte. For this project silicone glued to the compartment proved to work.

6.3.2 Further Improvements of the Electrochemical Cell

Compressing the seal is essential to prevent leakage of the electrolyte during the fatigue bending test. The current solution requires the user to squeeze the compartment parts together to fasten the clasps, which can be a challenging task for a single person if a tool is not used. A solution to this could be to design a specialized tool to assemble the compartment for the electrochemical cell or change the clasps for another method.

6.4 Materials

There is a large degree of freedom when it comes to the choice of materials for this tribometer. Since the whole tribometer is not submerged in the electrolyte, the compartment for the electrochemical cell and the ball holder are the only parts where the materials needs to be carefully chosen so that they do not interfere with the corrosion tests. For all the other parts the main concern is the strength of the materials.

6.5 How to Assemble the Tribometer

All of the parts will be connected to a 25×25 mm grid optical board.

It is recommended that the tribometer should be assembled in following order:

- The stepper motor parts (Figure 5.7.10).
 - Secure the stepper motor and the mount so that there are minimum nine available holes on the left and right side of the mount, and 5 holes behind the mount. This will assure that the supports will fit on the board.
- The test piece holder (Figure 5.4.18).
 - Assemble the test piece holder before attaching it to the optical board. Secure the test piece holders one hole away from the open sides of the stepper motor mount. Make sure that the test piece holder with an extra threaded hole faces to the right.
- The support applicators (Figure 5.7.8).
 - Secure the support applicator wall in the row of holes directly behind the back of the motor mount. Connect the rest of the support applicator pieces together.
- The load cell mount (Figure 5.5.2c).
 - Assemble the load cell mount. Secure the load cell mount one hole away from the test piece holder on the right.
- The left side of the friction mechanism support (Figure 5.4.3).
 - Assemble the left side of the friction mechanism support, then secure to the optical board two hole distances away from the left test piece holder.

- The BLDC motor attachments and mount (Figure 5.5.6).
 - Screw the BLDC motor to the motor mount. Connect the BLDC motor attachment to the motor with the coupling. Secure the motor mount with the attached BLDC motor to the designated holes on the left side of the friction mechanism support.
- The rest of the friction mechanism (Figure 5.4.21).
 - Assemble the right side of the friction mechanism support. Secure it one hole length to the left of the load cell mount.
 - Connect the main body and the rod attachment of the tribometer holder.
 - Thread the tribometer rod through one side of the friction mechanism supports, then the rod attachment and finally through the holes of the other friction mechanism support. Secure the rod on each threaded end with fitted nuts.
 - Connect the main body of the friction mechanism to the BLDC motor attachment, using the arm and attaching it with pins.

6.6 Performing the Tribotest

In this tribometer, the compartment for the electrochemical cell is completely separate from the rest of the machine. This makes it easier to perform the tribotest.

Before starting the tribotest, the compartment for the electrochemical cell needs to be fastened to the test piece. To make sure that this compartment is centered on the test piece, a separate tool is made. This tool is more like a box, where first the bottom part of the compartment for the electrochemical cell is placed. Then the test piece is placed on top, and after that the top of the compartment is placed. This tool is formed so there is only one possible way to lay all the components down and they will stand centered on each other. After fastening the side clasps of the compartment, it is ready to be filled with the electrolyte, which in this tribometer will be salt water.

The support beams and the fatigue load applicator also has to be adjusted to their preferred position. This position is depending on whether it is wished to have the friction test done on the compressive or the tensile side of the test piece.

The deflection of the test piece (given in Table 5.2.1) is the same size as the stroke length of the linear actuator stepper motor. These inputs are then given to the motors controllers.

After the compartment for the electrochemical cell is filled, the support beams and the load applicators are adjusted, and the motor is calibrated, the test piece with the compartment can be placed into the tribometer. After the test piece is slid onto the test piece holder, the pins can be put through the holes of the test piece and the holder, and the electrodes can be threaded into the loops that sits on the top of the compartment.

The friction ball is then put into the ball holder cap and the ball holder top is screwed on to hold the friction ball in place so it will not roll on the test piece. The ball holder, and if necessary, the cork, is put into place in the main body of the friction mechanism.

The testing is then ready to start. The test will go on for a few hours to simulate the actual life cycle of a mechanical component while data is collected from the load cell and the electrochemical process.

7 Limitations

Due to the requirements that were given for the tribometer, and the design that has been made on the background of this, the tribometer has some limitations.

The design of the compartment for the electrochemical cell brings some limitations to the tribometer. Because of the length of the compartment, the largest distance between the support applicators and the load applicators (a value) that can be reached is lower than if the whole tribometer was submerged in the electrolyte. With a lower a value, the force that is needed to reach 90% of the yield strength increases. This makes it so some materials, for example Ti6Al4V, can not be tested in this tribometer because the motor is not powerful enough to reach the needed force.

The compartment for the electrochemical cell also causes limitation in the size of the deflection. Because the compartment is sealed with the help of a silicon seal, the deflection that the test piece can have is limited. If the deflection of the test piece is too high, the seal will not be tight enough around the test piece to prevent leakage.

Both the compartment and the test piece holder come with some limitations for the tribometer. The compartment for the electrochemical cell and the test piece holder are only designed for one specific size of test piece, meaning that the tribometer can only perform tests when the test piece is this specific size. The compartment is only designed for a specific width and height and the test piece holder is designed for one specific width and length. The perpendicular distance between the test piece holder and the support beams is also designed precisely as big as the test piece's height since neither the test piece holder nor the support beams can move along the z-axis. If it was possible to change the size of the test piece, both the force needed to get to 90% of the yield strength and the deflection could be changed. This means that if it was possible to change the size it would also be possible to test more materials.

As mentioned earlier this tribometer can perform the tribotest on both the tensile side and the compressive side of the test piece. This is possible because the support beams and the load applicator are manually adjustable and depending on where on the test piece

these hit, the tribotest is done on either the tensile or the compressive side. But since this change happens manually and the location of the applied loads and the support beams have to change, it is not possible to perform the tribotest on the tensile side and the compressive side in the same test.

8 Conclusions

This project has given the group great insight into the field of tribology, a field that all of the group members had very little previous knowledge about. The project has also left the members of the group with valuable experiences about working and communicating with others, product development and writing academic texts. These were the goals that the group set before starting the project, and they were able to meet the goals by cooperating and solving problems together.

The main focus has been to design a prototype of a tribometer that can be used in the tribology laboratory at NTNU in Trondheim. The criteria that was given for the tribometer was that it should be able to test metallic samples exposed to corrosion, friction and bending fatigue simultaneously. Through brainstorming ideas and with the help from the supervisors, the group was able to come up with a design that meets these criteria.

Overall, working on this Bachelor's thesis has been a great way for the group to experience what it is like to work on bigger projects. It has been fun to be able to use the knowledge gained from previous courses in a more practical way, and to see the results of the work that has been put into these last three years of studying mechanical engineering at NTNU.

After submitting this Bachelor's thesis, the members of the group will be joining one of the supervisors in assembling the prototype of the tribometer in the tribology laboratory at NTNU.

References

- Ajay, V., Nakrani, J., Mishra, N. K., & Shrivastava, A. (2019). *Fatigue crack growth behavior of ss316l deposition from wire arc additive manufacturing*. <https://www.sciencedirect.com/science/article/pii/S2213846323001177> (accessed: 19.05.2024).
- ASTM International. (2013). *Astm e855-08 standard test methods for bend testing of metallic flat materials for spring applications involving static loading1*.
- Bakshi, B. R. (2019). *Sustainable engineering: Principles and practice*. Cambridge University Press.
- Boston University. (n.d.). *Mechanics of materials: Bending – normal stress*. <https://www.bu.edu/moss/mechanics-of-materials-bending-normal-stress/> (accessed: 20.05.2024).
- C. B. von der Ohe and R. Johansen and N. Espallargas. (2011). A multi-degradation test rig for studying the synergy effects of tribocorrosion interacting with 4-point static and cyclic bending. *Wear*.
- Carlota, V. (2023). *All you need to know about pla for 3d printing*. <https://www.3dnatives.com/en/pla-3d-printing-guide-190820194/#!> (accessed: 08.05.2024).
- Dam, R. F. (2024). *The 5 stages in the design thinking process*. <https://www.interaction-design.org/literature/article/5-stages-in-the-design-thinking-process> (accessed: 09.05.2024).
- Dings' Intelligent Control Technology Co. Ltd. (2024). *Size 24, stepper lead screw linear actuator*. https://www.faulhaber.com/fileadmin/Import/Media/EN_4221_BXTH_SC_DFF.pdf (accessed: 20.05.2024).
- ETH Corrosion. (2021). *Three electrode setup*. <https://www.youtube.com/watch?v=koCodYF1m9U> (accessed: 26.04.2024).
- Faulhaber. (n.d.). *Stepper motor basics*. https://www.faulhaber.com/fileadmin/Import/Media/AN001_EN.pdf (accessed: 13.05.2024).
- Faulhaber. (2021). *Brushless dc-servomotors: Series 4221g024bxt h sc*. https://www.faulhaber.com/fileadmin/Import/Media/EN_4221_BXTH_SC_DFF.pdf (accessed: 20.05.2024).
- Flintec. (2024). *What is a tension load cell, and how does it work?* <https://www.flintec.com/weight-sensors/load-cells/how-does-a-tension-load-cell-and-how-does-it-work> (accessed: 13.05.2024).

-
- Igual, A., Espallargas, N., & Mischler, S. (2020). *Tribocorrosion*. Springer.
- IMETRA. (n.d.). *Peek material properties*. <https://www.imetra.com/peek-material-properties/> (accessed: 08.05.2024).
- Johannessen, J. (2018). *Tekniske tabeller*. Cappelen.
- Kutz, M. (2012). *Handbook of environmental degradation of materials - second edition*. Elsevier.
- Lehigh University. (n.d.). *Tribometry and instrumentation*. <https://www.lehigh.edu/~intribos/tribodesign.html> (accessed: 23.04.2024).
- Lesics. (2014). *Brushless dc motor, how it works ?* <https://www.youtube.com/watch?v=bCEiOnuODac> (accessed: 02.05.2024).
- Loadstar Sensors. (n.d.). *Res2 s-beam jr. load cell*. <https://www.loadstarsensors.com/res2.html> (accessed: 21.05.2024).
- Lower, S. (n.d.). *16.8: Electrochemical corrosion*. [https://chem.libretexts.org/Bookshelves/General_Chemistry/Chem1_\(Lower\)/16%3A_Electrochemistry/16.08%3A_Electrochemical_Corrosion](https://chem.libretexts.org/Bookshelves/General_Chemistry/Chem1_(Lower)/16%3A_Electrochemistry/16.08%3A_Electrochemical_Corrosion) (accessed: 22.04.2024).
- Morshed, A., Wu, H., & Jiang, Z. (2021). A comprehensive review of water-based nanolubricants, 28–29. https://www.researchgate.net/publication/354517522_A_Comprehensive_Review_of_Water-Based_Nanolubricants
- NASA. (n.d.). *Newton's laws of motion*. <https://www1.grc.nasa.gov/beginners-guide-to-aeronautics/newtons-laws-of-motion/> (accessed: 01.05.2024).
- Panduro. (n.d.). *Lag dine egne silikonformer - sett med 2x300 ml silikonkomponent*. https://panduro.com/nb-no/products/skap-dekorer/stoping/stopematerialer/lag-dine-egne-silikonformer-sett-med-2-%C3%97300-ml-silikonkomponent-500859?gad_source=1&gclid=CjwKCAjw-OwBhBnEiwAgwzrUssxo7jmvR1Z0BEAddsKu7ZWtEkQsIhraslpZRUD6ucbiqI3x/96shxoCnQUQAvD_BwE#fo_c=3247&fo_k=e1aa1e38d44c05a433e3e7122d76122&fo_s=gplano (accessed: 03.05.2024).
- ProductPlan. (n.d.). *What is product development?* <https://www.productplan.com/learn/what-is-product-development/> (accessed: 09.05.2024).
- RS. (2023). *The complete guide to dc motors*. <https://uk.rs-online.com/web/content/discovery/ideas-and-advice/dc-motors-guide> (accessed: 02.05.2024).
- SINTEF. (n.d.). *Digitalisering*. <https://www.sintef.no/fagomrader/digitalisering/> (accessed: 09.05.2024).
-

-
- SINTEF. (2013). Tribocorrosion: A threat to materials. https://www.sintef.no/globalassets/upload/materialer_kjemi/faktaark/tribocorrosion.pdf
- Society of Tribologist and Lubrication Engineers. (n.d.). *Introduction to tribology*. https://www.stle.org/files/What_is_tribology/Tribology_Wear.aspx (accessed: 23.04.2024).
- Solutions, A. H. K. P. M. (2019). *What is a captive actuator?* <https://www.youtube.com/watch?v=JWSLN6FHIO4> (accessed: 13.05.2024).
- SRM Industries. (2023). *The pros and cons of silicone rubber: Is it the perfect material for your project?* <https://srm-industries.com/the-pros-and-cons-of-silicone-rubber-is-it-the-perfect-material-for-your-project/> (accessed: 01.05.2024).
- Stansbury, E. E., & Buchanan, R. A. (2000). *Fundamentals of electrochemical corrosion*. ASM International.
- Tennessee Tech University. (n.d.). *Static equilibrium*. <https://www2.tntech.edu/leap/murdock/books/v2chap3.pdf> (accessed: 19.05.2024).
- The Engineering Mindset. (2021). *How stepper motors work - electric motor*. <https://www.youtube.com/watch?v=09Mpkjcr0bo=> (accessed: 02.05.2024).
- United Nations. (n.d.-a). *The 17 goals*. <https://sdgs.un.org/goals> (accessed: 09.05.2024).
- United Nations. (n.d.-b). *Sustainability*. <https://www.un.org/en/academic-impact/sustainability> (accessed: 09.05.2024).
- United Nations Development Programme. (n.d.). *What are the sustainable development goals?* <https://www.undp.org/sustainable-development-goals> (accessed: 09.05.2024).
- University of Pennsylvania. (n.d.). *Three point and four point bending*. <https://www.med.upenn.edu/pcmd/3pt-4pt-bending.html> (accessed: 22.04.2024).
- WAYKEN Rapid Manufacturing. (2022). *A complete guide to peek material & properties*. <https://waykenrm.com/blogs/peek-material-and-properties/> (accessed: 08.05.2024).
- Wente, E. F., Nutting, J., & Wondris, E. (2023). *Steel*. <https://www.britannica.com/technology/steel/Effects-of-heat-treating> (accessed: 19.05.2024).
- Worldsteel Organisation. (2024). *What is steel?* <https://worldsteel.org/about-steel/what-is-steel/> (accessed: 19.05.2024).
- Yakout, M., Elbestawi, M., & Veldhuis, S. C. (2019). *Density and mechanical properties in selective laser melting of invar 36 and stainless steel 316l*. <https://www.sciencedirect.com/science/article/pii/S0924013618304953> (accessed: 19.05.2024).
-

REFERENCES

- Zemic Europe. (2024). *Load cells and force sensors*. <https://www.zemiceurope.com/en/loadcell> (accessed: 13.05.2024).
- Zhoa, J., & Yu, Y. (2011). *Brushless dc motor fundamentals*. https://www.monolithicpower.com/media/document/Brushless_DC_Motor_Fundamentals.pdf (accessed: 02.05.2024).

Appendix A
Calculations

Calculations for force and deflection for different materials

Using Equations 2.4.2 and 2.4.3 and the calculated formula for the maximum needed moment to get to the maximum stress value, the force can be calculated:

$$\sigma_{max} = \frac{M_{max} \times \frac{h}{2}}{I_z}$$

$$M(x) = -\frac{F}{2} \times a$$

$$\sigma_{max} = \frac{\frac{F}{2} \times a \times \frac{h}{2}}{I_z} \rightarrow F = \frac{4 \times \sigma_{max} \times I_z}{a \times h}$$

$$I_z = \frac{b \times h^3}{12} \rightarrow F = \frac{\sigma_{max} \times b \times h^2}{3 \times a}$$

σ_{max} is given as 90 % of the yield strength of the material:

$$\sigma_{max} = \sigma_y \times 90 \%$$

The deflection can then be calculated using formula 2.3.3

$$\delta = \frac{F \times a \times (3 \times L^2 - 4 \times a^2)}{4 \times b \times h^3 \times E_b}$$

For SS316L:

$$\sigma_{max} = 170 \text{ MPa} \times 90 \%$$

$$\sigma_{max} = 153 \text{ MPa}$$

$$F = \frac{153 \text{ MPa} \times 15 \text{ mm} \times (2.5 \text{ mm})^2}{3 \times 20 \text{ mm}}$$

$$F = 230.0625 \text{ N}$$

$$\delta = \frac{230.0625 \text{ N} \times 20 \text{ mm} \times (3 \times (90 \text{ mm})^2 - 4 \times (20 \text{ mm})^2)}{4 \times 15 \text{ mm} \times (2.5 \text{ mm})^3 \times 193000 \text{ MPa}}$$

$$\delta = 0.5772621762 \text{ mm}$$

For SDSS UNS S32750:

$$\sigma_{max} = 550 \text{ MPa} \times 90 \%$$

$$\sigma_{max} = 495 \text{ MPa}$$

$$F = \frac{495 \text{ MPa} \times 15 \text{ mm} \times (2.5 \text{ mm})^2}{3 \times 20 \text{ mm}}$$

$$F = 773.4375 \text{ N}$$

$$\delta = \frac{773.4375 \text{ N} \times 20 \text{ mm} \times (3 \times (90 \text{ mm})^2 - 4 \times (20 \text{ mm})^2)}{4 \times 15 \text{ mm} \times (2.5 \text{ mm})^3 \times 210000 \text{ MPa}}$$

$$\delta = 1.783571429 \text{ mm}$$

For mild steel:

$$\sigma_{max} = 350 \text{ MPa} \times 90 \%$$

$$\sigma_{max} = 315 \text{ MPa}$$

$$F = \frac{315 \text{ MPa} \times 15 \text{ mm} \times (2.5 \text{ mm})^2}{3 \times 20 \text{ mm}}$$

$$F = 492.1875 \text{ N}$$

$$\delta = \frac{492.1875 \text{ N} \times 20 \text{ mm} \times (3 \times (90 \text{ mm})^2 - 4 \times (20 \text{ mm})^2)}{4 \times 15 \text{ mm} \times (2.5 \text{ mm})^3 \times 210000 \text{ MPa}}$$

$$\delta = 1.135 \text{ mm}$$

For bearing steel:

$$\sigma_{max} = 520 \text{ MPa} \times 90 \%$$

$$\sigma_{max} = 468 \text{ MPa}$$

$$F = \frac{468 \text{ MPa} \times 15 \text{ mm} \times (2.5 \text{ mm})^2}{3 \times 20 \text{ mm}}$$

$$F = 731.25 \text{ N}$$

$$\delta = \frac{731.25 \text{ N} \times 20 \text{ mm} \times (3 \times (90 \text{ mm})^2 - 4 \times (20 \text{ mm})^2)}{4 \times 15 \text{ mm} \times (2.5 \text{ mm})^3 \times 210000 \text{ MPa}}$$

$$\delta = 1.686285714 \text{ mm}$$

For inconel 625

$$\sigma_{max} = 580 \text{ MPa} \times 90 \%$$

$$\sigma_{max} = 522 \text{ MPa}$$

$$F = \frac{522 \text{ MPa} \times 15 \text{ mm} \times (2.5 \text{ mm})^2}{3 \times 20 \text{ mm}}$$

$$F = 815.625 \text{ N}$$

$$\delta = \frac{815.625 \text{ N} \times 20 \text{ mm} \times (3 \times (90 \text{ mm})^2 - 4 \times (20 \text{ mm})^2)}{4 \times 15 \text{ mm} \times (2.5 \text{ mm})^3 \times 208000 \text{ MPa}}$$

$$\delta = 1.898942308 \text{ mm}$$

For Ti6Al4V

$$\sigma_{max} = 880 \text{ MPa} \times 90 \%$$

$$\sigma_{max} = 792 \text{ MPa}$$

$$F = \frac{792 \text{ MPa} \times 15 \text{ mm} \times (2.5 \text{ mm})^2}{3 \times 20 \text{ mm}}$$

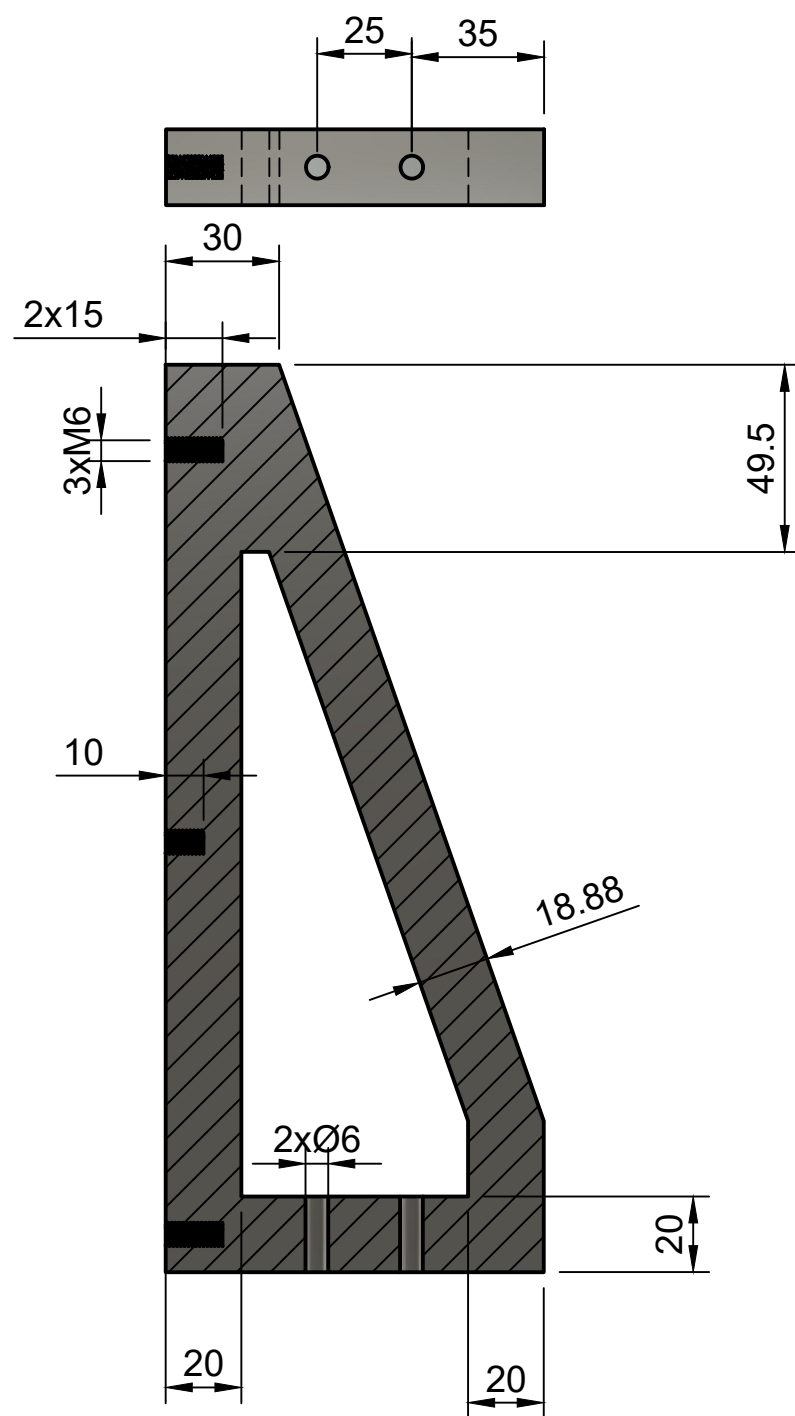
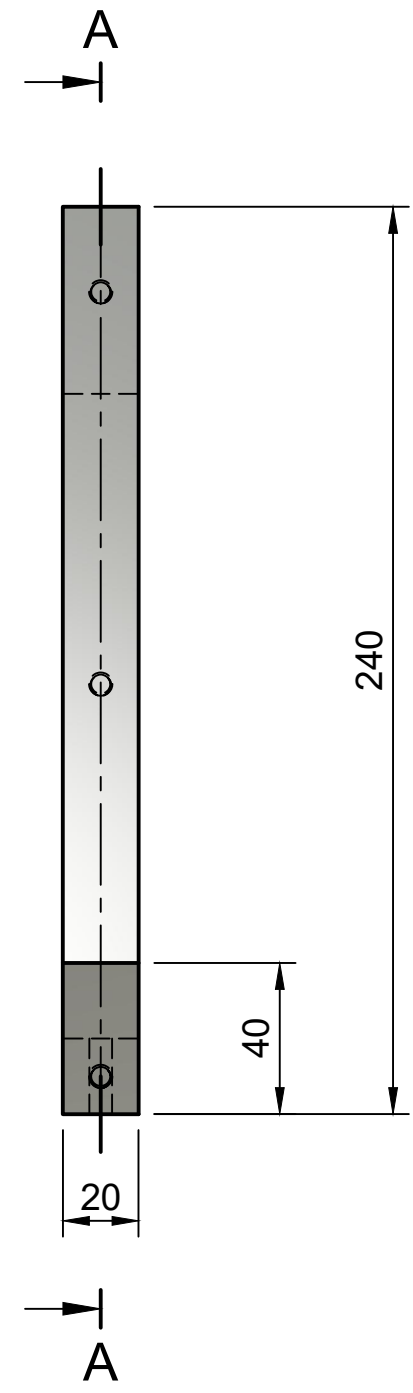
$$F = 1237.5 \text{ N}$$

$$\delta = \frac{1237.5 \text{ N} \times 20 \text{ mm} \times (3 \times (90 \text{ mm})^2 - 4 \times (20 \text{ mm})^2)}{4 \times 15 \text{ mm} \times (2.5 \text{ mm})^3 \times 113800 \text{ MPa}}$$

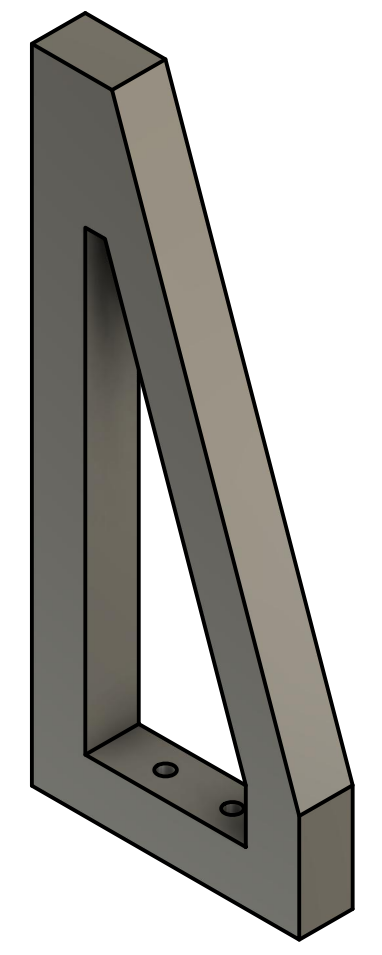
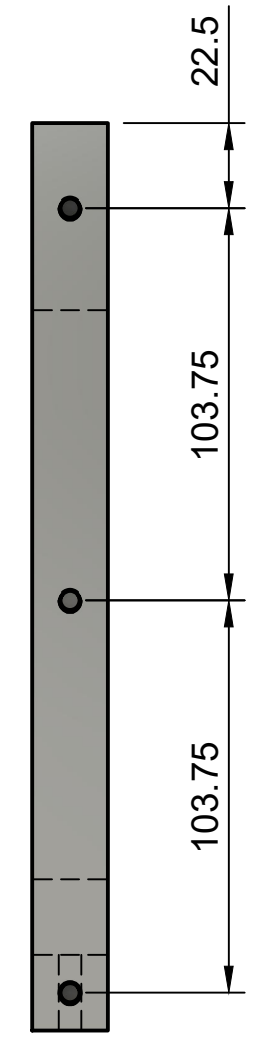
$$\delta = 5.266080844 \text{ mm}$$

Appendix B
Machine Drawings

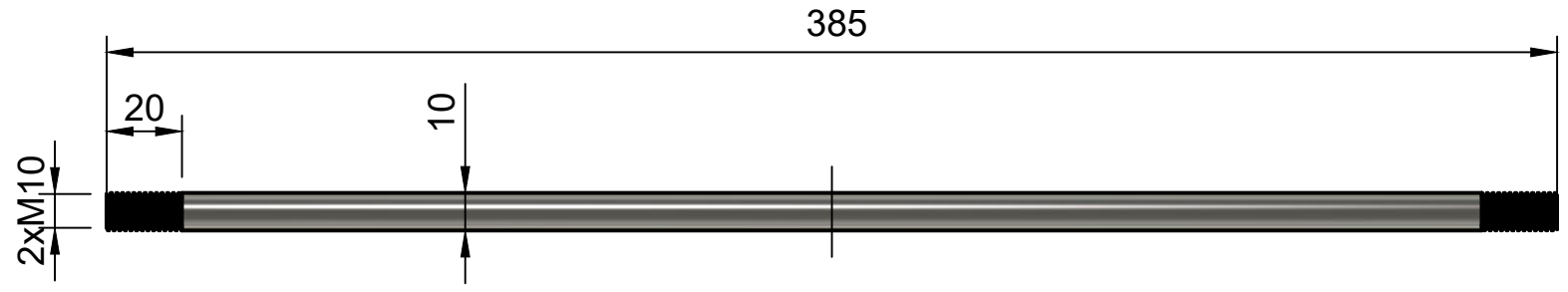
4x Triangular beam



A-A (1:2)

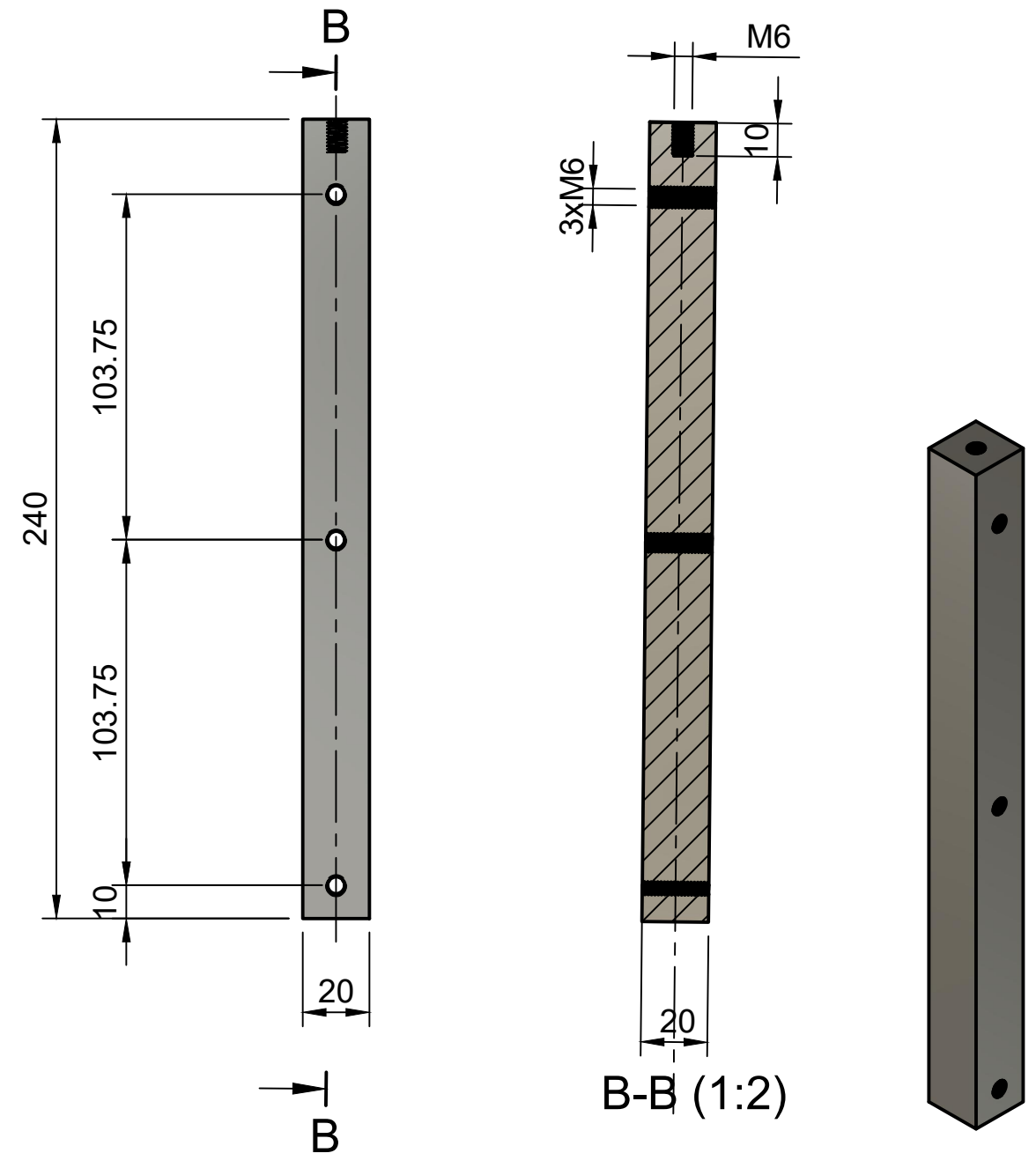


2x Rod

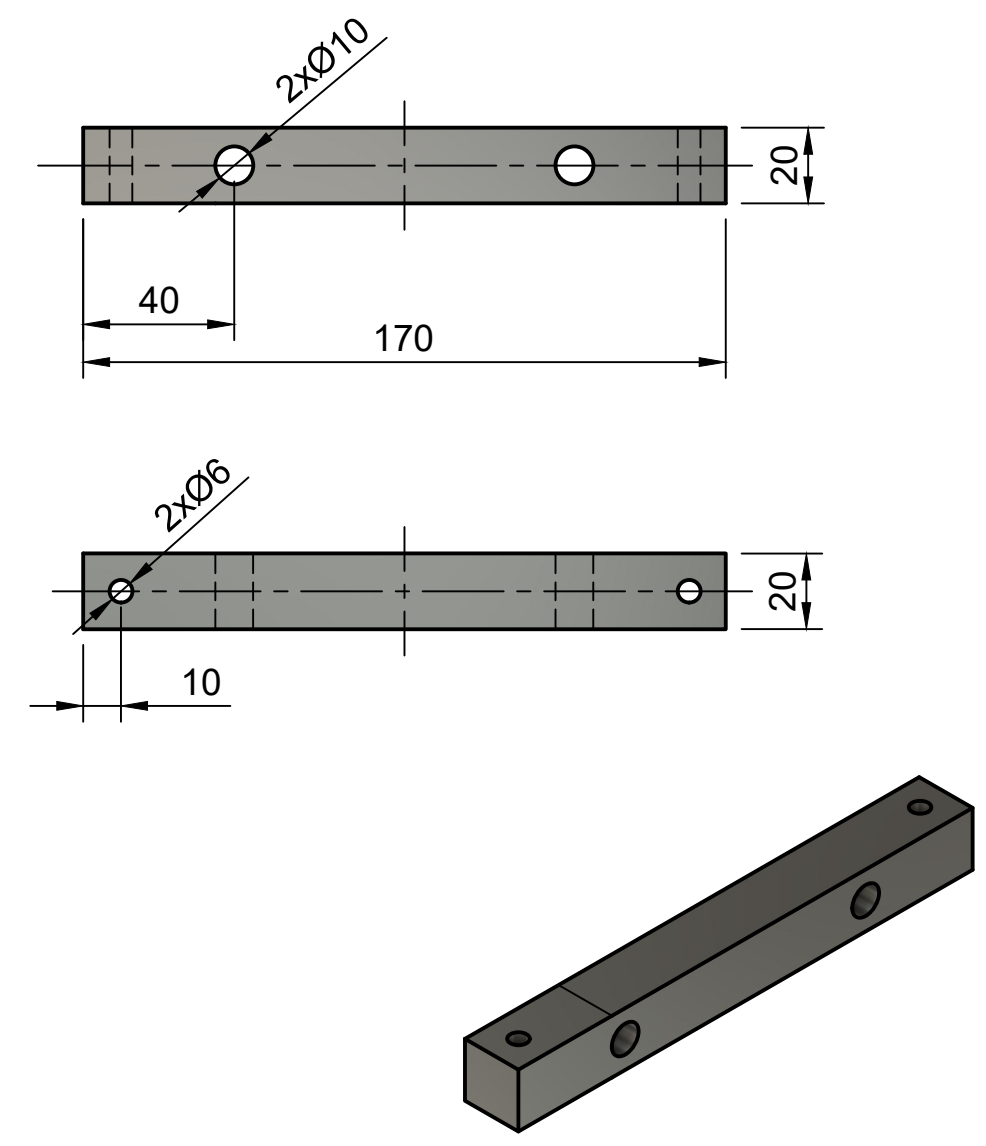


Name Elin	Title Triangular beam and rod
Scale 1:2	Material Stainless Steel
Number	1

2x Support beam - right side

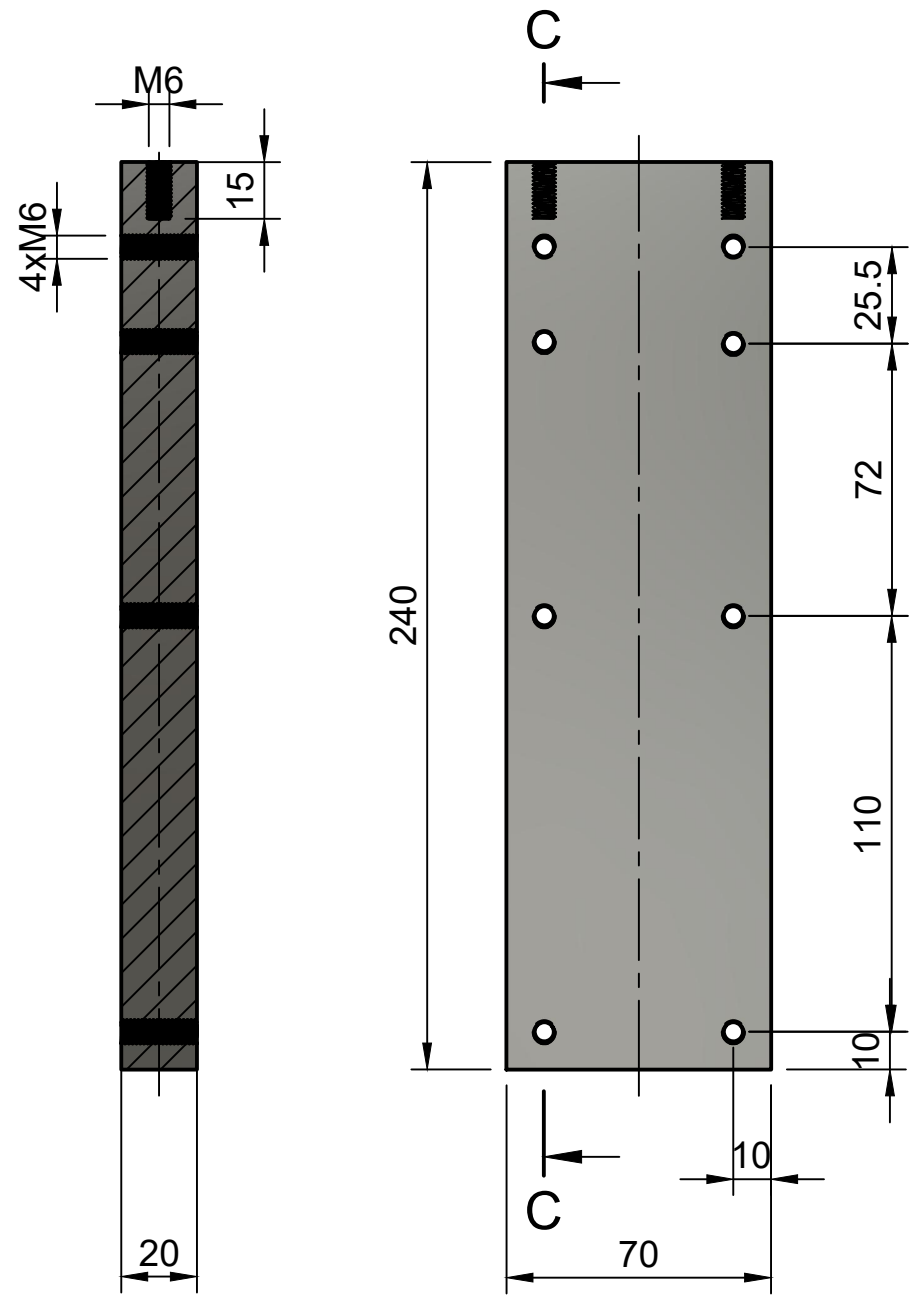


1x Support for rods - right side



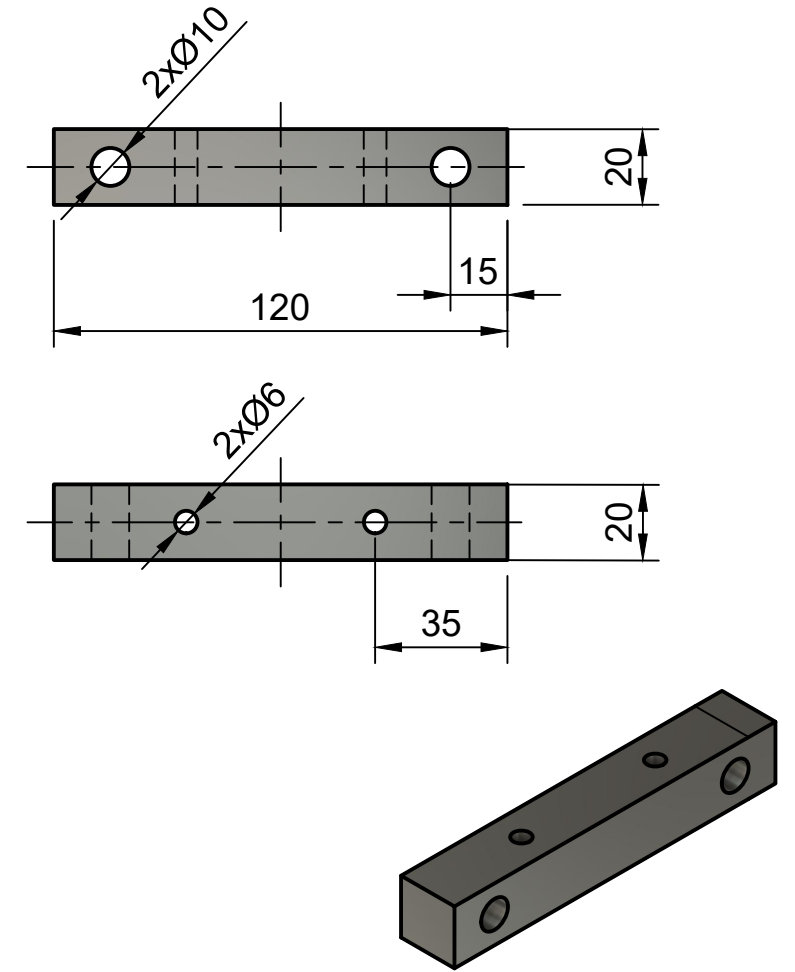
Name	Elin	Title	Support right side
Scale	1:2	Material	Stainless Steel
Number	2		

1x Supportwall - left side



C-C (1:2)

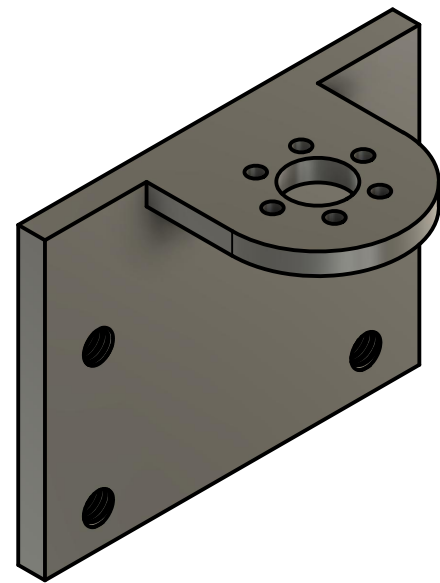
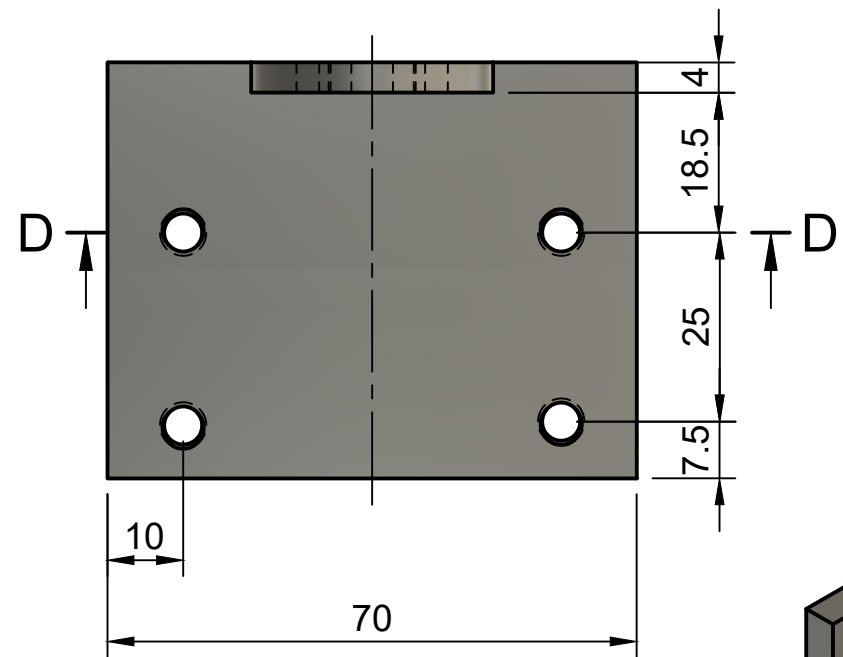
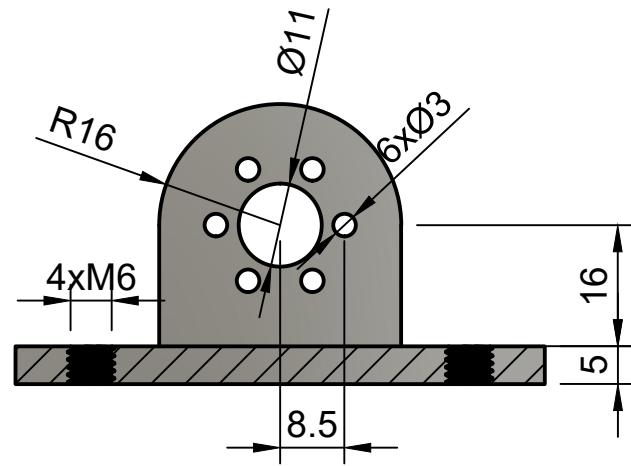
1x Support for rods - left side



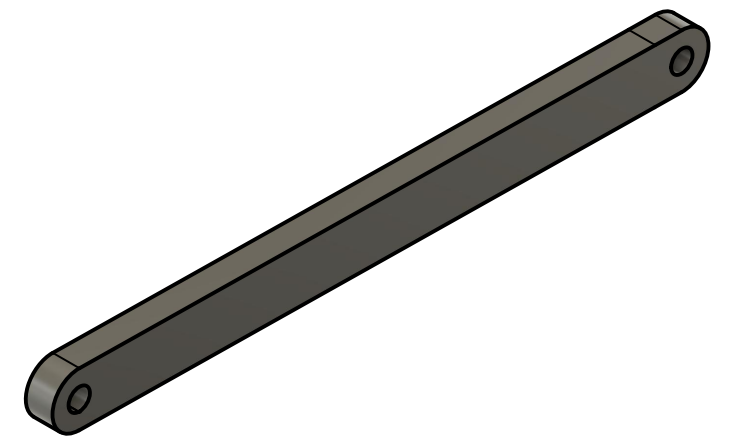
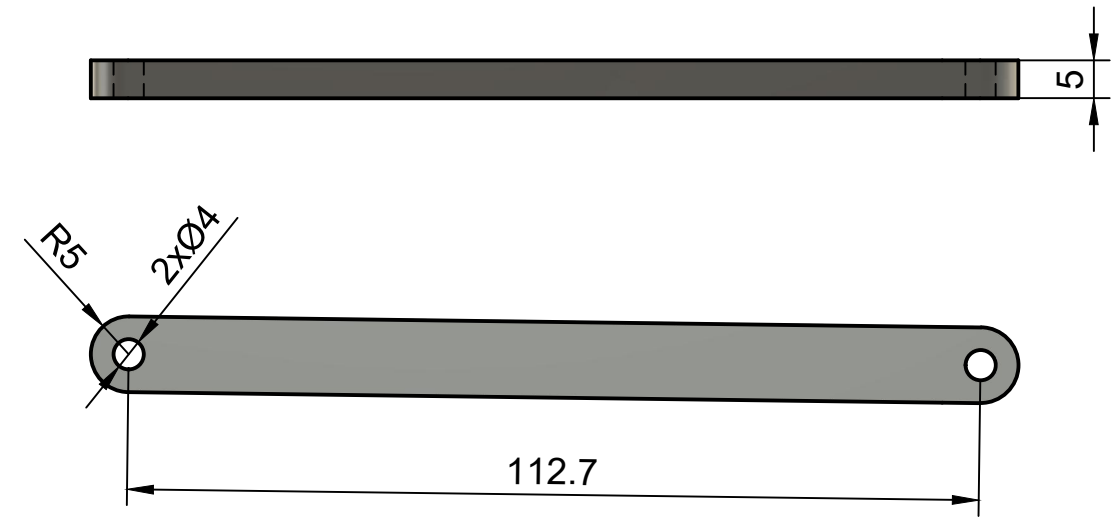
Name Elin	Title Support left side
Scale 1:2	Material Stainless Steel
Number	3

1x Motor mount

D-D (1:1)

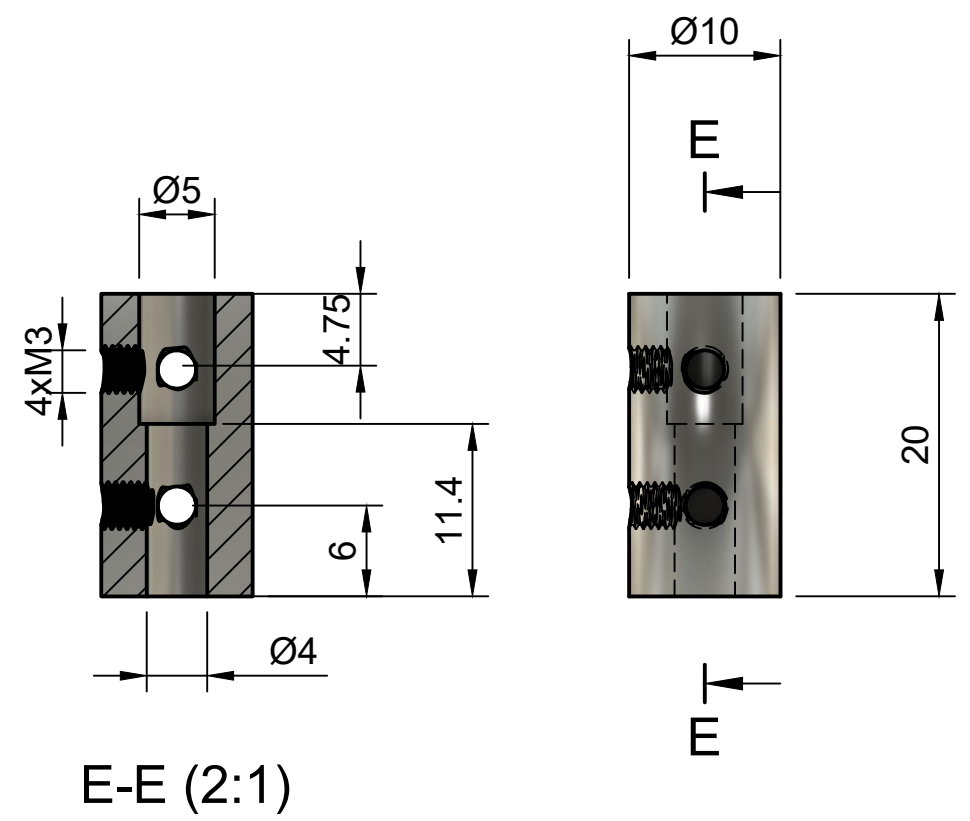


1x Arm

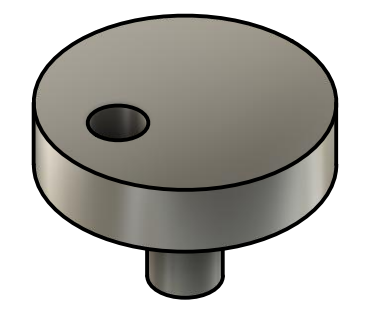
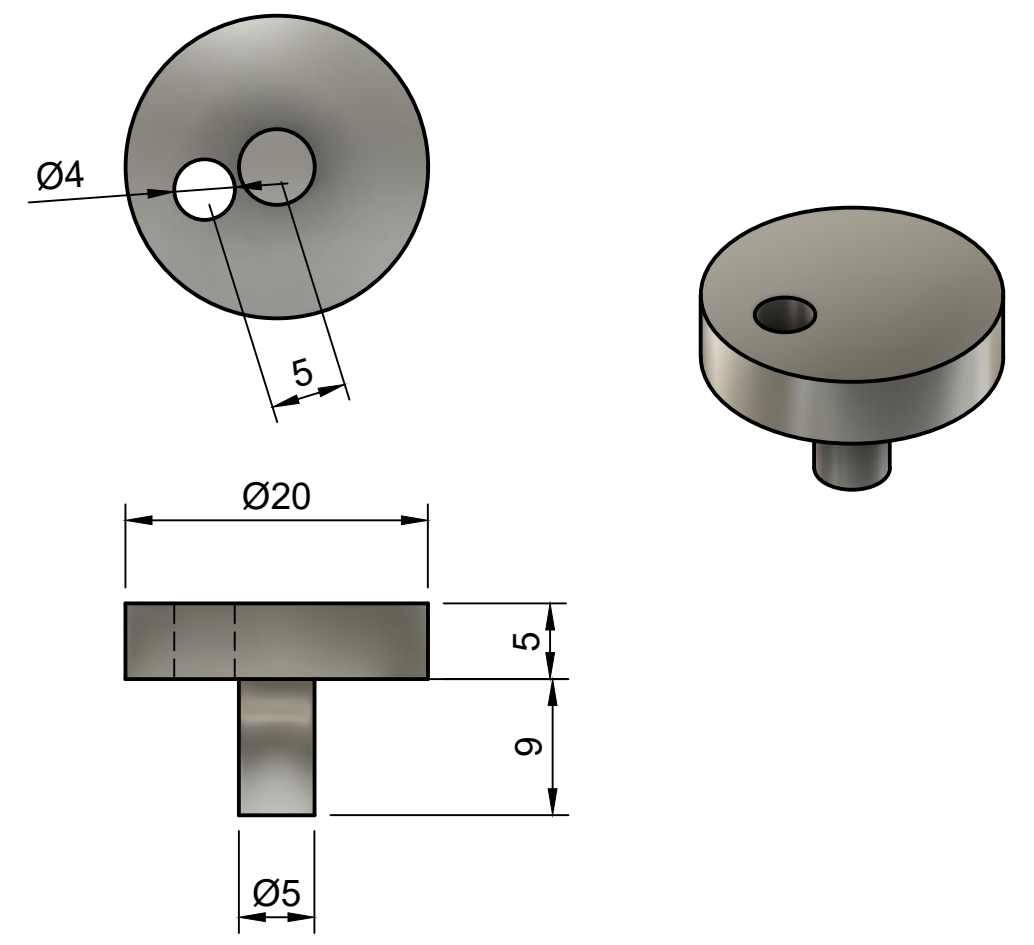


Name Elin	Title Motor mount and arm
Scale 1:1	Material Stainless Steel
Number	4

1x Motor - attachment coupling

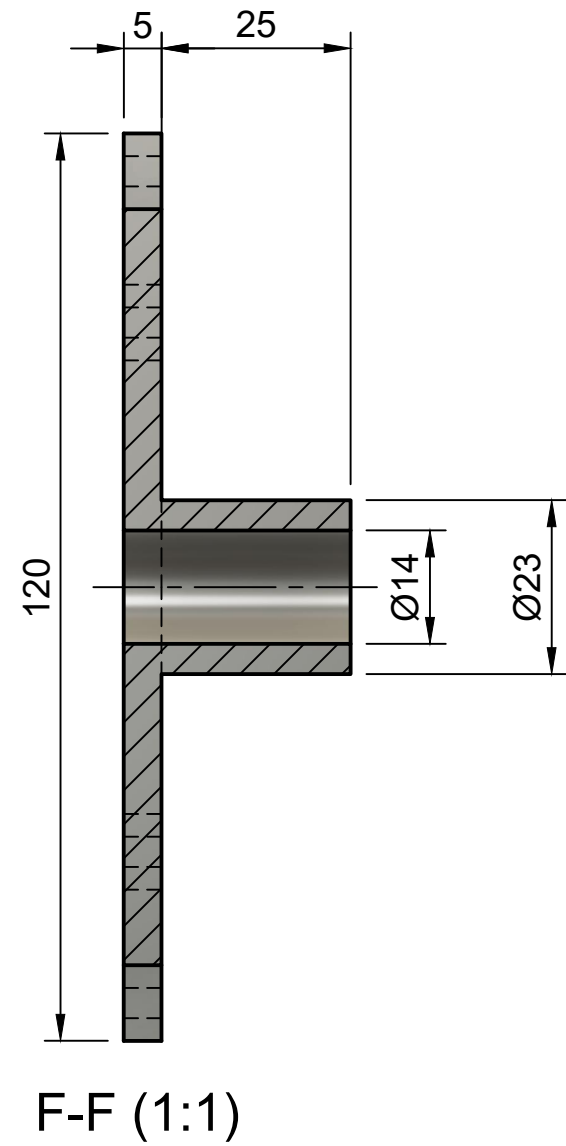
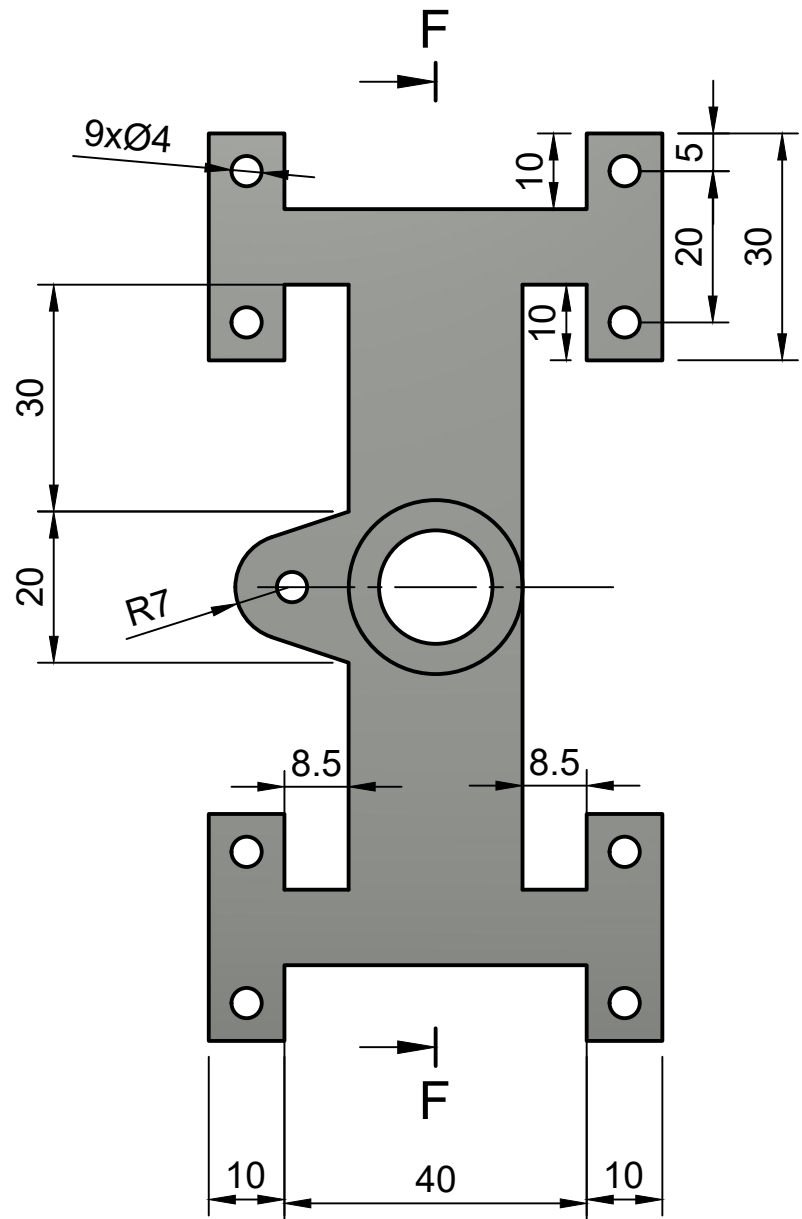


1x Motor attachment

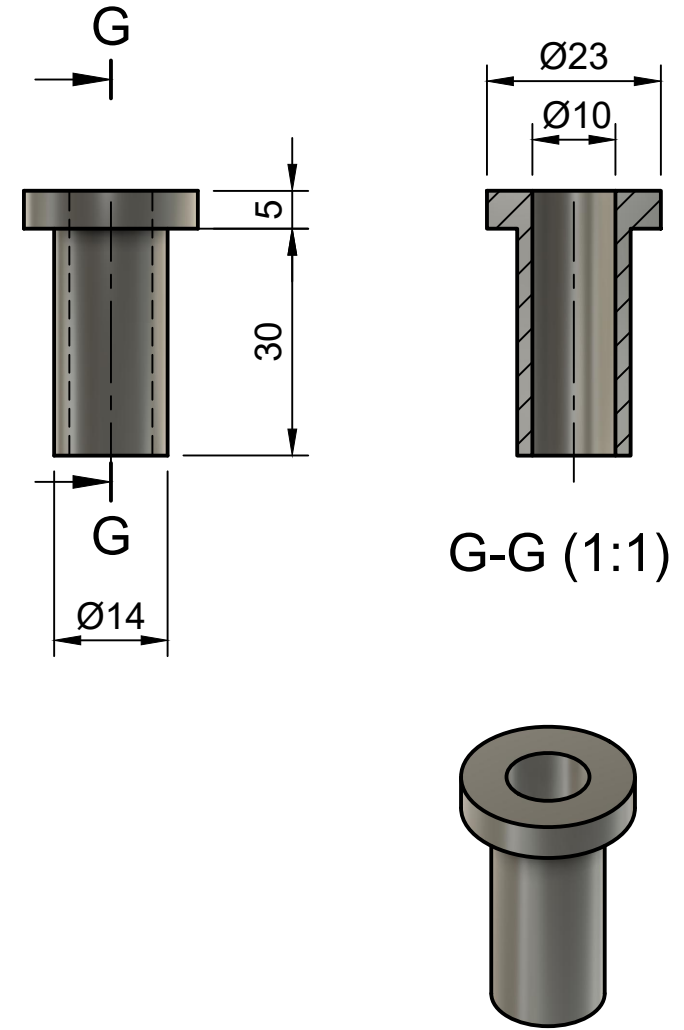


Name Elin	Title Motor attachments
Scale 2:1	Material Stainless Steel
Number	5

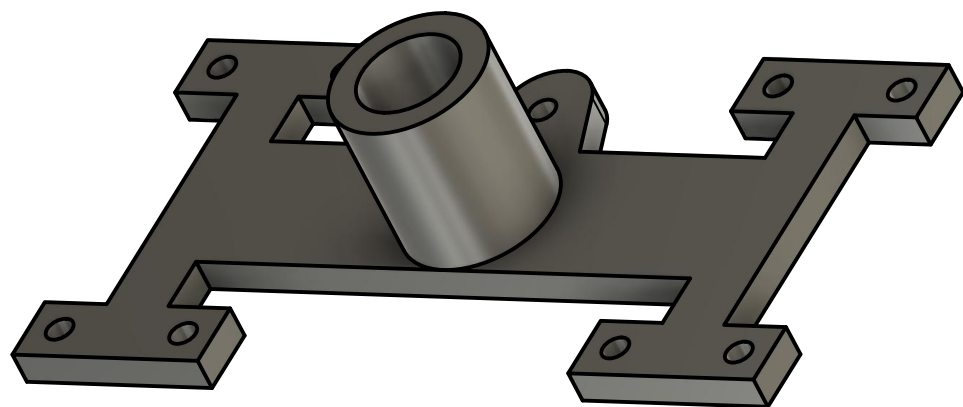
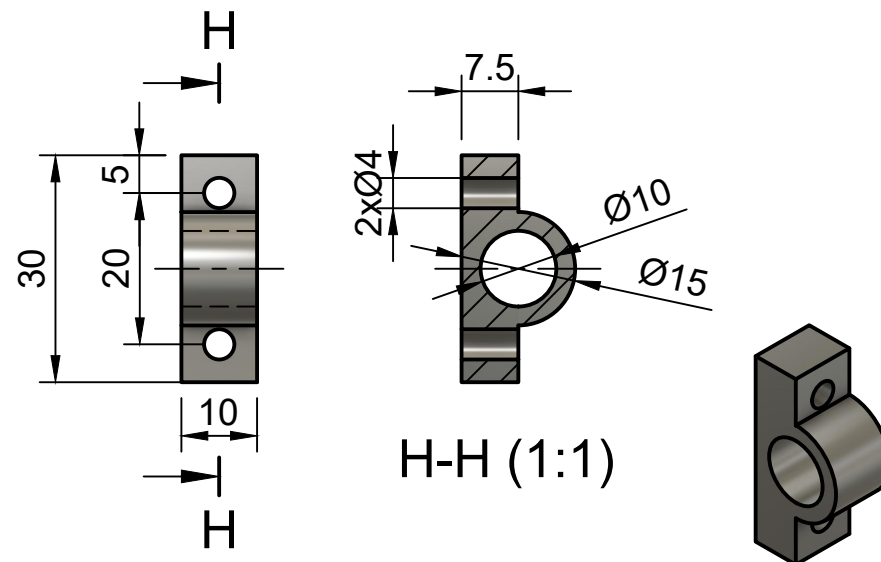
1x Main body of friction mechanism



1x Cork for friction mechanism

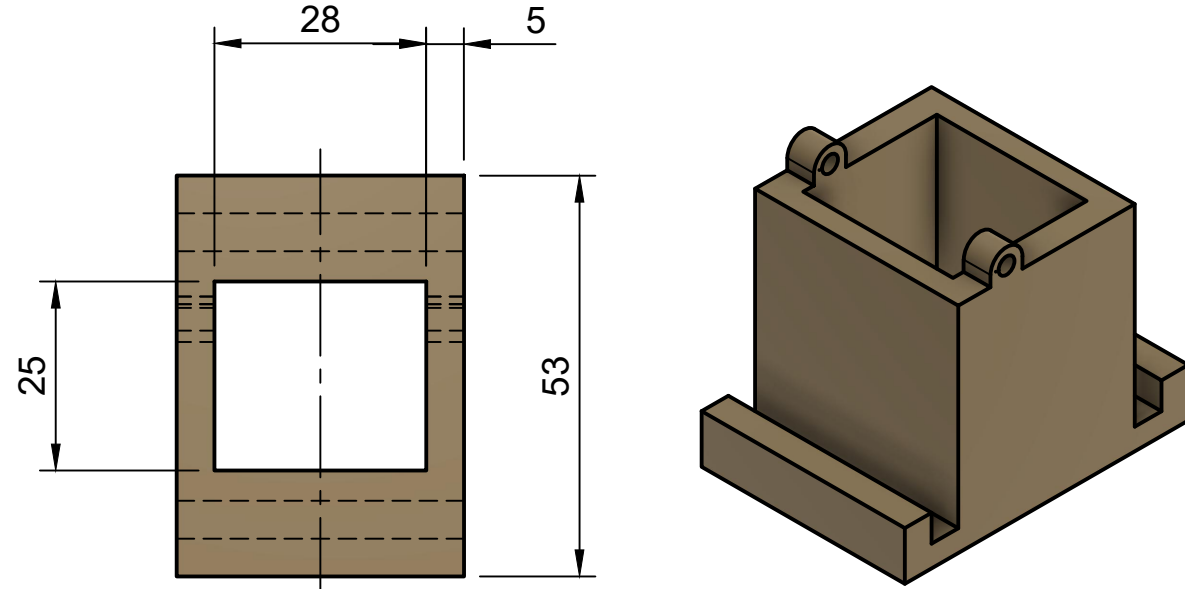


4x Rod attachments

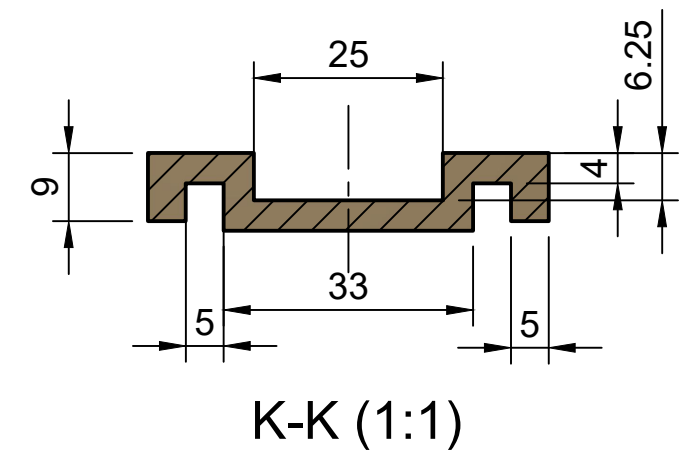
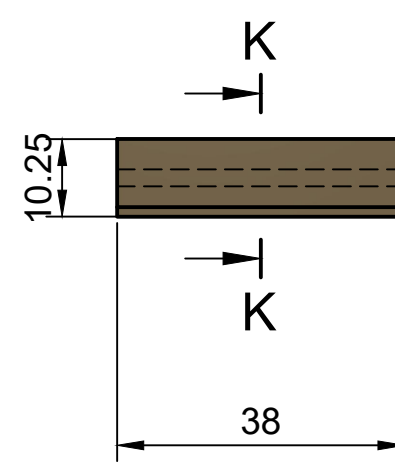
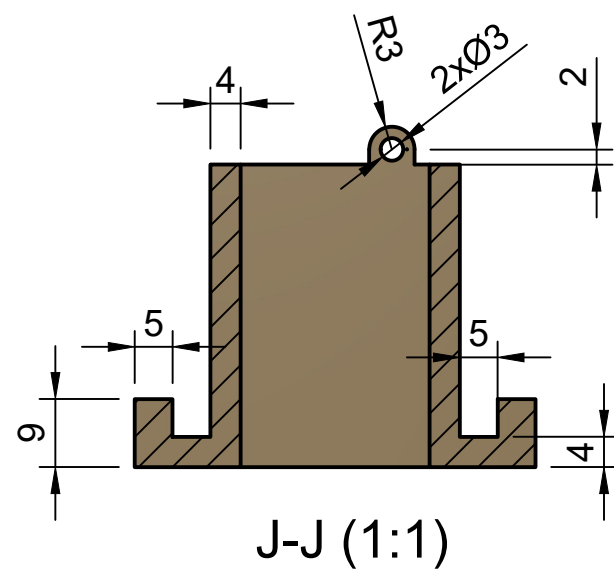
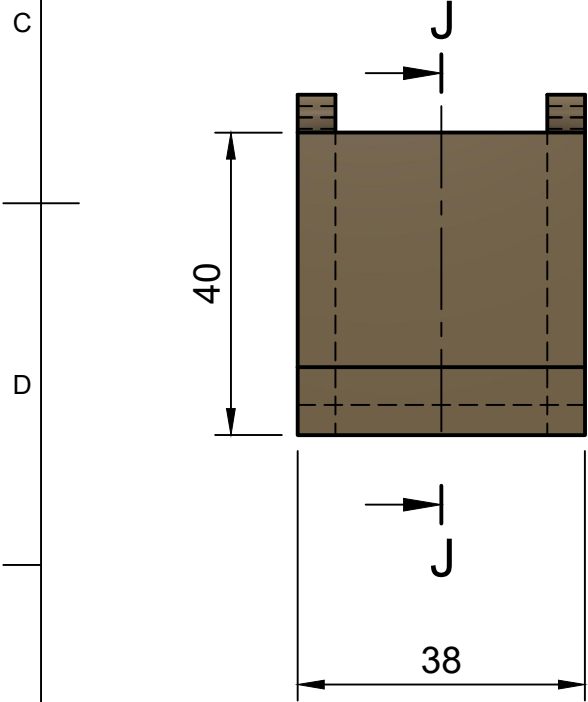
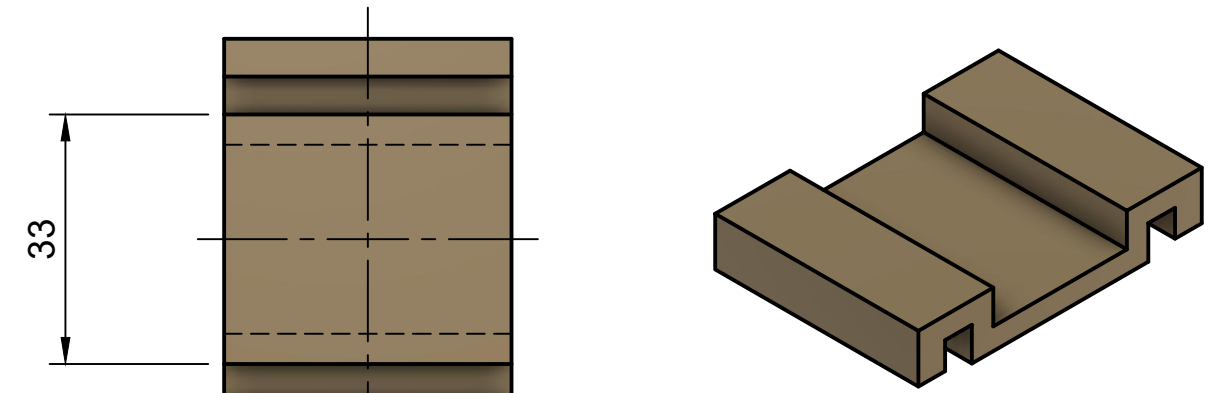


Name Elin	Title Friction mechanism
Scale 1:1	Material Stainless Steel
Number 6	

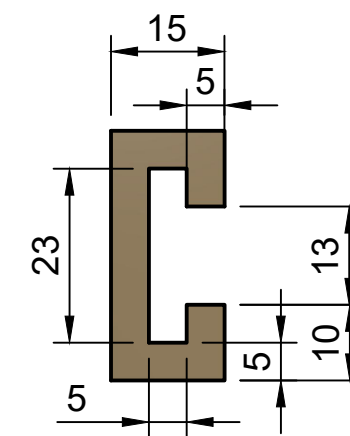
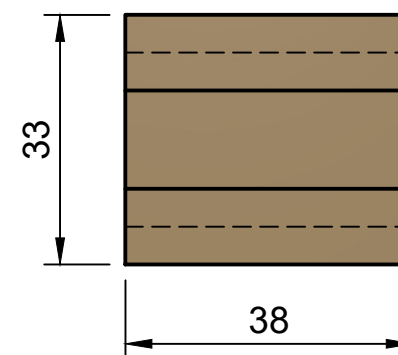
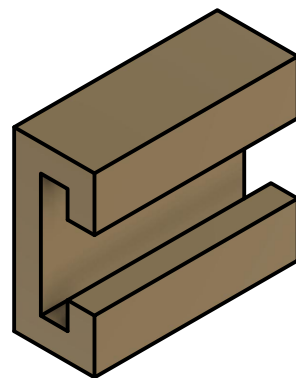
1x Top of compartment
for electrochemical cell



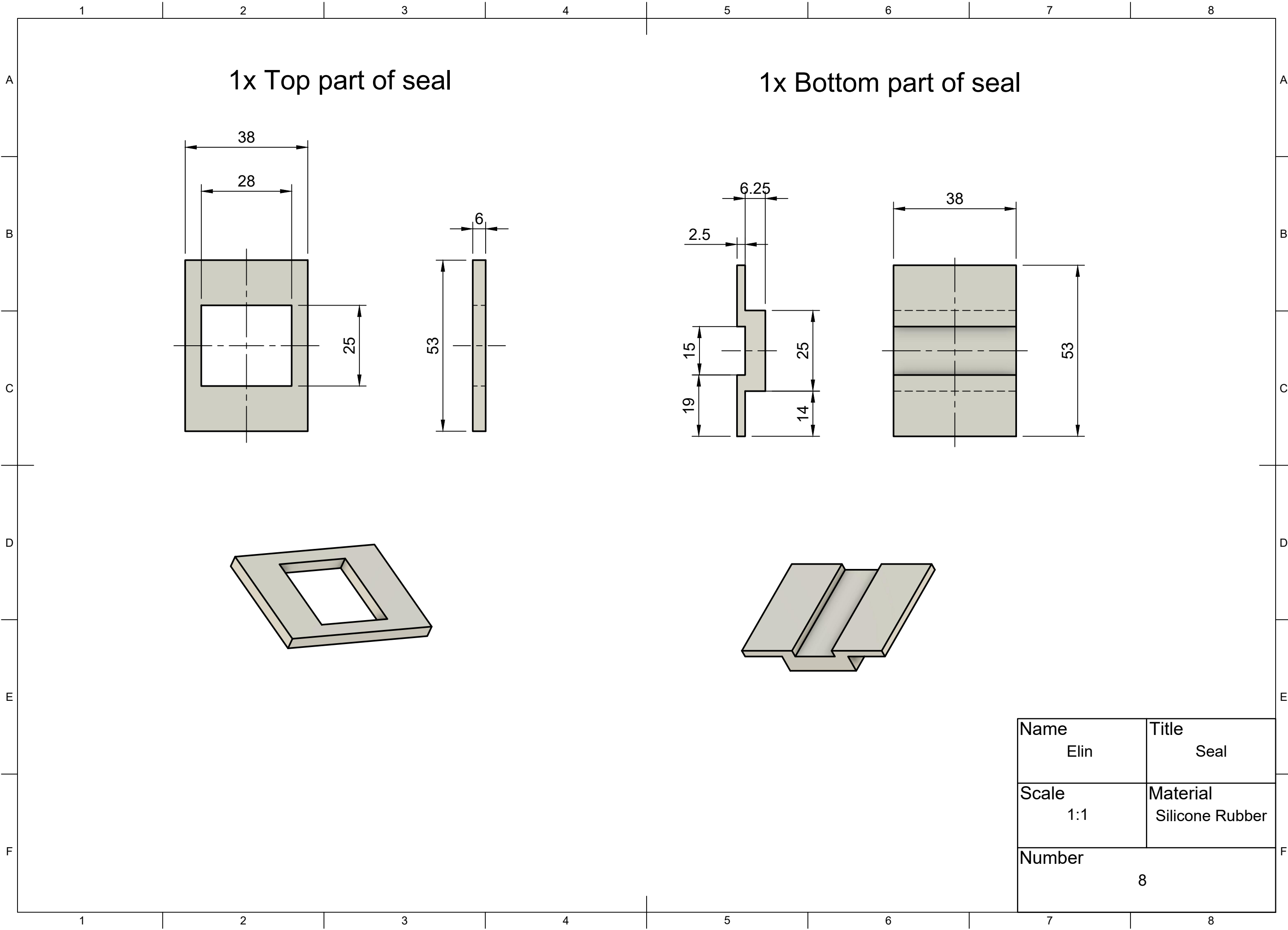
1x Bottom of compartment
for electrochemical cell



2x Clasps



Name Elin	Title Compartment - electrochemical
Scale 1:1	Material PEEK
Number	7

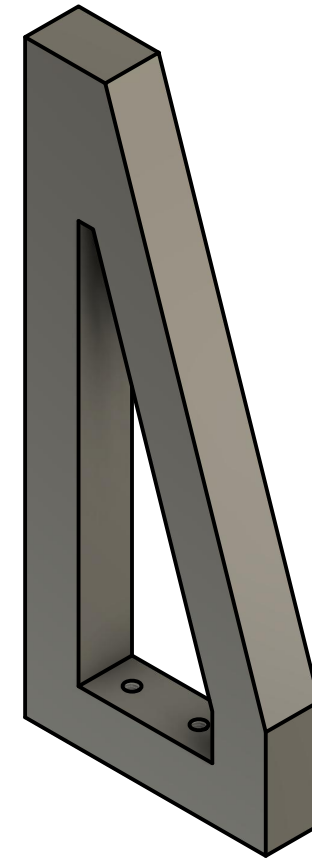
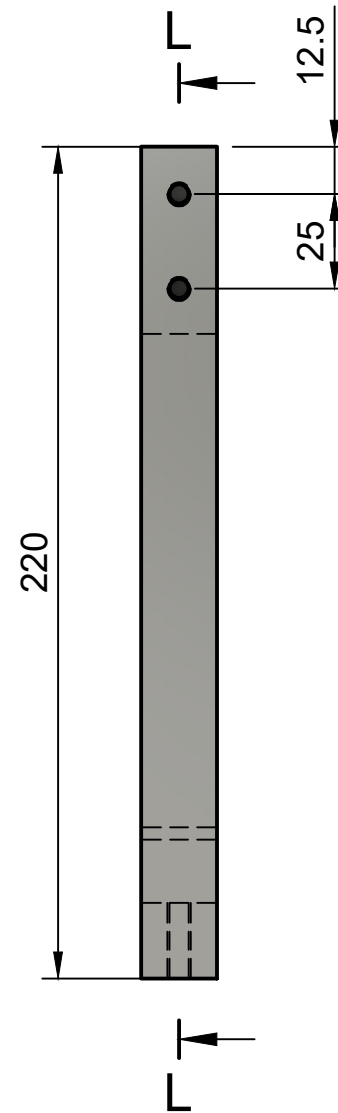
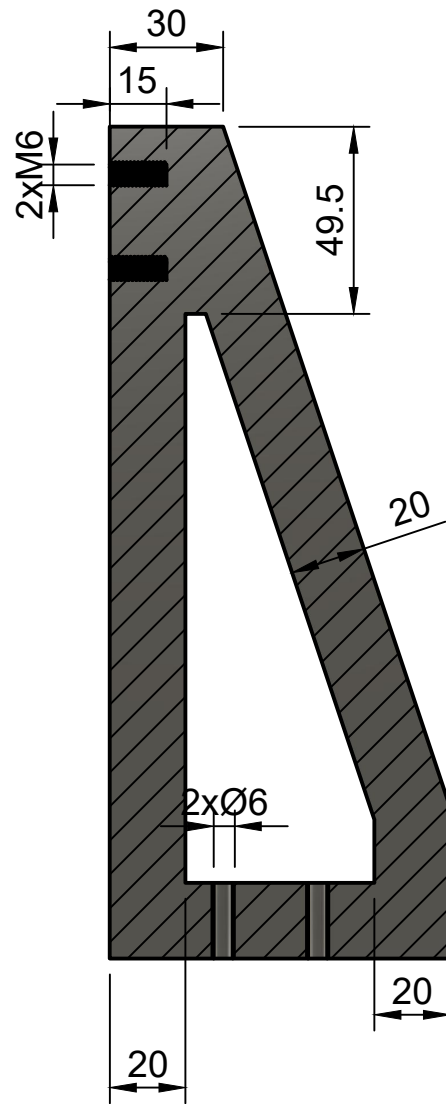
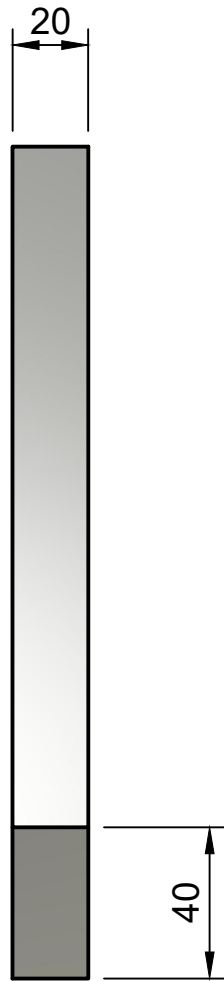
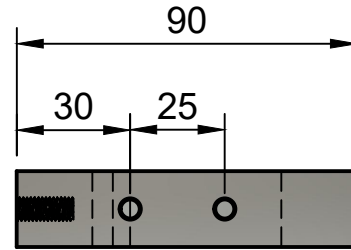


1x Top part of seal

1x Bottom part of seal

Name Elin	Title Seal
Scale 1:1	Material Silicone Rubber
Number	8

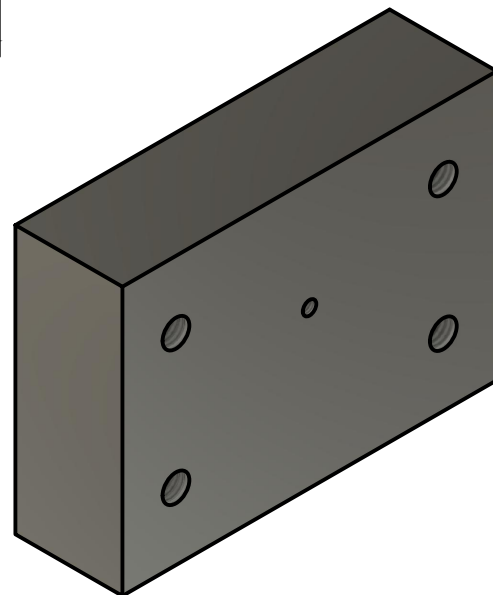
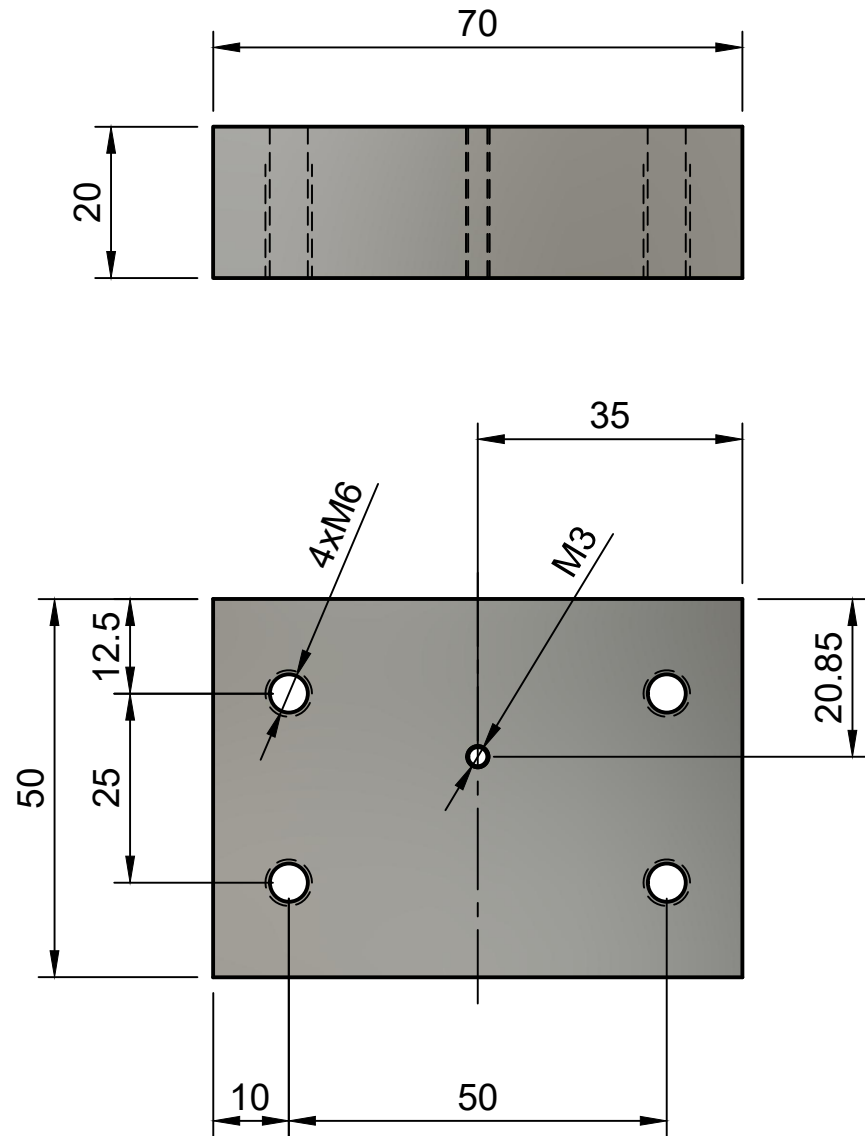
2x Triangular beam for load cell mount



L-L (1:2)

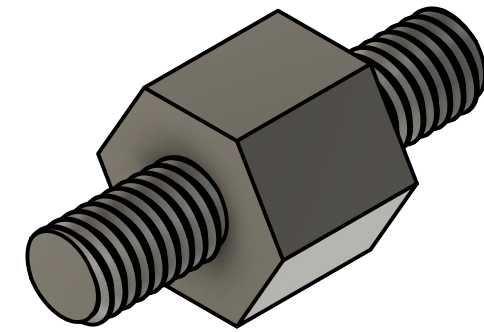
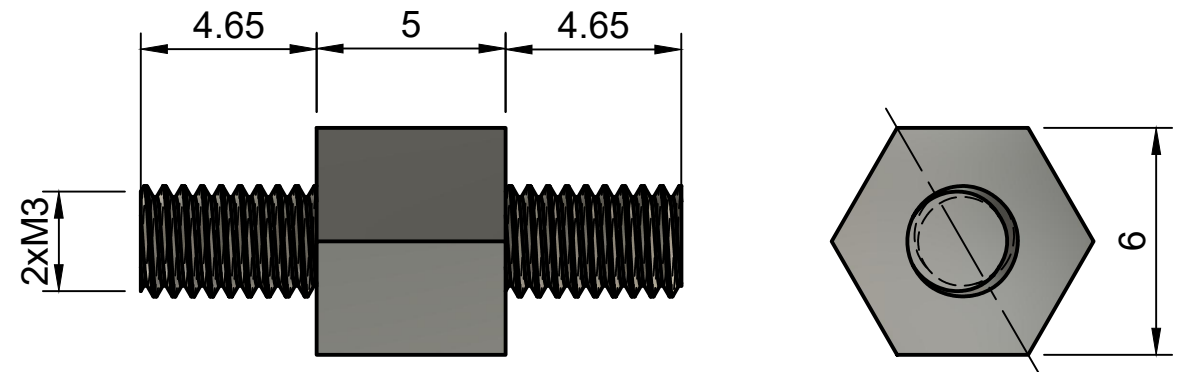
Name	Elin	Title	Load cell mount
Scale	1:2	Material	Stainless Steel
Number	9		

1x Support wall for load cell



1x Double ended bolt for load cell

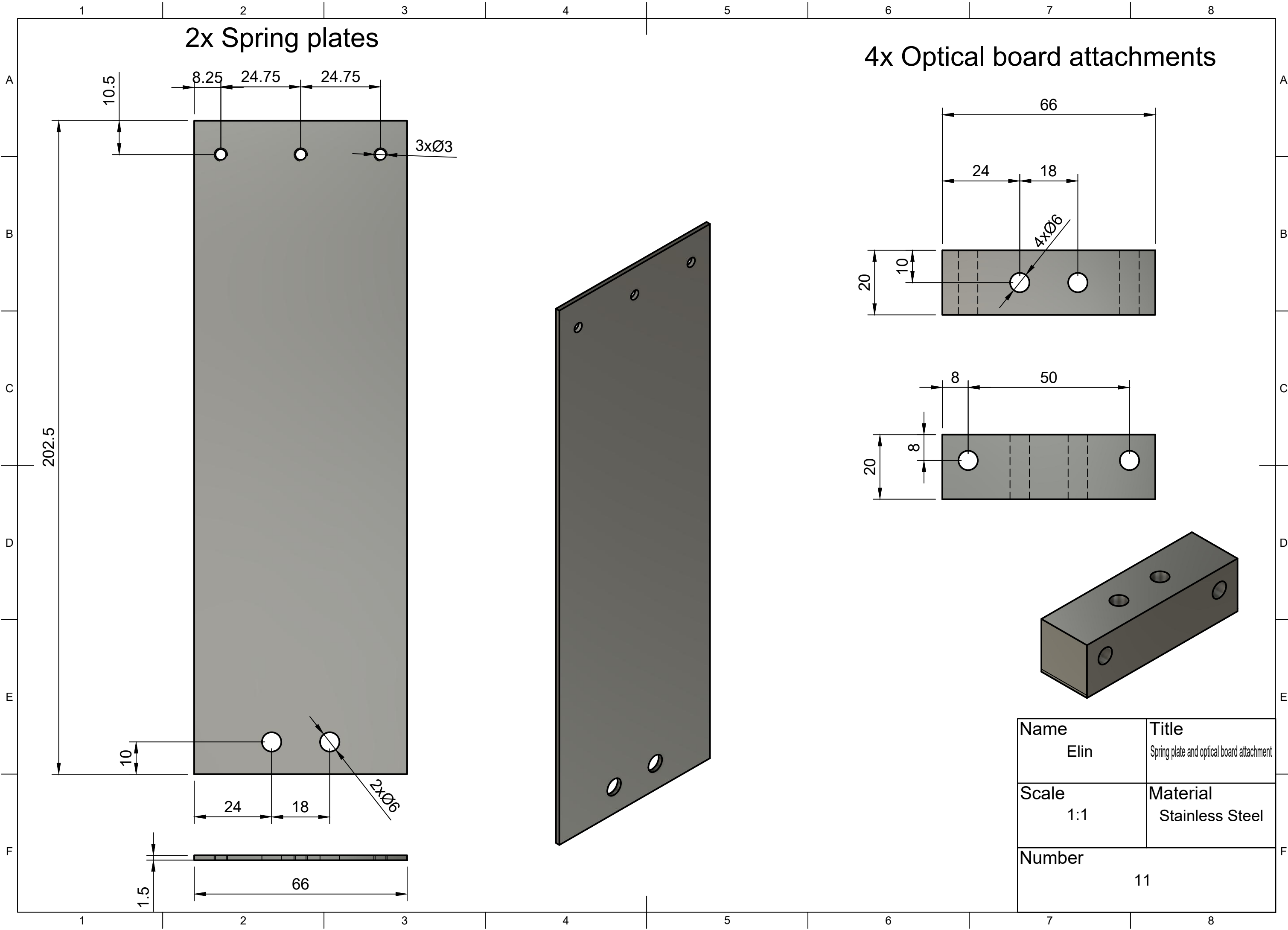
(5:1)



Name Elin	Title Load cell support wall and bolt
Scale 1:1	Material Stainless Steel
Number	10

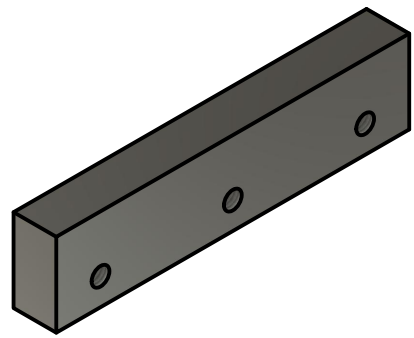
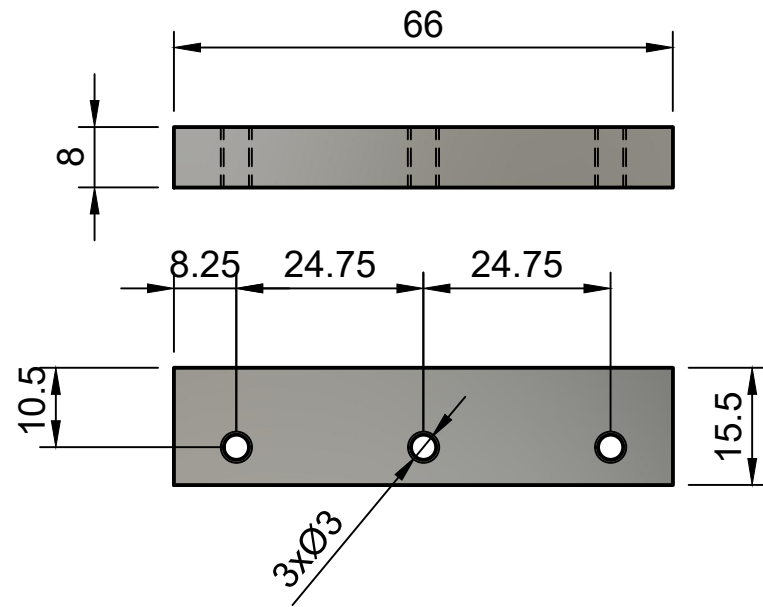
2x Spring plates

4x Optical board attachments

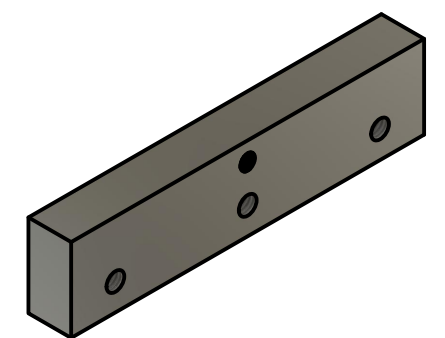
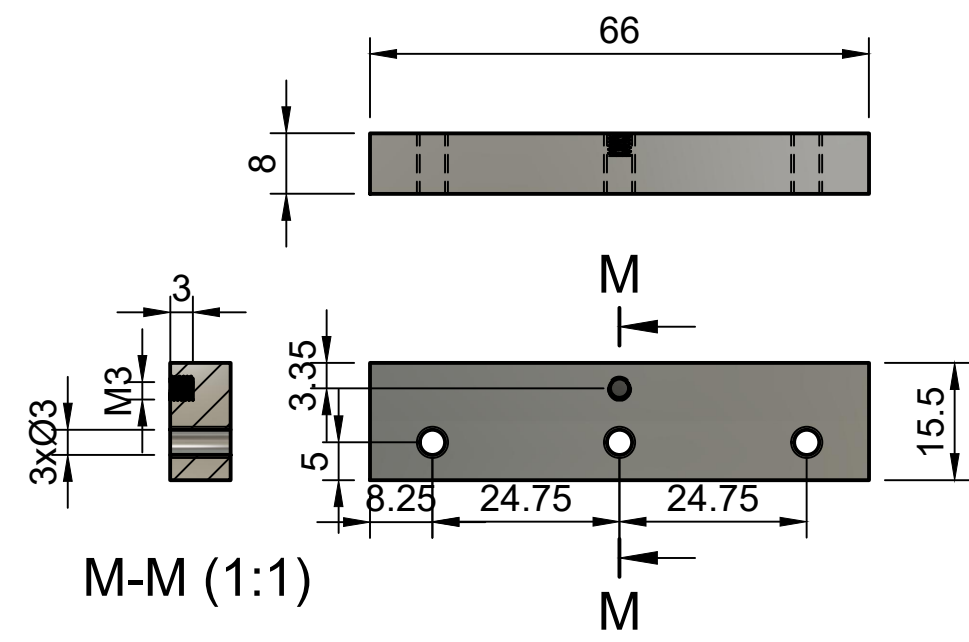


Name	Elin	Title	Spring plate and optical board attachment
Scale	1:1	Material	Stainless Steel
Number	11		

1x Upper attachment - left side

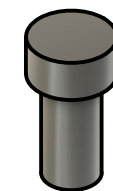
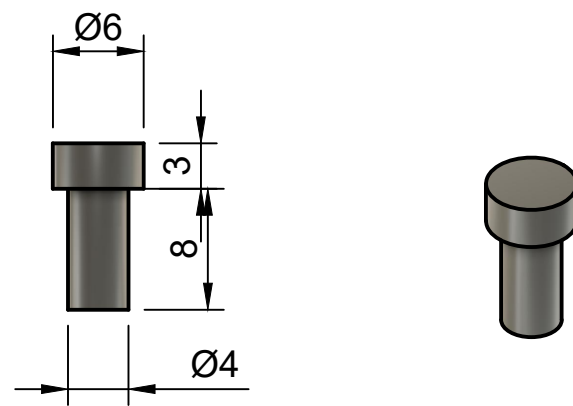


1x Upper attachment - right side



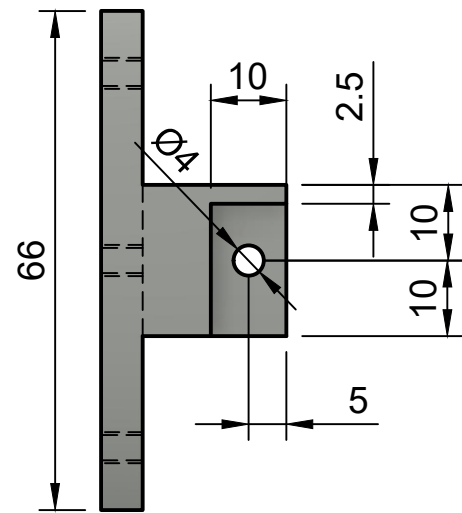
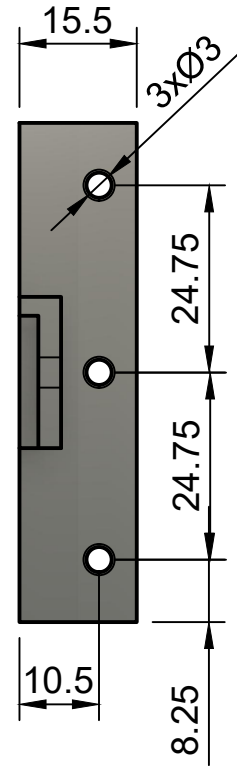
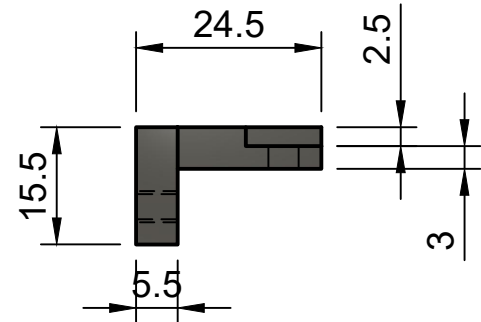
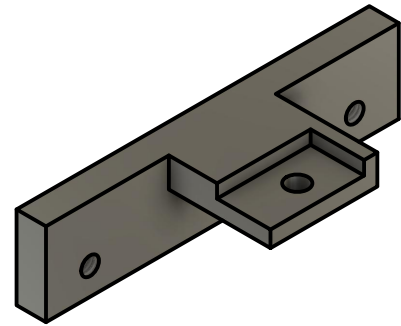
2x Pin for test piece holder

(2:1)

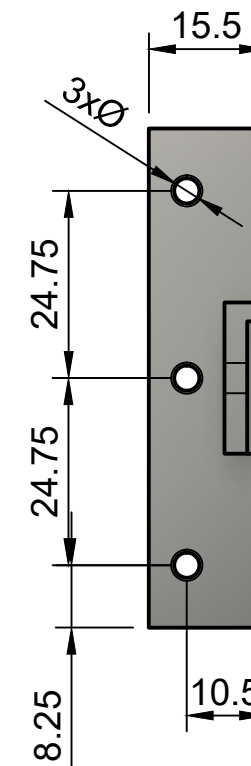
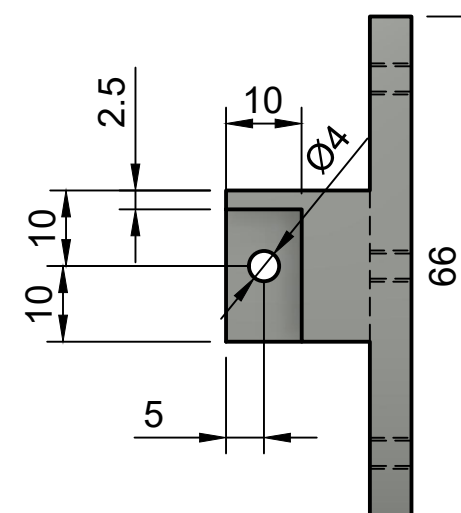
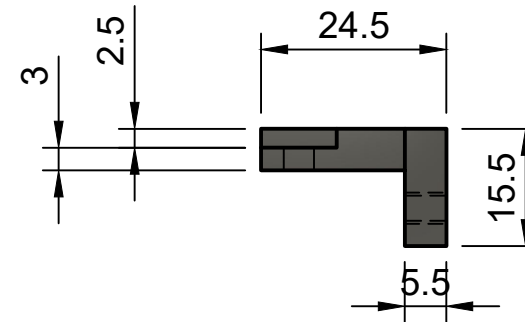
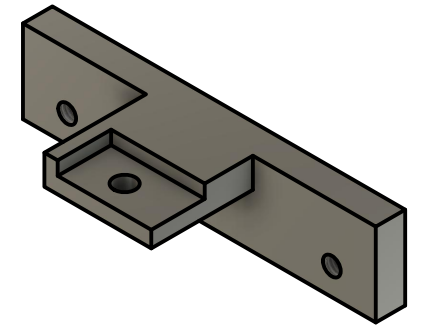


Name Elin	Title Upper attachment and pin
Scale 1:1	Material Stainless Steel
Number	12

1x Test piece holder - left side

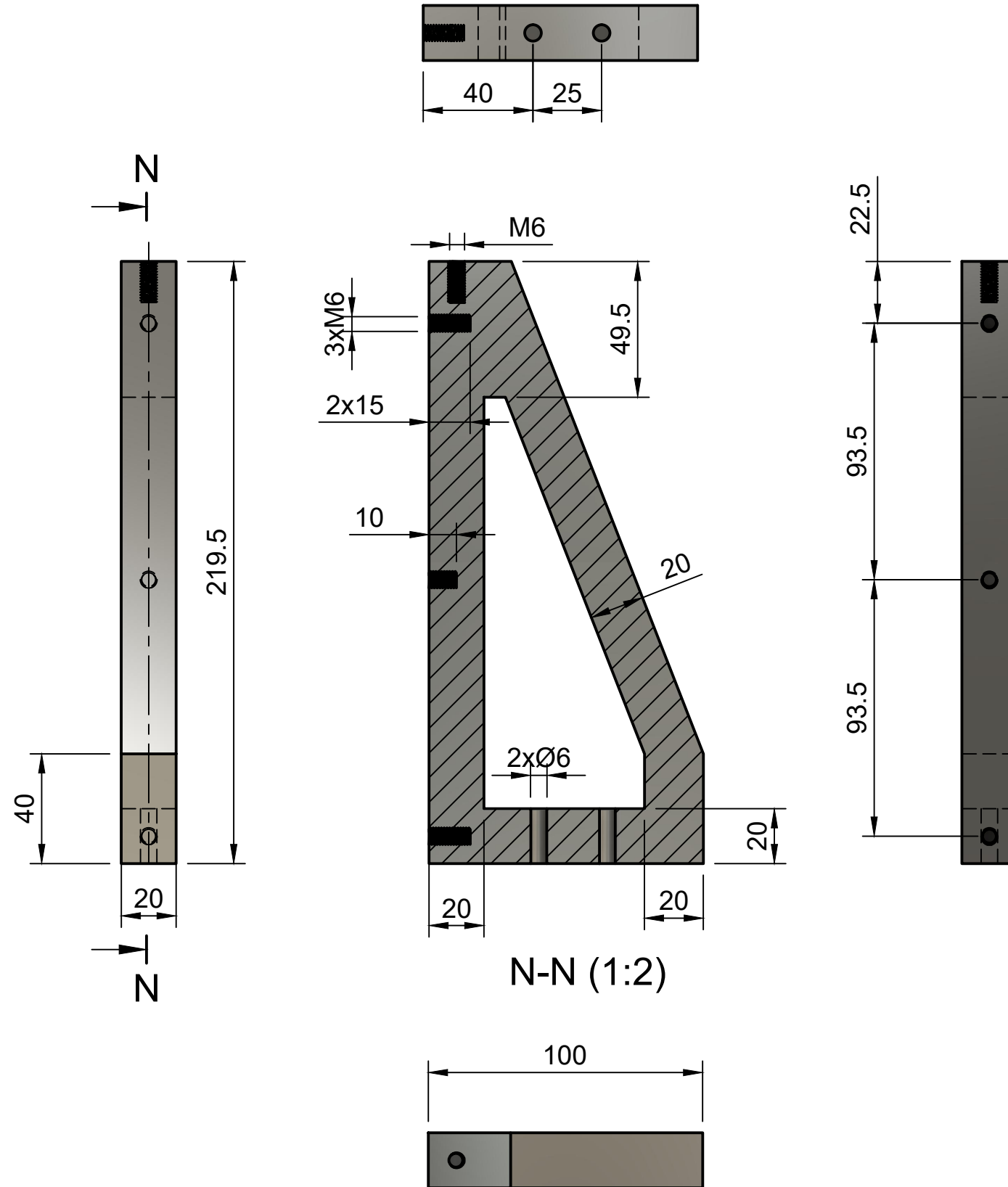


1x Test piece holder - right side



Name Elin	Title Test piece holder
Scale 2:1	Material Stainless Steel
Number 13	

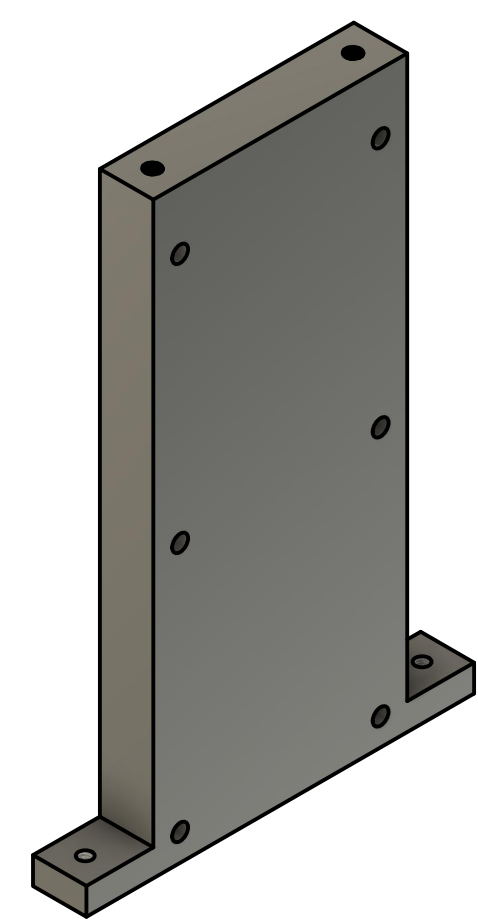
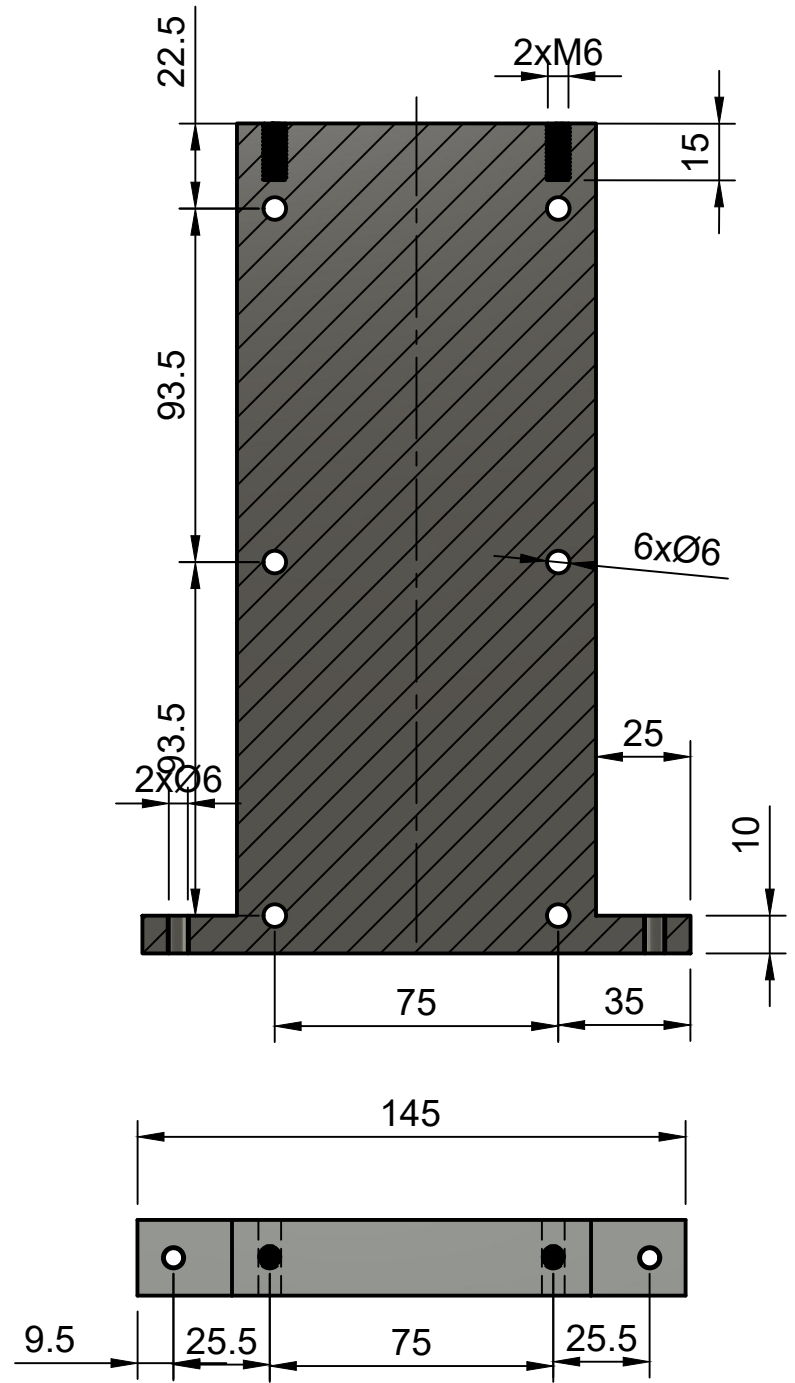
2x Triangular beam for support applicators



Name	Elin	Title	Triangular beam support
Scale	1:2	Material	Stainless Steel
Number	14		

1x Support applicator wall

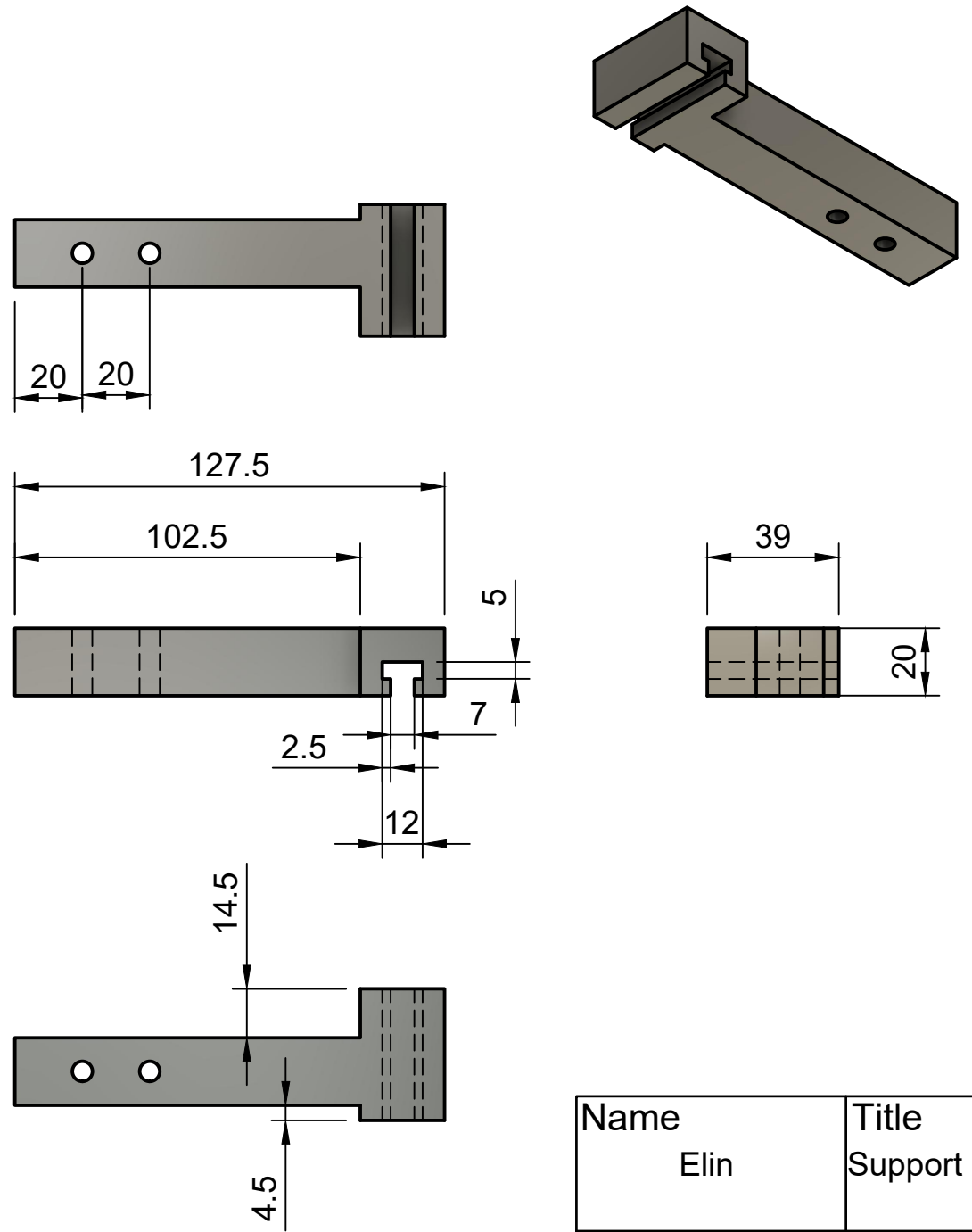
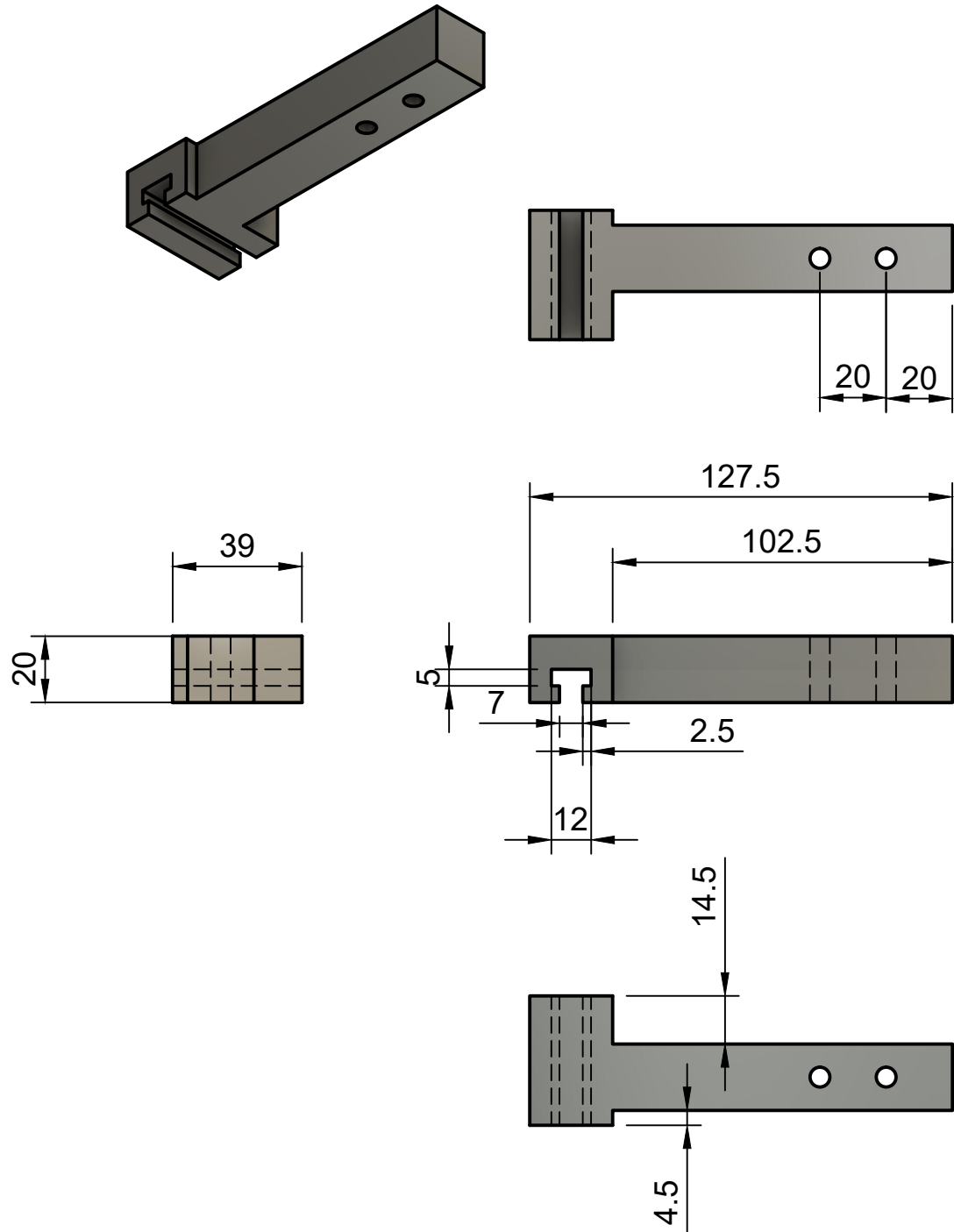
P-P (1:2)



Name	Elin	Title	Support applicator wall
Scale	1:2	Material	Stainless Steel
Number	15		

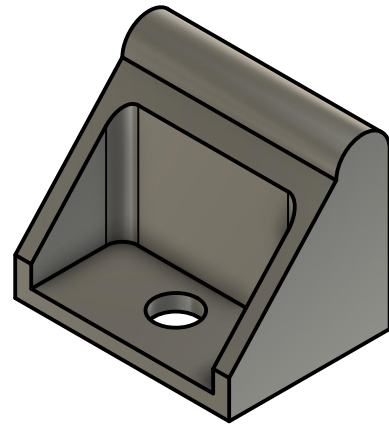
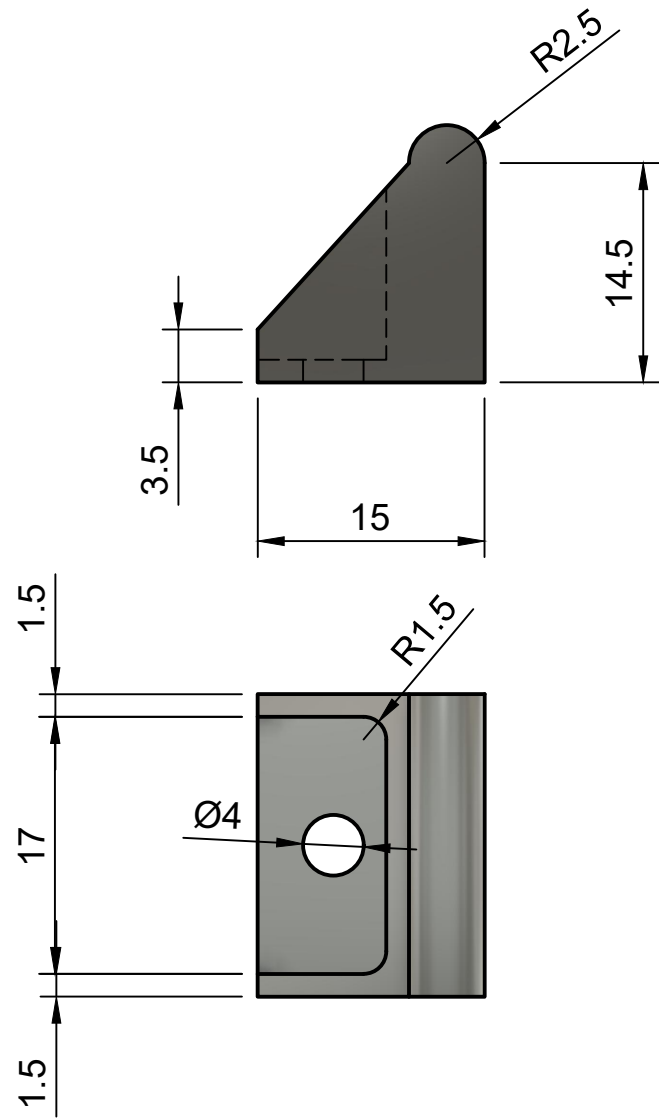
1x Support applicator arm - left side

1x Support applicator arm - right side

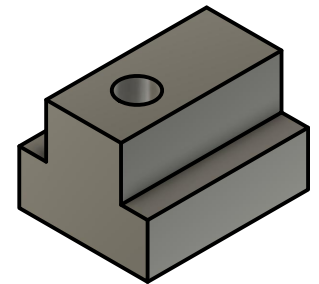
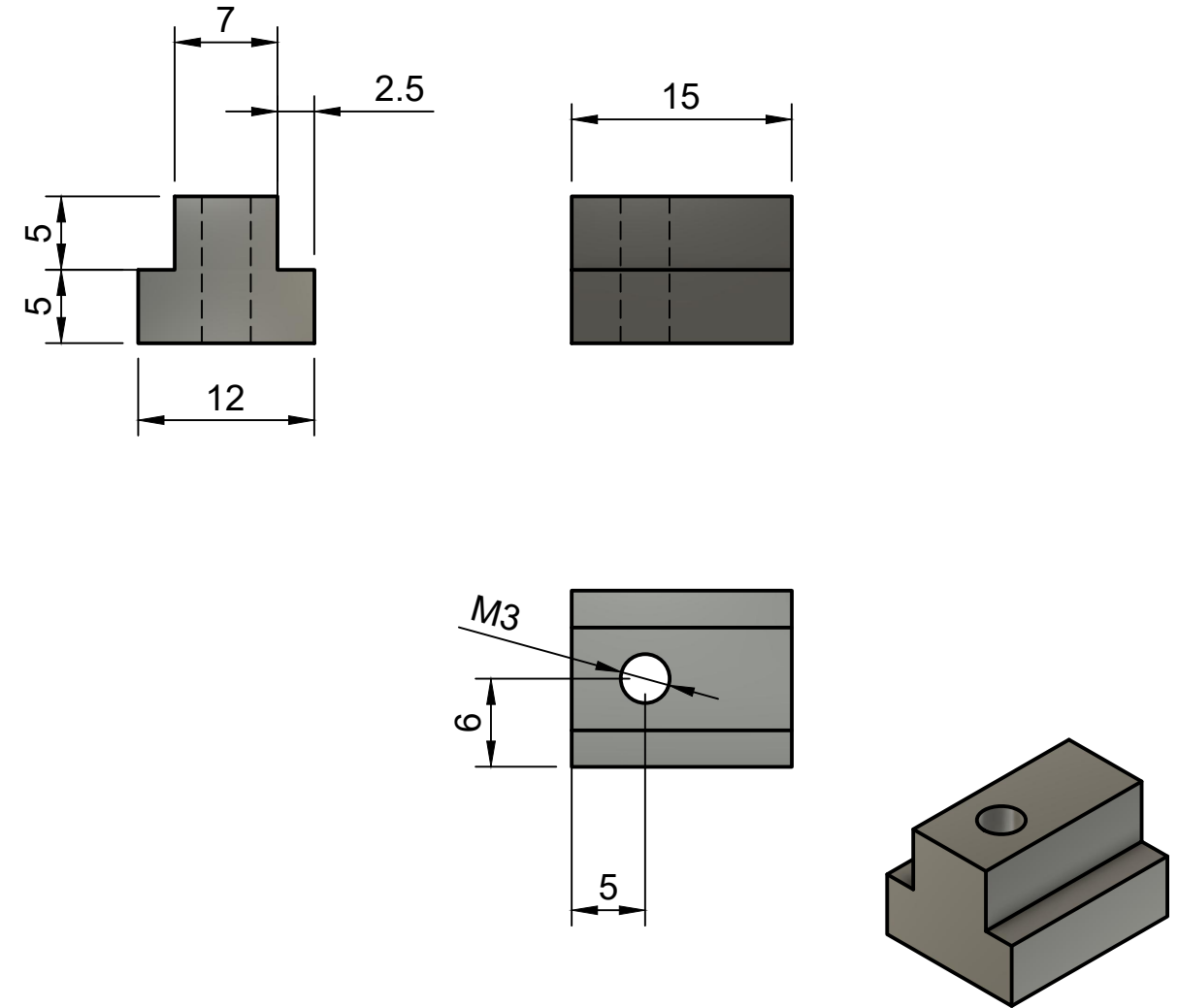


Name Elin	Title Support applicator
Scale 1:2	Material Stainless Steel
Number	16

4x Applicator

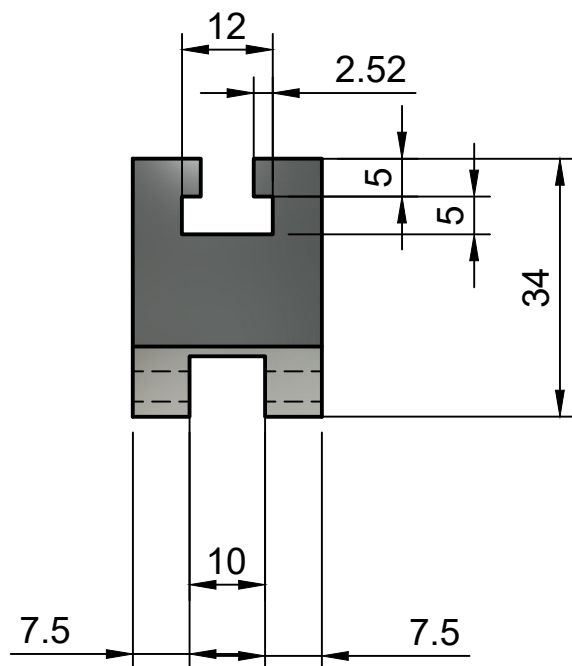
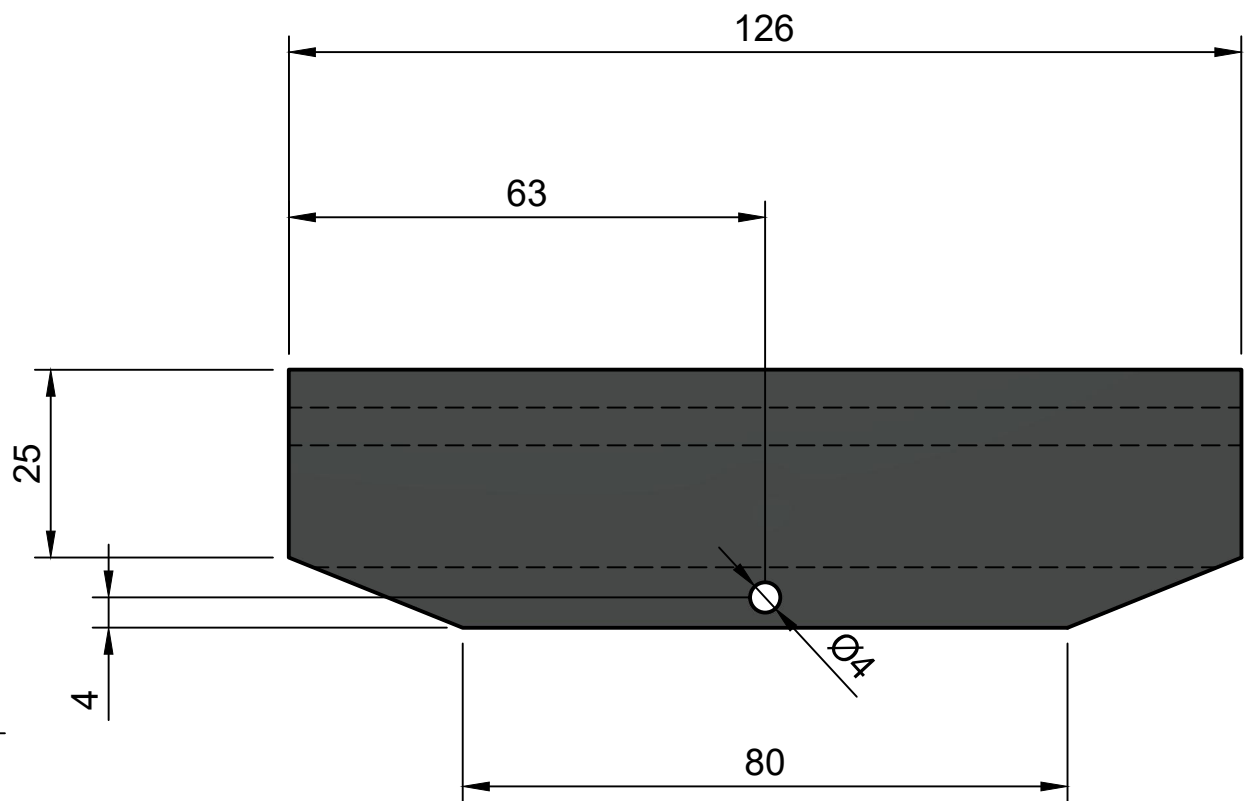


4x T-bolt

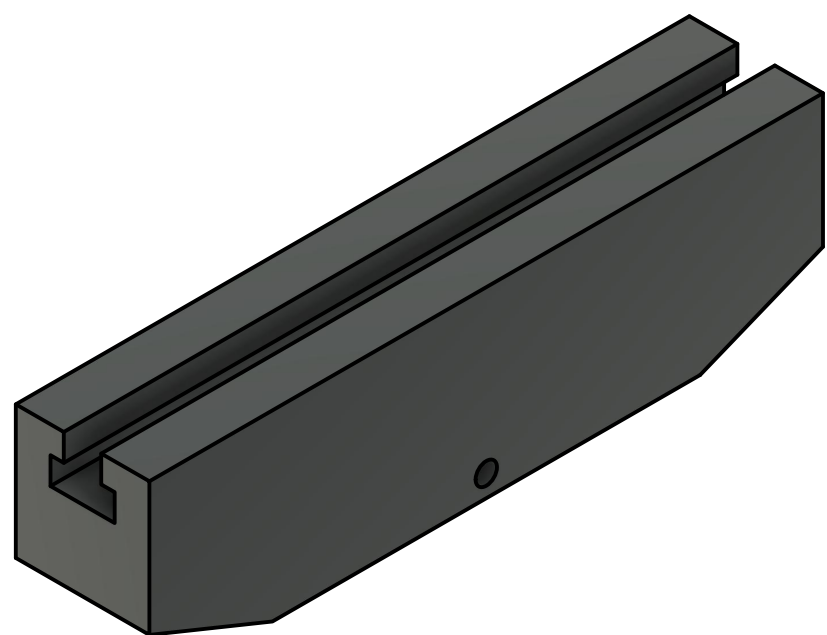
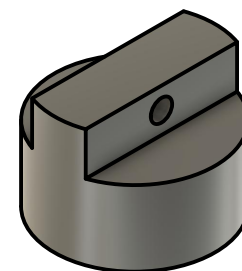
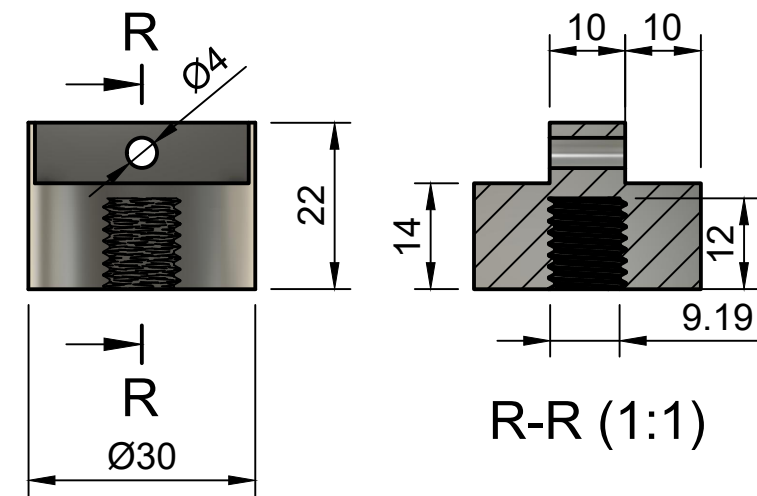


Name Elin	Title Applicator and T-bolt
Scale 2:1	Material Stainless Steel
Number	17

1x T-rail load applicator

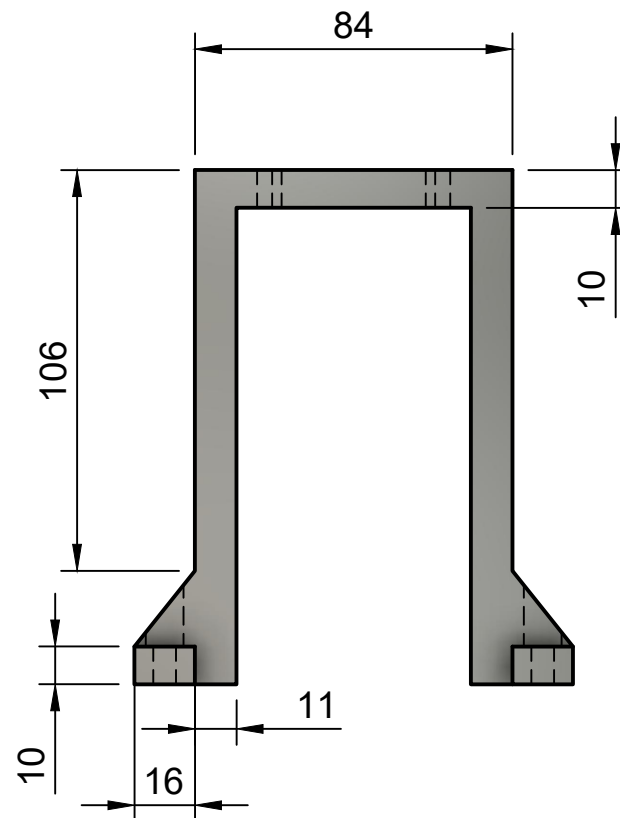
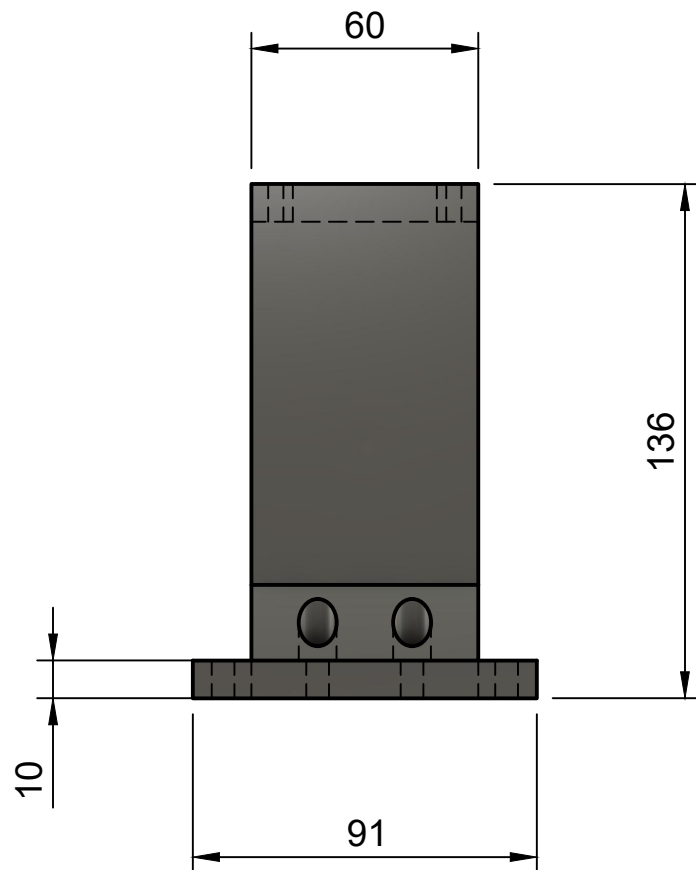
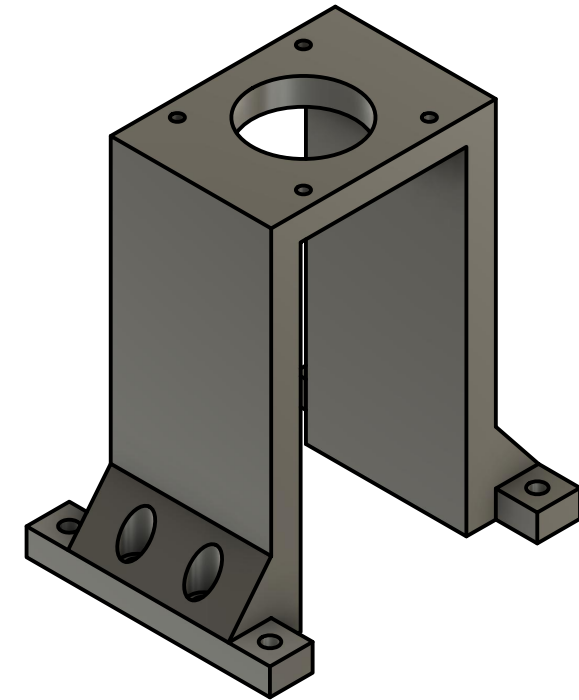
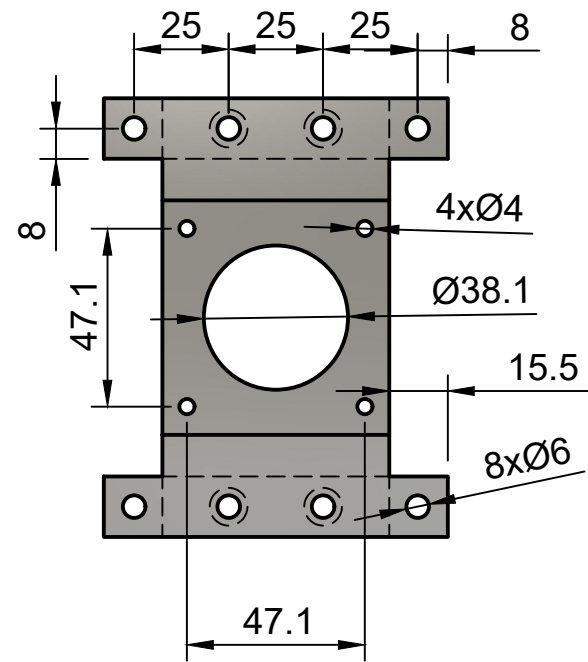


1x Motor attachment for load applicator



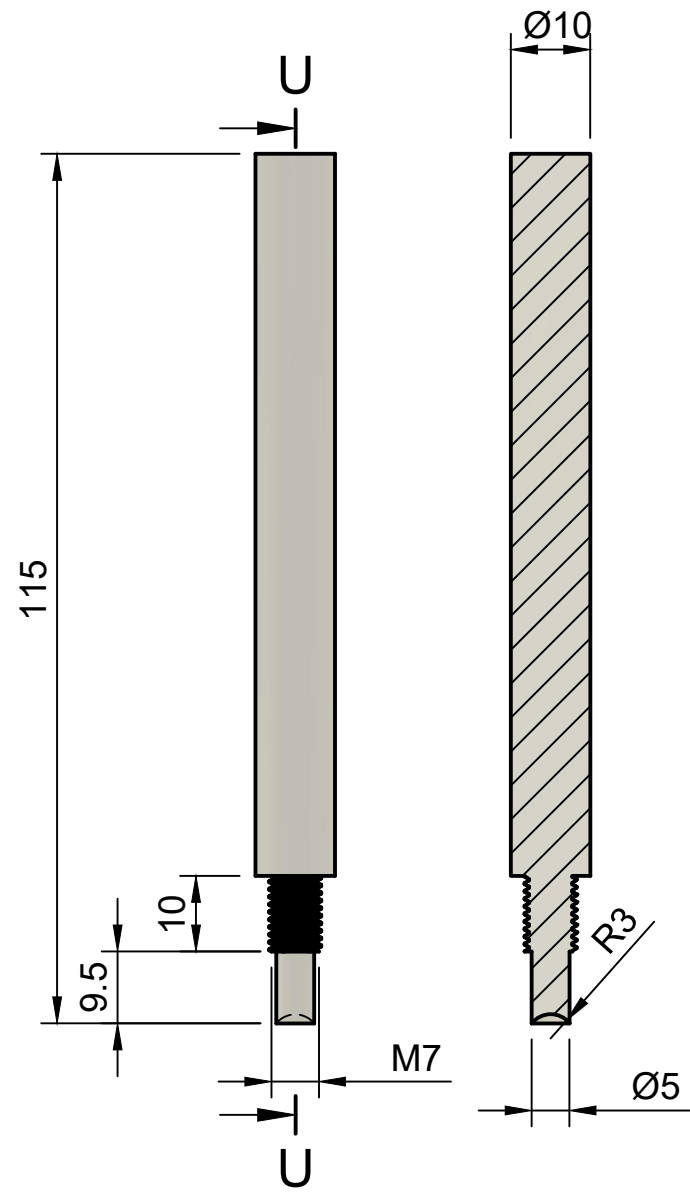
Name Elin	Title T-rail and motor attachment
Scale 1:1	Material Stainless Steel
Number	18

1x Motor mount for stepper motor



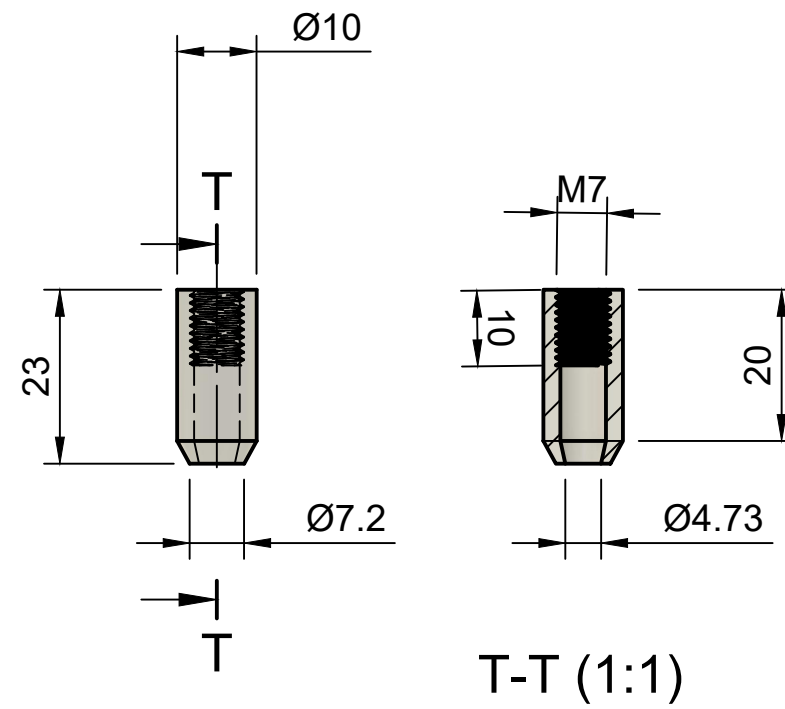
Name Elin	Title Motor mount
Scale 1:2	Material Stainless Steel
Number	19

1x Ball holder top



U-U (1:1)

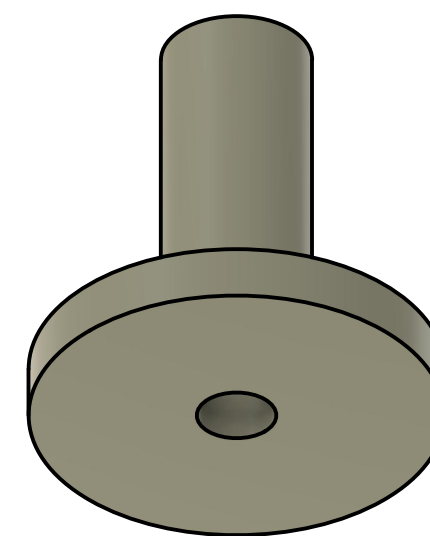
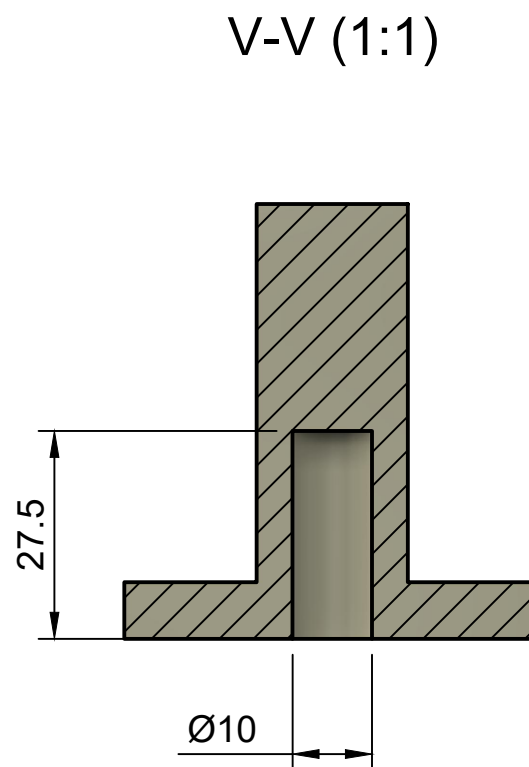
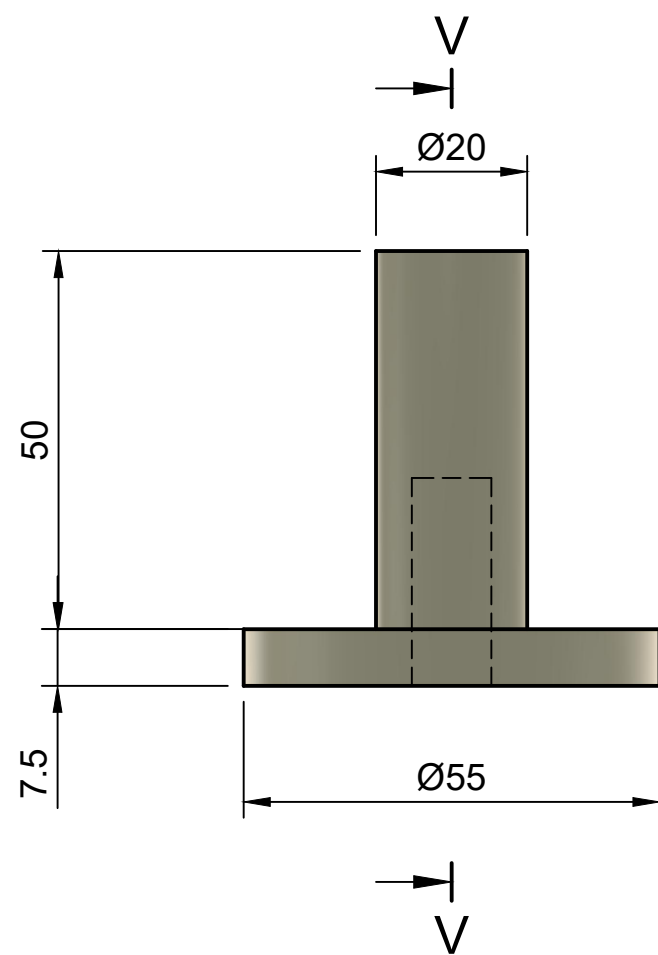
1x Ball holder cap



T-T (1:1)

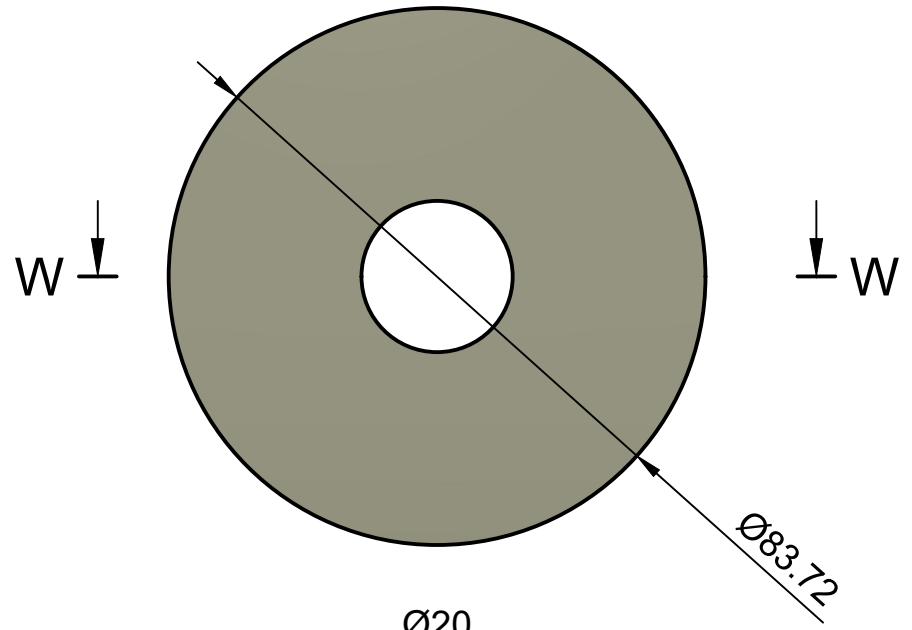
Name Elin	Title Ball holder
Scale 1:1	Material PEEK
Number	20

1x Ball holder hat

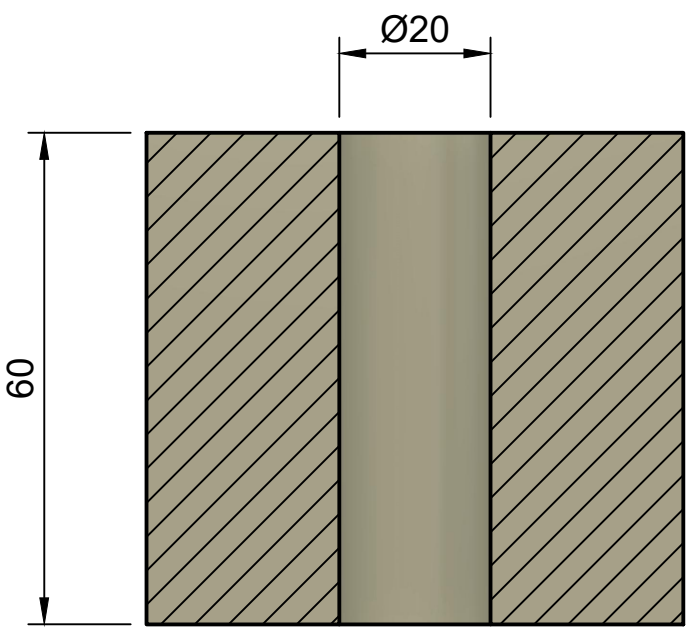
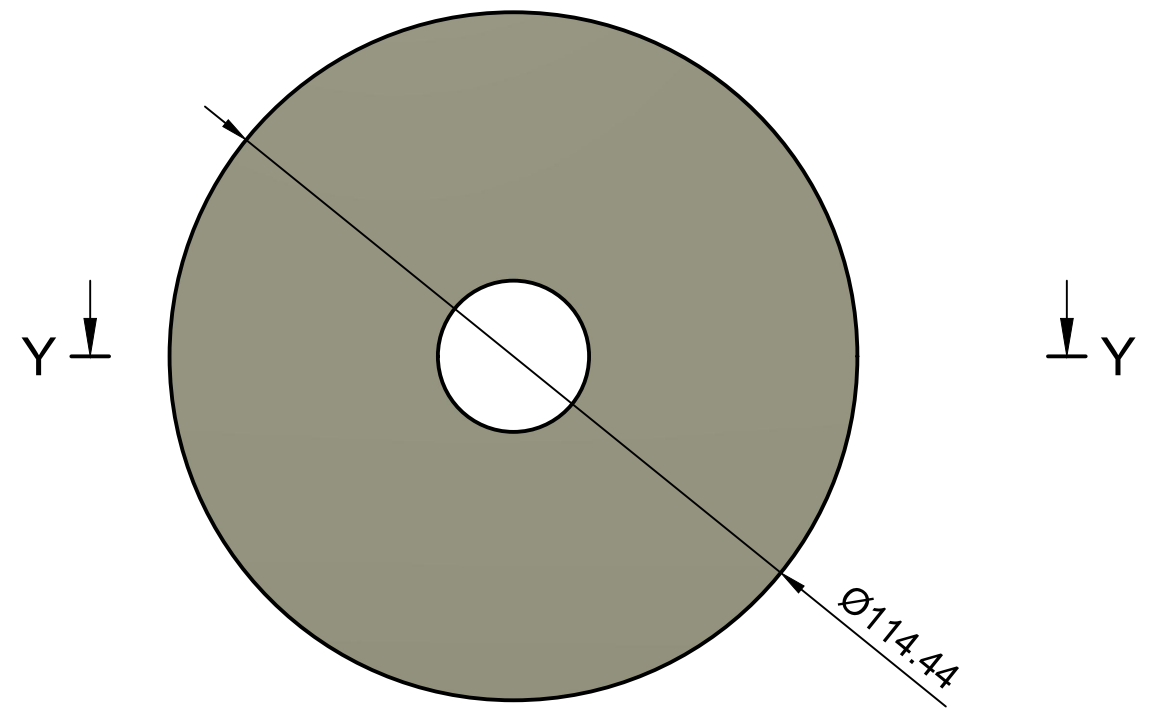


Name Elin	Title Ball holder
Scale 1:1	Material PEEK
Number	21

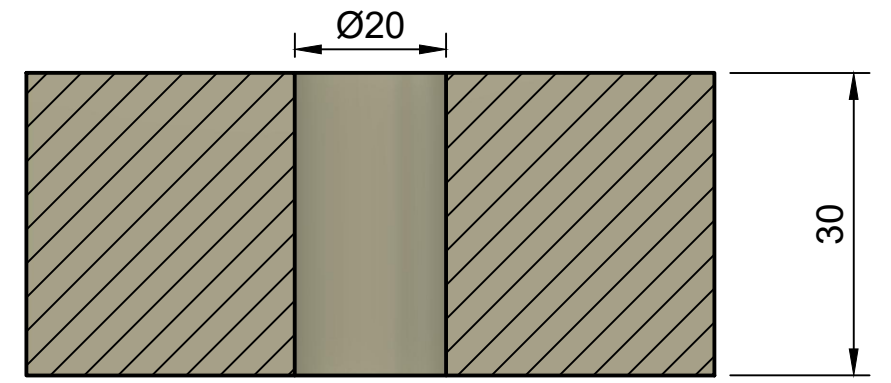
1x Tall 20 N dead weight



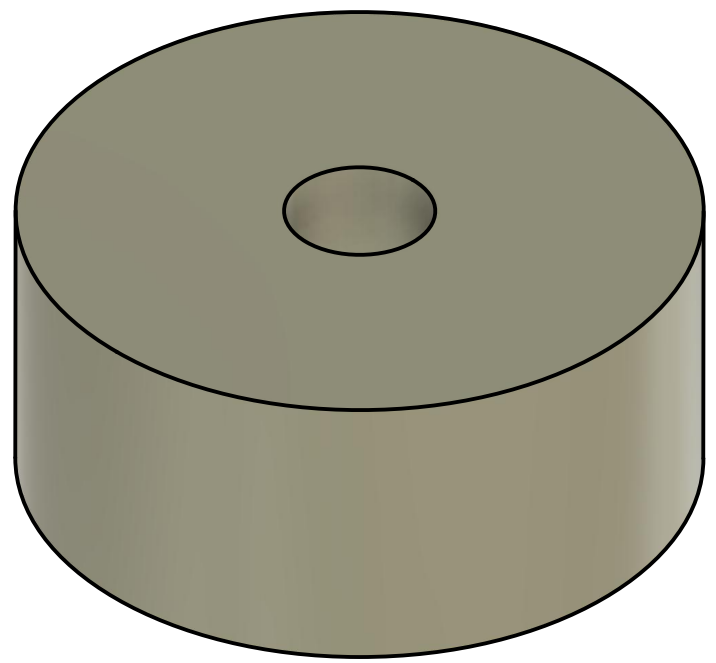
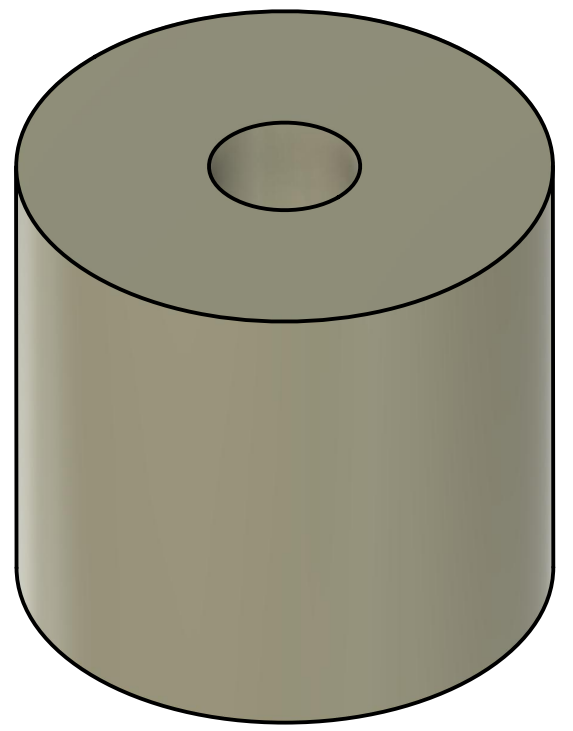
1x Short 20 N dead weight



W-W (1:1)

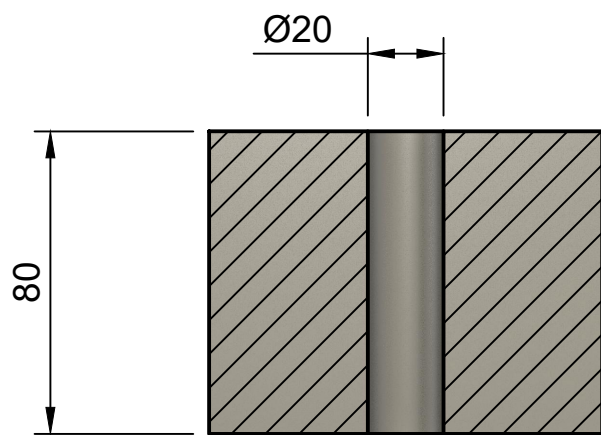
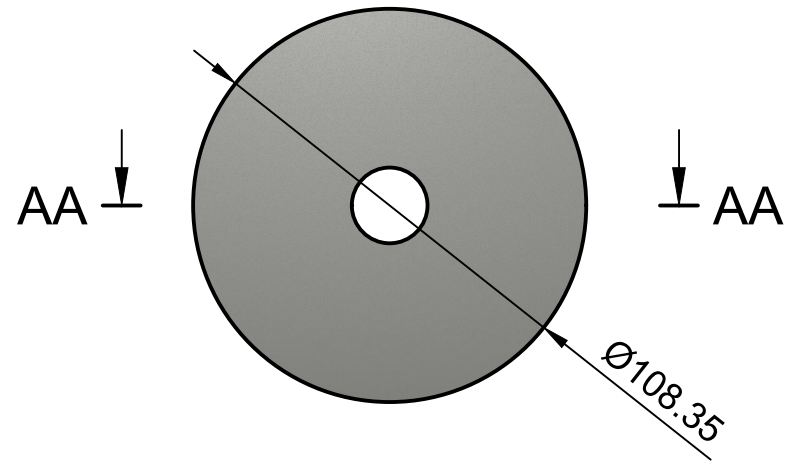


Y-Y (1:1)

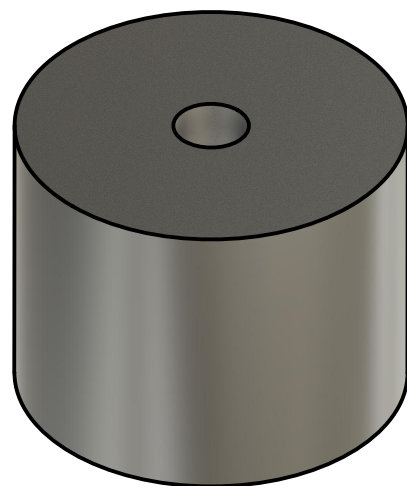


Name Elin	Title 20 N dead weight
Scale 1:1	Material Stainless Steel
Number 22	

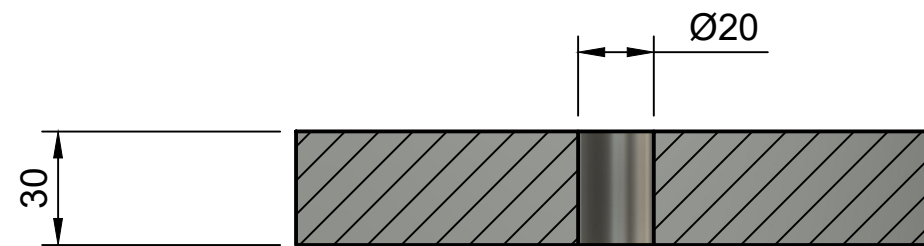
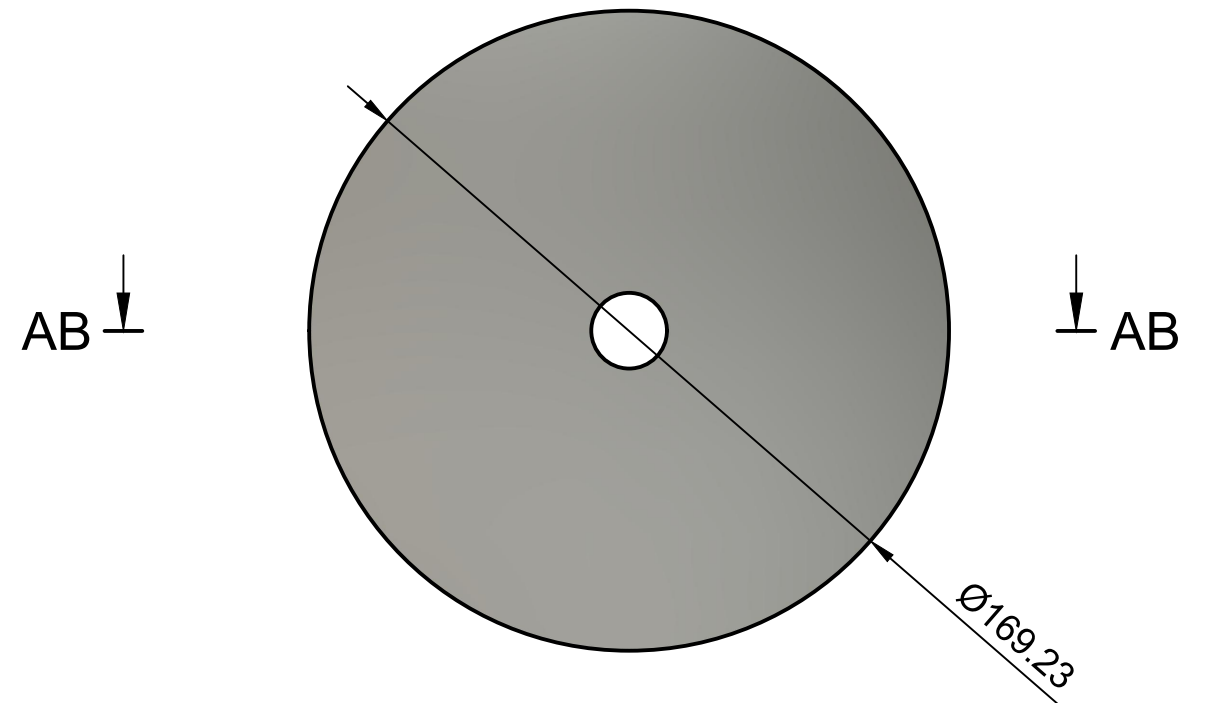
1x Tall 50 N dead weight



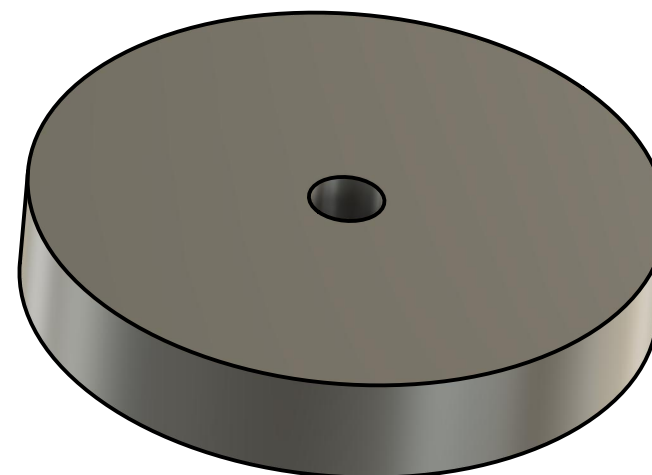
AA-AA (1:2)



1x Short 50 N dead weight

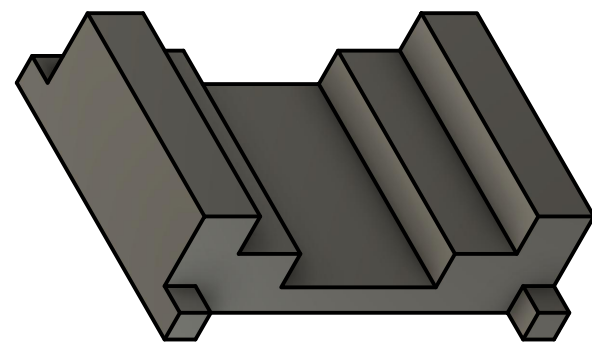
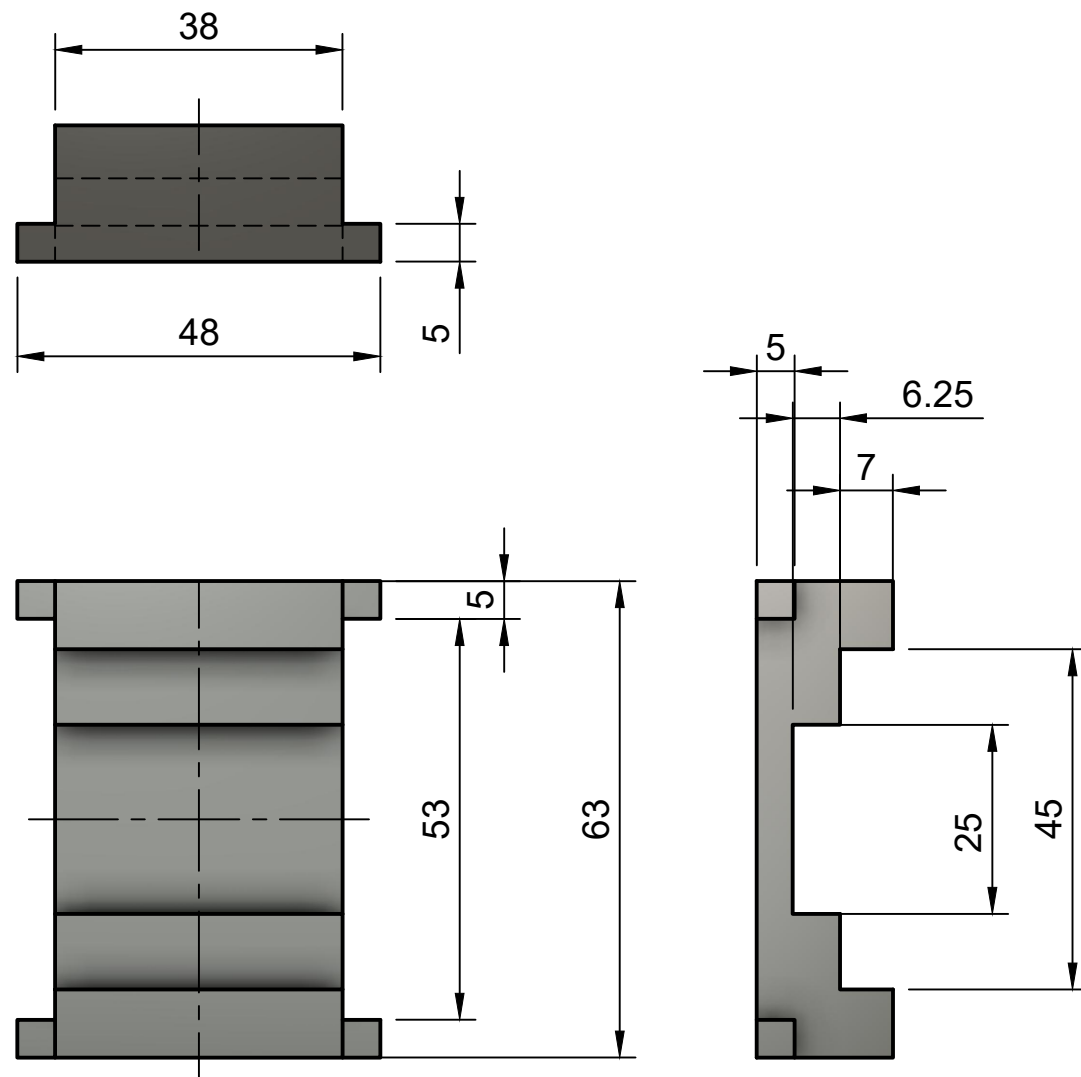


AB-AB (1:2)

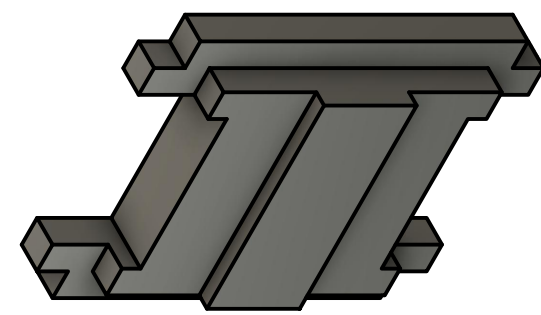
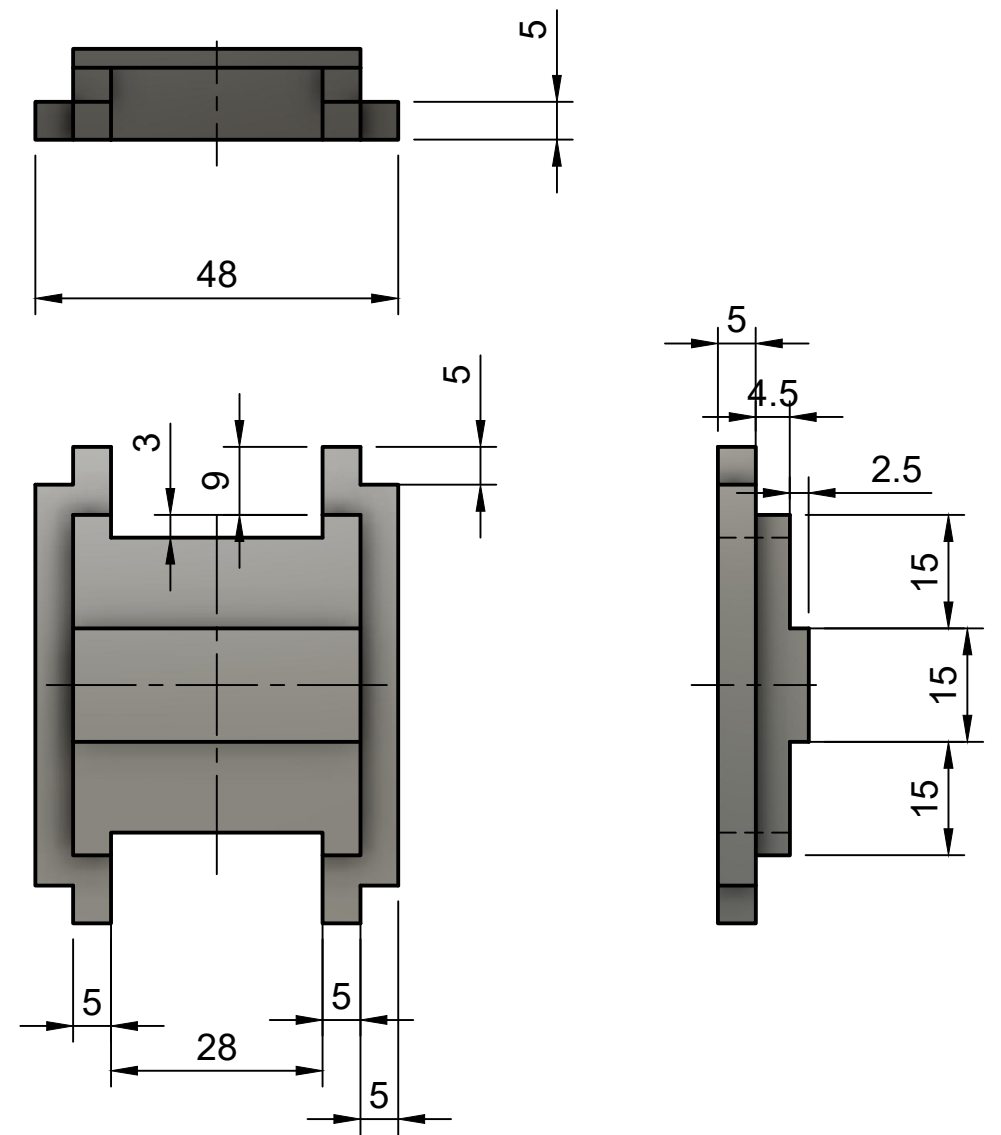


Name Elin	Title 50 N dead weight
Scale 1:2	Material Stainless Steel
Number	23

1x Lower part of the mould for the bottom seal

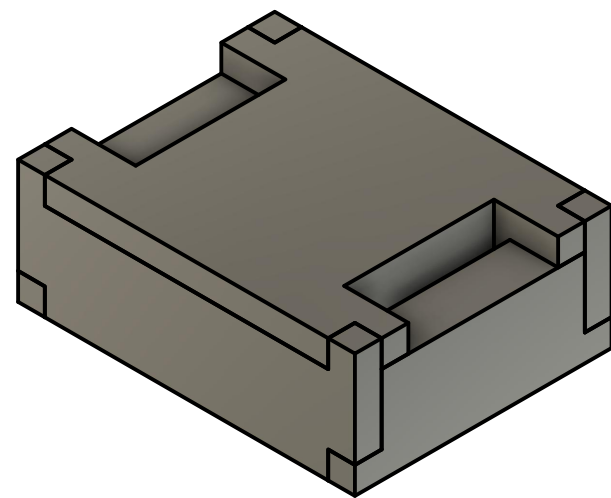
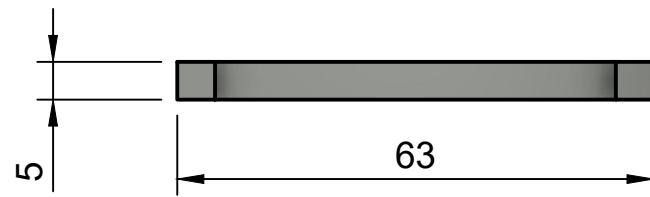
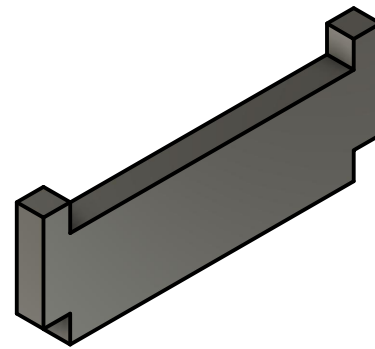
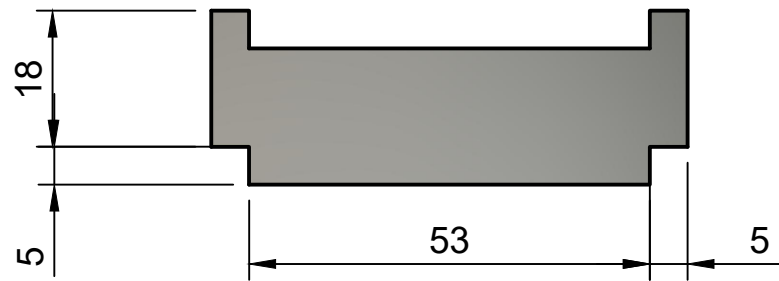


1x Upper part ("lid") of the mould for the bottom seal

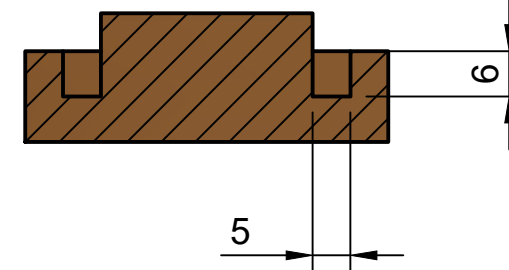


Name Elin	Title Mould bottom seal
Scale 1:1	Material PLA
Number	24

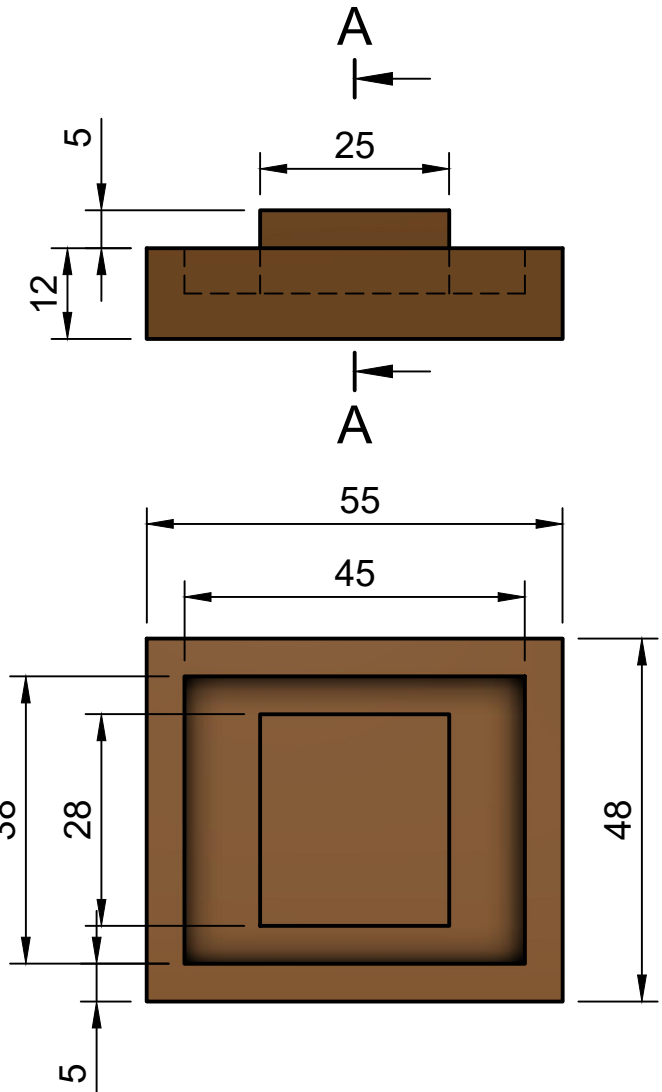
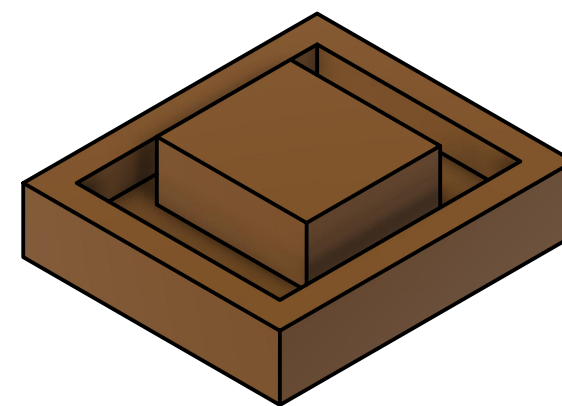
2x Side parts of the
mould for the bottom seal



1x Mould for the top seal



AC-AC (1:1)



Name Elin	Title Mould seal
Scale 1:1	Material PLA
Number	25



 **NTNU**

Norwegian University of
Science and Technology